POLYTECHNIQUE MONTRÉAL

affiliée à l'Université de Montréal

et

l'Université du Québec en Abitibi-Témiscamingue

Impacts of Mine Dewatering on Groundwater Flow and Dissolved Mass Transport: Conceptual Examples Applied to The Canadian Shield

FELIX ABANTO TRUJILLO

Département des génies civil, géologique et des mines

Mémoire présenté en vue de l'obtention du diplôme de *Maîtrise ès sciences appliquées*

Mineral Engineering – Environmental Hydrogeology

December 2025

POLYTECHNIQUE MONTRÉAL

affiliée à l'Université de Montréal

et

l'Université du Québec en Abitibi-Témiscamingue

Ce mémoire intitulé:

Impacts of Mine Dewatering on Groundwater Flow and Dissolved Mass Transport: Conceptual Examples Applied to The Canadian Shield

présenté par **Felix ABANTO TRUJILLO**

en vue de l'obtention du diplôme de *Maîtrise ès sciences appliquées*

a été dûment accepté par le jury d'examen constitué de :

Faneva RARISON, président
Eric ROSA, membre et directeur de recherche
Carmen NECULITA, membre et codirectrice de recherche
Lucie COUDERT, membre et codirectrice de recherche
Alain ROULEAU, membre externe

DEDICATION

Dedicated to all who strive to understand hidden flow and transport of water through fractured rock and to those who work towards responsible mine closure planning.

ACKNOWLEDGEMENTS

I want to thank my project director, Eric Rosa, for all the support he has provided to me with his problem-solving skills; more specifically, his technical, financial and moral support were very important to the success of this project. His guidance and motivation helped me to structure this project and surpass challenges. I also want to take the opportunity to thank my co-directors, Lucie Coudert and Carmen Neculita for their availability and similar support provided.

I also want to give a special thank to Brahim Maylal for his time and constant support with the numerical modelling portion. His knowledge, patience and efforts were also key for the progress of this project which I sincerely value and appreciate.

Last but not least, I want to thank my parents and my partner and family of dogs for their unwavering support and patience through this journey. Your encouragement made all the difference.

RÉSUMÉ

Cette étude examine l'écoulement des eaux souterraines et le transport de solutés dans des systèmes rocheux fracturés influencés par les ouvertures minières. Des structures géologiques ont été utilisées pour modéliser un assemblage de fractures et de joints susceptibles d'améliorer la connectivité entre les discontinuités structurales. La compréhension de ces voies d'écoulement préférentielles est essentielle pour interpréter la dynamique de l'infiltration d'eau dans une mine et pour tester des approches numériques simplifiées qui peuvent être utilisées pour la planification de l'opération et de la fermeture. L'objectif était de comparer la capacité de certains modèles de continuum équivalent (MCE) homogènes et hétérogènes développés dans GeoStudio 3D (SEEP3D & CTRAN3D) à simuler l'écoulement des eaux souterraines et le transport de soluté dissous non réactif à travers une gamme d'analyses de sensibilité changeant les paramètres géométriques, hydrauliques et d'advection-dispersion. Des critères supplémentaires, y compris l'analyse des nombres de Péclet et de Courant, ont été utilisés pour évaluer la robustesse des simulations de transport de soluté non réactif par advection-dispersion et identifier les conditions dans lesquelles les performances des MCE sont considérées comme fiables ou limitées. Les résultats montrent que les MCE peuvent reproduire les solutions analytiques lorsque la conductivité hydraulique (K) des zones de fractures est homogène sur un domaine cubique de 2 km. Néanmoins, des écarts importants ont été observés avec une géométrie complexe et des caractéristiques discrétisées présentant des valeurs de K hétérogènes au sein d'un même domaine. Les résultats suggèrent en outre que les MCE homogènes simplifiés peuvent fournir des informations précieuses sur l'écoulement et le transport de soluté dissous dans un aquifère rocheux fracturé soumis à une dépressurisation causée par le dénoyage d'une mine, par exemple. Les premières conclusions concernant les limites des MCE suggèrent que les modèles devraient être affinés en améliorant la représentation des fractures et en introduisant une formulation stochastique potentielle avec des données de surveillance pour assurer la fiabilité de GeoStudio afin de soutenir l'interprétation du dénoyage des mines et la prise de décision en matière de gestion des eaux souterraines.

ABSTRACT

This study investigates groundwater flow and solute transport in fractured bedrock systems influenced by the mining openings where geological structures were used to model a conjunction of fractures and joints sets potentially enhancing the connectivity of structural discontinuities. Understanding these preferential pathways is critical to interpret the mine inflow dynamics and for testing simplified numerical approaches that can be used for operation and closure planning. The objective was to compare the capacity of some homogeneous and heterogeneous equivalent continuum models (ECMs) developed in GeoStudio 3D (SEEP3D & CTRAN3D) to simulate groundwater and dissolved non-reactive solute transport across a range of sensitivity analyses changing geometry, hydraulic, and advection-dispersion parameters. Additional criteria, including the analysis of the Péclet and Courant numbers, were used for evaluating the robustness of mass transport simulations and identify structural conditions where the ECM performance is considered reliable or limited. Results show that the ECMs can reproduce analytical solutions when the hydraulic conductivity (K) of fracture zones is homogeneous over a 2 km cubic domain. Nevertheless, major deviations were observed with complex geometry and discretized features presenting heterogeneous K values within the same domain size. The results further suggest that simplified homogeneous ECMs can provide valuable insight into flow and non-reactive solute transport by advection-dispersion in a fractured bedrock aquifer undergoing depressurization caused by mine dewatering, for instance. Early findings regarding ECMs limitations suggest that models should be refined by improving the fracture representation, introduce potential stochastic formulation with monitoring data to ensure the reliability of GeoStudio to support mine dewatering interpretation and groundwater management decision-making.

TABLE OF CONTENTS

.

LIST OF TABLES

LIST OF FIGURES

LISTE OF SYMBOLS AND ABBREVIATIONS

BATEA	Best Available Technology Economically Achievable
CCME	Canadian Council of Ministers of the Environment
CTRAN/W	Contaminant Transport Modelling Software by GeoStudio 2D module
CTRAN3D	Contaminant Transport Modelling Software by GeoStudio 3D module
DCM/DPM	Dual Continuum Model/Dual Permeability Model
DFM	Discrete Fracture Matrix
DFN	Discrete Fracture Network
DTW	Depth to Water
EC	Electrical Conductivity
ECM	Equivalent Continuum Model
EFM	Equivalent Fracture Model
Eh	Redox Potential
EPM	Equivalent Porous Media
FEFLOW	Finite Element subsurface flow system
FRA	Fractured Rock Aquifer
FZ	Fracture Zone
GMS	Groundwater Modelling System
GMWL	Global Meteoric Water Line
GSI	Geological Strength Index
GW	Groundwater
GWQ	Groundwater quality
i	Hydraulic gradient
ICP-MS	Inductively Coupled Plasma Mass Spectrometry
K	Hydraulic Conductivity
K_f	Fracture Permeability
K_m	Matrix Permeability
LOM	Life-of-Mine
MCE	Milieu Continu Équivalent

MODFLOW	Modular Finite-Difference Groundwater Flow Model
MODPATH	Modular 3D Particle Tracking Post-Processing Model
MT3D-USGS	Modular Transport Model for Multi-Species Contaminant Transport
n	Porosity
NAPL	Non-aqueous phase liquid
PCOCs	Potential Constituents of Concern
REV	Representative Elementary Volume
RO	Reverse Osmosis
RQD	Rock Quality Designation
SEEP/W	Seepage Modelling software by GeoStudio 2D module
SEEP3D	Seepage Modelling software by GeoStudio 3D module
SRB	Sulfate-reducing Bacteria
TDS	Total Dissolved Solids

CHAPTER 1 INTRODUCTION

It is estimated that nearly 30% of the Canadian population relies on groundwater as a drinking water source (ECCC, 2017). This percentage even reaches 70% in the Abitibi-Témiscamingue Region (Cloutier et al., 2016). Regional aquifers used for drinking water supply are often influenced by industrial activities, particularly mining operations in the Canadian Shield, which have a significant impact on the local environment and hydrogeological conditions. Even if there has been previous work done in the past to better understand their impacts, it is still important for mining companies to continue refining their knowledge through hydrogeological studies supported by hydrogeological modelling (Labbé et al, 2024).

Hydrogeological modelling of fractured rock aquifer has significantly progressed over the years through the development of different applications and approaches (Chen et al., 2022). In fact, other than the mining industry, hydrogeological modelling of fractured rock has been conducted to better understand the impacts of nuclear waste, agricultural activities and shale gas development (Chesnaux et al., 2012; Praamsma, 2016; Hadgu et al., 2017; Peterson, 2017). Moreover, in the mining industry, modelling in fractured rocks is used not only for fate and transport, but also to assess rock mechanics and the effects of blasting in fractures (MacQuarrie & Mayer, 2005; Pine et al., 2006; Elmo & Stead, 2010). The scientific community has primarily adopted a range of conceptualizations for representing fractures in numerical modelling, including continuum and dual-continuum framework, equivalent porous medium (EPM) models and equivalent continuum models (ECM), channel network models and discrete fracture network (DFN) approaches (Chen et al., 2022). These methodologies have become the most widely accepted and applied due to their ability to capture the complex behaviour of fracture rock systems at varying scales. However, each approach has advantages and limitations, which complicates the widespread use of specific conceptual and numerical models. Scaling can have an impact on the results of the fracture representation chosen (Cacas et al., 1990). A larger scale can ignore heterogeneity and anisotropy using the ECM method since mine development induces damages which affect the effective hydraulic conductivity (Kleine et al., 1997). Representing precisely fracture geometry is challenging due to the irregular shape of fractures across the medium. However, a constructive way to capture preferential pathways in groundwater is to identify and discretizes the faults which are

easier to identify within a domain. A fault is a large fracture where movement has occurred along a break (Bense et al., 2013). In some cases, the evaluation of combined approaches, more specifically the ECM and DFN methods, have refined interpretation of fracture networks (Ma et al., 2023). Despite the numerical modelling advancement, there are still uncertainties tied to the socio-economic impact of mine dewatering and drainage (Sreekanth et al., 2020).

Precambrian crystalline aquifers are typically characterized by fracture networks where groundwater shows strong vertical variations in salinity and total dissolved solids (TDS), including brines at depth which is controlled by long-term interactions as observed in different mines in the Canadian Shield (refer to Fig. 1.1) (Frape et al., 1984; Bottomley et al., 1994). Studies at Con Mine demonstrate that mine inflows are often mixtures of three components: fresh meteoric water, ice sheet meltwater and deep brines, and studies have also shown that hydraulic gradients imposed by underground openings can induce meteoric water at depth in relative short time (Douglas et al., 2000). Chesnaux et al. (2012), used GeoStudio to show how natural or artificial hydraulic connections between a granular aquifer and an underlying fracture bedrock aquifer can significantly alter drawdown behaviour, transmissivity estimates, and hydrogeochemistry. Mine openings have been known to impact both the stress field and groundwater regime by creating large, depressurized zones (mine dewatering), modifying flow paths and enhancing hydrogeochemical processes (Rouleau et al., 2013). To characterize regional fractured bedrock aquifers, Gagné (2014) has developed a methodology to use structural mapping, pressure data and hydrogeochemical monitoring data from several mines in the Abitibi-Témismcamigue region. The data available helped to estimate equivalent hydraulic conductivities at a large scale which are typically used in ECMs. These types of models must still capture key boundary conditions and preferential flowpaths to provide realistic predictions of flow and dissolved non-reactive solute transport (Chesnaux et al., 2012).

The situation becomes even more complex in the case of models designed to simulate both groundwater flow and dissolved solute transport. Solute transport mechanisms are indeed challenging to capture and evaluate in numerical modelling fractured systems. DFN models can help capture the complexity of hydrogeochemical processes which can impact the decision making for plume mitigation (Molson et al., 2012). In parallel, ECMs can become practical because they allow representation of groundwater flow systems with a greater simplicity, although they may fail to capture the complexity of mass transport processes. In this context, the general objective of this

study is to compare the performance of homogeneous and heterogeneous ECMs across a range of sensitivity analyses that vary geometry, hydraulic properties, and advection–dispersion parameters. The sub-objective 1 is to assess the ability of homogeneous versus heterogeneous ECMs to reproduce groundwater flow patterns and non-reactive solute transport behaviour in fractured bedrock aquifers influenced by underground mine depressurization (i.e. dewatering). The sub-objective 2 is to evaluate the sensitivity of ECMs to variations in geometry, hydraulic conductivity, fracture-zone representation, porosity, and advection–dispersion parameters. The hypothesis is that if the dominant flow and solute transport is the geometry and connectivity of the main structures, then a homogeneous ECM can approximate the bulk behaviour of a heterogenous ECM. Conversely, when strong contrasts in properties. In the contrary, when strong spatial contrasts in properties create channeling or storage effects, the homogeneous ECM will diverge. The approach is specifically tested using SEEP3D and CTRAN3D components of the GeoStudio software. Another working hypothesis is that the flow and transport are led by the orientation of the faults and the preferential flows formed while having steady inflows and that mine dewatering can heavily impact the effective hydraulic conductivity. The focus is set on specific mining site located in the Canadian Shield, where models were developed using different software to simulate groundwater flow at different stages of the Life of Mine (LOM) cycle.

Figure 1.1: Locations of mines sampled as part of Bottomley et al., 1994 study in the Canadian Shield (shaded area)

The manuscript is divided into seven chapters, including this introduction. Chapter 2 presents a knowledge base of fractured systems and their limitations associated with numerical modelling. In Chapter 3, the regional geology and hydrogeological setting are discussed. Chapter 4 describes the methodology used to conceptualize the numerical model. Analysis and results of the groundwater flow and transport simulations are discussed in Chapter 5. The benefits, limitations and opportunities tied to the methods, analysis and interpretation used, are described in Chapter 6. The conclusion and recommendations are presented in Chapter 7.

CHAPTER 2 KNOWLEDGE BASE OF NUMERICAL MODELLING IN FRACTURE SYSTEMS

2.1 Physical characteristics applied in numerical modelling of fractured rock

One of the main challenges of modelling fracture systems is to have an accurate fracture representation of the study area. In fact, it is difficult to identify all the different structural geological deformations in the rock. This highly variable environment is referred to as heterogenous and anisotropic. A fracture network is a connection of fractures that can influence the fluid flow patterns and create preferential flow paths (Bear et al., 1993). Within a given rock matrix, the fracture networks often show considerably large permeability differences (Selroos et al., 2002). The fracture permeability must be considered along with the rock matrix permeability for the numerical modelling representation to adequately represent effective permeability. This permeability also depends on several factors, such as depth, hydraulic properties, discontinuities, and hydrogeochemical conditions (Gagné, 2014). The level of complexity in the representation of the fractures and rock matrix will depend on the defined objectives and on software and data limitation (Hadgu, et al., 2017). The advantages and disadvantages of each method and approach to represent the fracture network have to be evaluated. Some of the parameters that are critical to consider to better understand groundwater flow and solute transport are described in the following subsections.

2.1.1 Physical parameters in fracture network

The orientation, aperture, density, extension or continuity, degree of connectivity, degree of separation, rugosity, permeability and structural discontinuities can be considered in numerical modelling to represent fractures (Bernard, 1982). The groundwater flow conditions are localized to ease up the characterization of the fracture network and the random selection of test locations can lead to considerable differences in parameter estimates including permeability (Bernard, 1982). Here it is assumed that the permeability refers to intrinsic properties of uniform material. The effective permeability includes the combined effect of fractures and the rock matrix which induces the real flow. In numerical modelling, effective permeability tensors are derived using upscaling

and homogenization techniques (NRC, 1996). In addition to the complexity of the interpretation, it is difficult to determine the number and types of samples that are required per site (Hadgu et al., 2017). Generally, if more information is collected, it is more feasible to lean into a discrete method rather than an equivalent continuum method. Several different geological and environmental processes may contribute to the creation of fractures within a given domain that have distinct characteristics (Bear et al., 1993). These subsystems of fracture can be identified with regular, preferred, and/or random orientations, and with varying hydraulic conductivities and degrees of interconnectedness (Bear et al., 1993). These unique properties may be considered a distinct continuum that can be integrated into a model if there is an adequate representative elementary volume (REV). Logically, if the volume of the domain is not representative, there would be more variation in properties such as porosity and permeability, since they are sensitive to the fracture aperture. Hence, it is important to reflect the effects seen at a smaller scale. Fig. 2.1 illustrates the variation of porosity in a same domain of a point as a function of the size of the averaging volume; there is a minimum volume to obtain the REV (Bear and Bachmat, 1990). Primary porosity in a rock can be formed during the initial crystallization (Freeze & Cherry, 1979). Secondary porosity on the other hand, is related to the void space that are developed in a rock after the initial formation. While the secondary porosity increases the storage of the rock, it is the connectivity of these voids that primarily controls the permeability. In fact, the permeability is governed by the degree of fracture openness, interconnection, and spatial organization. In addition to fracturing, weathering and dissolution can increase the secondary porosity (Freeze & Cherry, 1979). The concept of dual porosity is also used in numerical models where the fluid flow occurs primarily through fractures, while the rock matrix serves as a storage domain. It accounts for the exchange of water or solutes between the fast-flowing fractures and the slower, diffusive matrix, providing a more realistic representation of a fracture media (Anderson et al., 2015). Unlike fractured aquifers, the fluid movement in porous rock (and granular aquifers), found in coastal regions, primarily depends on the interconnectedness of the pores instead of the fractures. The case of fractured bedrock aquifers is especially complex because even within a same fracture, there can be very different hydraulic properties depending on the intersection and openings between two fracture surfaces (Selroos et al., 2002). The solute migration in poorly fracture settings can take several million years in the rock shield (Al Yacoubi, 2021). The openings in fracture are potential channels that connect with other open section to form a continuum network (Bear et al., 1993). More specifically, the fracture

aperture is the width of the open space between fracture surfaces. It controls how much flow and how fast fluids can move through the fracture system. Fracture density refers to the number of fractures per unit volume or area, which impacts the permeability and storage capacity of the rock mass (Anderson et al., 2015). It is generally assumed that the hydraulic conductivity of the rock mass decreases with depth (Neretnieks, 1990) as shown in Fig 2.2.

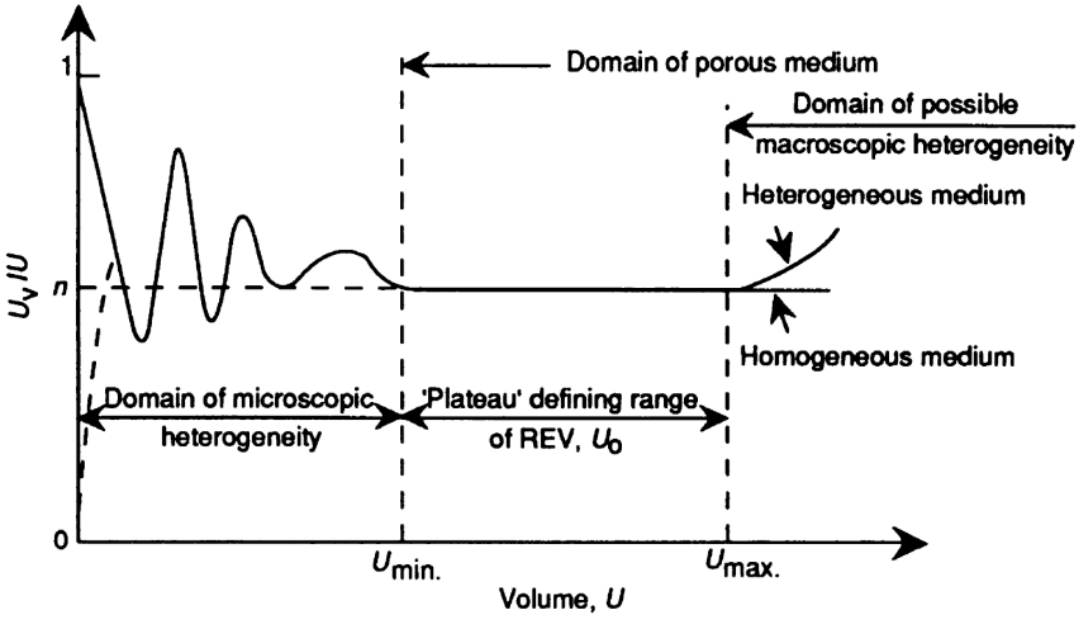

Figure 2.1: Variation of porosity in a same domain of a point as a function of the size of the averaging volume (Bear and Bachmat, 1990)

Fracture density is an important parameter. A higher density would potentially suggest more potential pathways for fluid flow. The scale of the fluid movement depends on the fracture extension also referred to as the length of the fracture. Longer fractures tend to increase the potential for connectivity and large-scale flow (Anderson et al., 2015). However, the efficiency of this connectivity depends on how many discontinuities is encountered within a fracture plane. The degree of separation is also tied to the connectivity. It refers to the spacing between adjacent fractures, measured as the perpendicular distance between two fracture planes (Selroos et al., 2002). The fluid flow also depends on the rugosity of the fracture, also referred to as the roughness of the fracture surfaces which increases the flow resistance. The extension or continuity is the measurable length of a fracture plane from one end to the other with no interruption; long fractures can act as major flow conduit, while short fractures might limit the flow or create a physical barrier

(NRC, 1996). Table 2.1 summarizes the physical parameters of fractures that are critical for numerical modelling mentioned above.

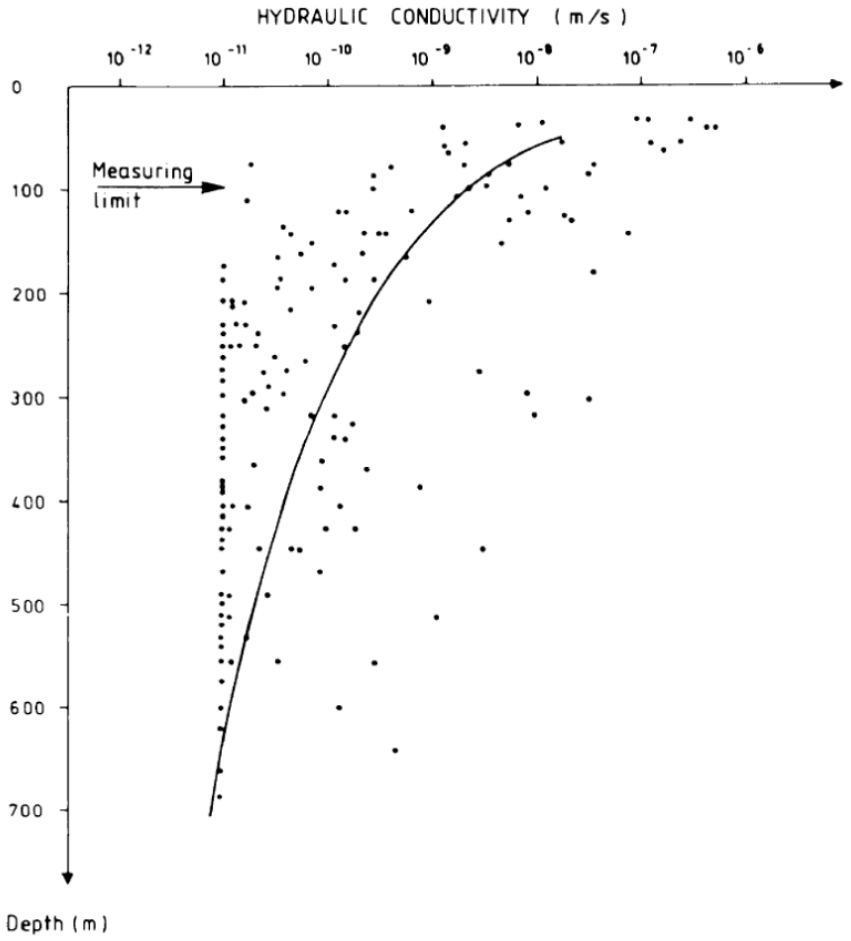

Figure 2.2: Hydraulic conductivity varying according to the depth (Neretnieks, 1990)

Table 2.1 Summary of physical parameters of fractures critical for numerical modelling.

Parameter	**Definition**	**Influence on flow**
Fracture density	Number of fractures per unit of area or volume	Control bulk permeability and storage
Fracture extension (continuity)	Length of individual fracture	Long fractures enhance regional flow and connectivity
Degree of connectivity	Degree of intersection between fractures forming a network	Highly connected network allow more fluid movement
Degree of separation	Distance between adjacent fractures	Closer spacing increases interaction and flow potential
Aperture	Width of the open space within a fracture	Directly controls flow
Rugosity	Surface irregularity of the fracture surface	High rugosity increases resistance, affects effective aperture
Fracture orientation	Strike and dip of fractures relative to stress and flow gradients	Influences anisotropy of flow and mechanical stability
Porosity	Proportion of void space within rock and or fracture network	Affects storage capacity and fluid saturation
Permeability	Ability of a medium to transmit a fluid	Determines how easily fluids can move through the fracture system

The more these parameters are used to describe the fractures in a medium, the more precision there can be in simulation results. However, the accuracy also depends on the method applicable to represent the fracture network in the area of study, a topic discussed in more detail in the following section.

2.1.2 Geometrical Representations of fractures

Fractures in numerical models are typically represented using two main approaches: the discrete fracture method and the equivalent continuum approach. Nonetheless, it is very complex to

represent a fracture field because of the anisotropy and heterogeneity caused by the structural geological deformations to consider (Bernard, 1982). A domain can be simplified by using an equivalent continuum approach, but it also depends on the modelling objectives and limitations (Anderson et al., 2015). The continuum approach treats a material as a continuous medium in which properties are defined at every point, smoothing out the discrete nature of individual particles and assuming homogeneity at the scale of interest (Bernard, 1982). In fact, if not enough data is available regarding the fracture zone characteristics, it is recommended to represent it as an equivalent continuum medium under homogeneous conditions (Selroos et al., 2002). The idea is to have simulation results that are relatively accurate considering the complexity of the study domain. The continuum medium for the rock matrix is generally represented with common geometrical domains such as sphere, a block or a slab (MacQuarrie & Mayer, 2005). Contrary to the discrete method approach, the ECM approach does not analyze individually each element. This implies a lot of hypotheses since there is a simplification at a large scale of the fracture network and this could ignore several aspects associated with the groundwater flow (Selroos et al., 2002). Therefore, the fracture network is represented by an equivalent porous medium (EPM) to simplify the numerical simulation and the applicability of the Darcy's Law related to fluid flow (Selroos et al., 2002). The ECM relies on REV within which fracture and matrix heterogeneity can be averaged into effective properties, such as the effective permeability (Selroos et al., 2002). Such simplification can make the model more efficient to simulate effects related to advection, diffusion, groundwater flow and mass transport. Selroos et al. (2002) and Hadgu et al. (2017), are examples of studies that compare both approaches. Hadgu et al. (2017) showed how the effective permeability and porosity of the mesh of each block is simplified with a permeability tensor which considers the opening, aperture and the distribution of the fracture in an ECM. In this context, each block mesh has a series of fractures with the same properties. The fracture zone is determined by analyzing the orientation and the structural grid. If the structural grid does not contain any fracture, the grid still has permeability and porosity, according to the rock matrix. The advection depends on the portion of the fracture in the structural grid and on the portion without fracture that happens across the porous volume led by matrix porosity. Depending on the simulation, the shape of the fractured zone can be chosen in order to better capture all fractures within the same model domain (Hadgu et al., 2017). Simulation results of groundwater flow and mass transport using the ECM approach can potentially be similar to a discrete fracture network (DFN) approach as long as

effective mesh properties are integrated in the model, or even by increasing the study scale (Hadgu et al., 2017). The connectivity effects and the diffusion matrix are key parameters that could make one approach more feasible adequate than the other. Sensitivity analysis can also be conducted to assess the influence of material properties, geometry, and boundary conditions on model results.

The fracture network could also be represented with the double ECM or also referred to as dual continuum model (DCM). To be more specific, the DCM is a continuum medium for the matrix and a continuum medium for the fractures. MacQuarrie & Mayer (2005) suggest using this approach in systems where fractures control the flow and mass transport and where the rock matrix provides significant storage and reactive surface area. Not only does the DCM approach help to simplify the domain, but it also treats two media independently. Fig 2.3 illustrates the conceptualization of this approach. However, the main disadvantage, like in an ECM, is the lack of representation of discrete fractures or fracture zones in some environments. Assumptions pertaining to fracture density and extension can further move the simulation away from real conditions. In addition, simulations can become oversimplified when hydraulic properties of fractures are considered homogeneous in time and space. There could also be a large variation of results depending on the scale of the study domain. Despite such limitations DCMs allow the consideration of fracture-matrix interaction.

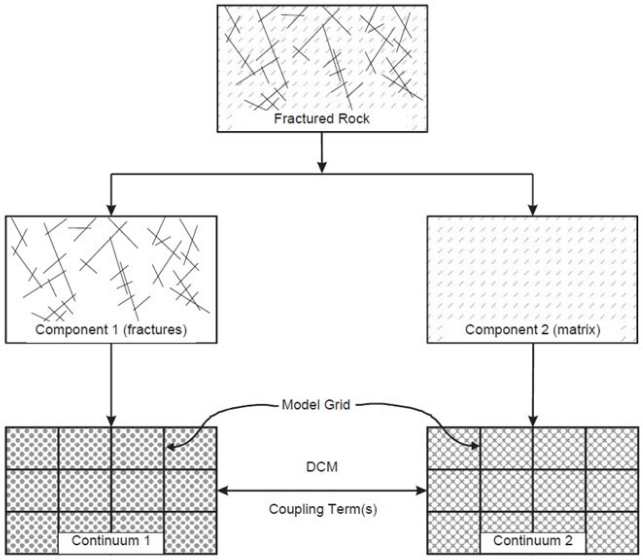

Figure 2.3: Conceptualization of DCM from MacQuarrie & Mayer (2005)

Contrary to the ECM and DCM, the DFN approach considers each fracture in the rock matrix and treats it individually. The discretization of each fracture requires access to sufficient hydraulic data and geometric information. The DFN approach represents the geometry and connectivity of fractures in the domain with greater details than the ECM. This can help better understand the mass transport, the flow and the geotechnical behaviour of the fracture rock system (Anderson et al., 2015). The DFN is often recommended when it is important to understand the fate and transport of solutes in the groundwater system (Hadgu et al., 2017). It can help consider the heterogeneity and anisotropy of the environment and allow the evaluation of the fracture-matrix chemical exchanges. This is important to adequately represent the migration of a contaminant plume and avoid misleading operational and closure forecasts (Molson et al., 2012). Fig. 2.4 illustrates an example of a DFN representation using dfnWorks (Hadgu et al., 2017). The fracture network needs to be well identified in the domain, and its physical properties need to be characterized. The mass transport in groundwater is often influenced by diffusion and sorption. This requires the model to include diffusion and sorption matrices (Hadgu et al., 2017). In fact, one of the main disadvantages using the DFN approach can happen during the simulation of the reactive transport since there are several complex geochemical reactions to consider. For example, the alteration of an adjacent matrix to the fracture surface can be limited by the small zone subjected to molecular diffusion and kinetic reactions (MacQuarrie & Mayer, 2005). Local geometry and tests can limit the scale chosen (Cacas et al., 1990). At a larger scale, there is a lot of data to process to execute the simulation, it can become challenging. This can present significant challenges, particularly regarding data processing, computing performance and the time required for simulations. Furthermore, it can be complex to represent each fracture in an explicit format in the model mesh (Hadgu et al., 2017). It is important to note that fluid flow in the fracture rock is led by advection which also leads to displacements over long distances. It becomes complicated to englobe all the chain of reactions while preserving a same scale without adding more cells to the model (Selroos et al., 2002). Despite the challenges encountered, if properly recreated, the DFN method can help understanding mass transport in fractured bedrock aquifers. For example, Kleine et al. (1997) proposed a DFN representation to predict the likelihood gas pathways as a mine get progressively blasted. Indeed, the DFN approach is recommended when the objective is to reproduce anisotropic permeability and complex transport behaviour, such as channelling, and localized contaminant migration, which are often missed in continuum models. Modelling DFN helps to improve the problem definition

and operational decision (Kleine et al., 1997). Furthermore, this approach has been shown to be relevant to use to better understand rock mechanics and fracture propagation as part of failure modes assessments (MacQuarrie & Mayer, 2005; Pine et al., 2006; Elmo & Stead, 2010).

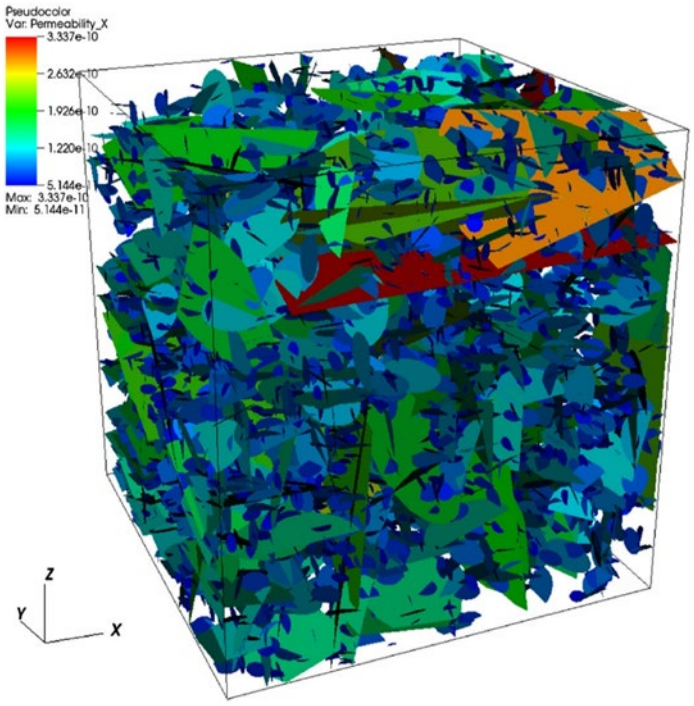

Figure 2.4: Discrete fracture network represented in dfnWorks, the permeability variation is shown. (Hadgu et al., 2017)

Similarly to the DCM, where the fracture continuum medium and rock matrix continuum medium are combined in a model, a DFN can be combined with a surrounding rock matrix continuum. The contrary can also be applied in modelling where a surrounding fracture continuum medium can be combined with a discrete element of the surrounding rock matrix. This approach is referred to as a hybrid and depends on the data available to characterize the domain (Wu et al., 2017). In some cases, this approach can be a more accurate way to represent geological formations, including the

fracture network and the rock matrix in the domain; it can help to better understand the preferential flow and mass transport in the fracture network even at a smaller scale (Wu et al., 2017). The hybrid approach is also recommended to better understand the geotechnical behaviour in fractured rock, especially in context when there is known or expected deformations and fracture propagation (Jing & Stephansson, 2007). In fact, a model that uses a similar approach helps to better understand rock mechanics of the surrounding by simulating the distribution of tension, deformation and the interaction between the fractures and rock matrix (Wu et al., 2017). It is important to note that while the hydraulic properties are critical for the flow modelling, the mechanical behaviour of the rock mass also plays a key role. The Hoek-Brown failure criterion, combined with the Geological Strength Index (GSI), offers a practical approach to estimate the reduced strength of fracture rock systems (Hoek et al., 2002). The mechanical stress redistribution and around the mine opening can induce new fractures or dilate existing ones, enhancing permeability in the immediate vicinity of the excavation (Zhou et al., 2023). The main advantage of using the hybrid approach is the fact that it can consider complex geometries in the domain and it can catch most of the effects between the fracture and the rock matrix. Similarly to DFN, it can make the simulation complicated and can take more time to process; there is a lot of data that needs to be processed (Mayer & MacQuarrie, 2007). In a hybrid method, using a discrete representation for fractures often requires some assumptions regarding the surrounding matrix properties. Conversely, when fractures are treated as part of a continuum, more assumptions are typically made about the fracture network, while the matrix is more explicitly characterized. As with any modelling approach, it is challenging to explicitly represent fractures with all their geometrical irregular and complex forms while still working at as consistent resolution in the numerical model. Alternatively, another method considered hybrid is the discrete fracture matrix (DFM). It uses fractures that are discretized with their features while also explicitly modelling the surrounding porous matrix. This allows the simulation to provide detailed fluid interactions between fractures and the matrix. The DFM approach is suggested when the media is moderately fractured and where the fracture locations are known. As Berre et al. (2019) highlight, the DFM approach offers a good compromise between the geometric accuracy of DFN and the computational efficiency of continuum models, particularly in hybrid or multi-scale modeling contexts as shown in Fig 2.5.

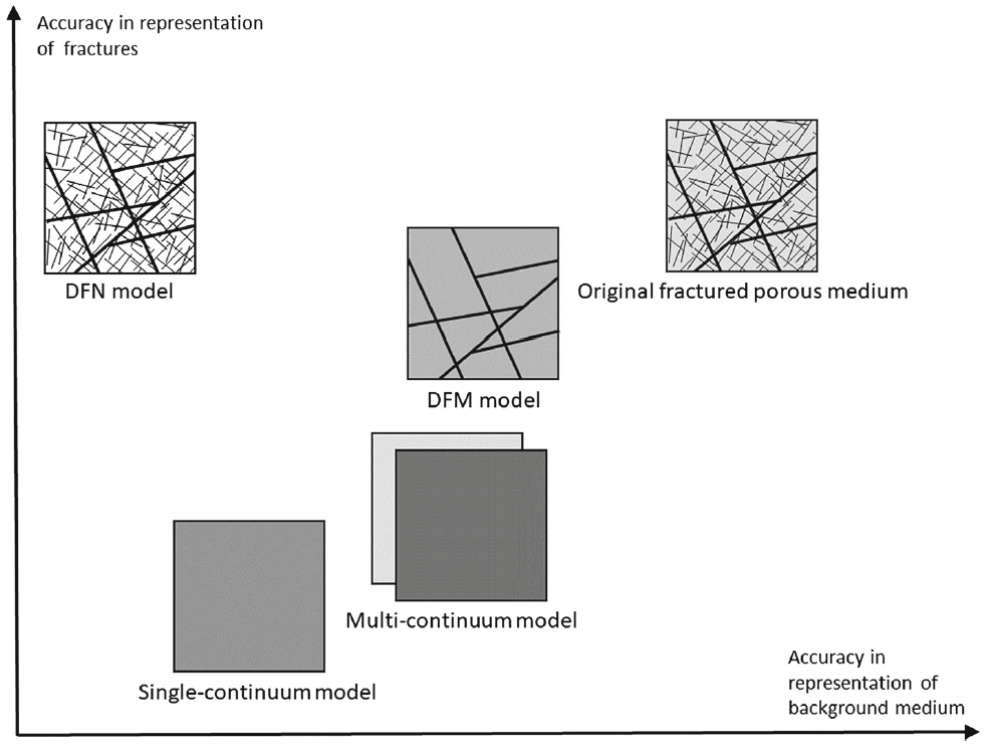

Figure 2.5: Conceptual models of a fractured porous medium. The DFM approach represents all fractures of the original medium, and the placement is very similar to the original medium in the illustration (Berre et al., 2019)

Other approaches can be used to represent a fractured domain, including the channel network method. This approach simplifies the discretization concept by representing fractures into one system where fractures are interconnected. If the fracture network is well identified, the channels formed can represent the preferential flow in the domain. It is similar to an ECM, since this approach is suggested for studies performed at a larger scale or where a REV is applicable (Ma et al., 2023). The channel network method helps to better understand the groundwater flow behaviour across a large region. This region can include several interactions with one or several aquifers in the surroundings. The main disadvantage of the channel network method is that it does not represent accurately the fracture properties. The stochastic method incorporates random spatial distribution and properties of fractures or hydraulic properties. This is particularly useful when the spatial variation in properties are not well-known. Statistical physical parameters can help to generate multiple realizations of the system. The stochastic method allows uncertainty

quantification and is preferably used for risk assessment (Neuman, 2005). The main disadvantage of this method is that it requires extensive statistical data that might move the model away from the real-world settings. Alternatively, studies including Billaux et al. (1989) or Pruess et al. (1999) that discusses methods to generate fracture networks in numerical modelling by using computer simulation since they cannot be well-constrained from field observations as shown in Fig 2.6.

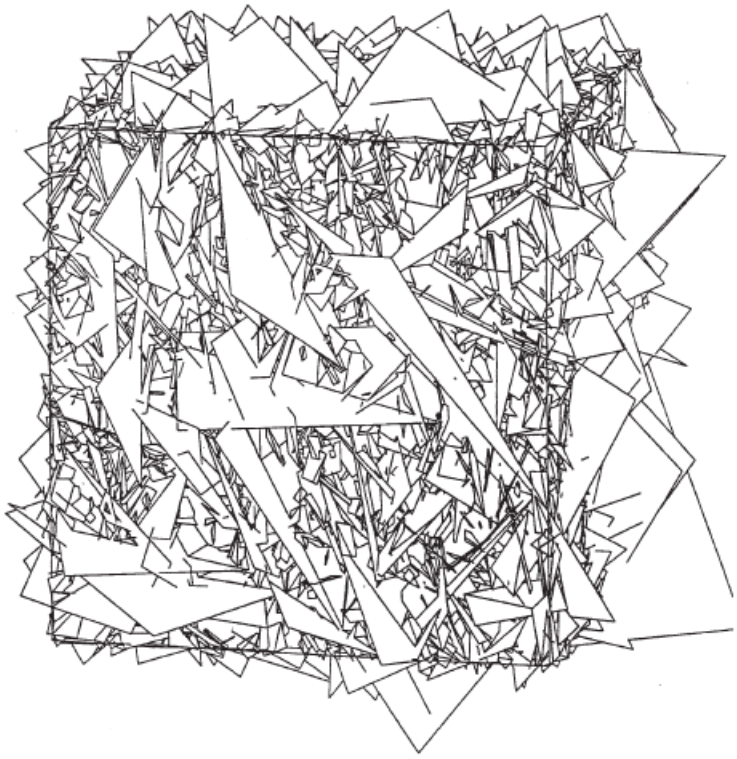

Figure 2.6: Computer-generated fractures of a 12.5 m sided cube of fractured rock (Pruess et al., 1999)

2.2 Hydraulic Behaviour and Flow Mechanism

As explained in section 2.1, physical parameters such as the aperture, orientation and connectivity of fractures, directly influence the way fluids move through fractured rock systems. Understanding the hydraulic behaviour of fractured media is essential for accurately simulating groundwater flow,

mass transport, and even resource extraction of the respective environment (Bear et al., 1993). Even if a rock wall seems impermeable, fracture can form pathways for the migration of contaminants that are emplaced in or released to the subsurface environment (NRC, 1996). An extensive summary of the different engineering applications and context where fractures represent a significant component to consider is provided by NRC (1996). Fortunately, numerical modelling is a tool used to better understand and predict transport of reactive and non-reactive solute. This section outlines the dominant flow mechanisms in fracture rock which includes flow through single fractures, fracture networks, and fracture-matrix interactions. It also describes how they are conceptualized and implemented in numerical models.

2.2.1 Flow in fractured rock

Fractures represent concentrations of void spaces in rock (NRC, 1996). Whether through their statistical and physical properties or by explicitly representing only the major fractures, depending on the site conditions and objectives, in numerical modelling, it is important to characterize fracture patterns (NRC, 1996). To have a representative scale, it must include enough fractures and all the physical characteristics that are applicable. In a larger scale, the flow is usually assumed to take place in a pseudo-homogeneous porous medium (Bear et al., 1993). In fact, Darcy's Law is not always applicable in fractured rock (Selroos et al., 2002). As described in Bear et al. (1993), flow in an individual fracture is often conceptualized by idealizing the fracture as two smooth, parallel plates and applying the cubic law to estimate transmissivity. This idealization provides a useful first-order approximation, but it does not fully reflect the complexity of real fractures. Fracture surfaces display physical properties that cause deviations from laminar, parallel-plate flow. Moreover, the cubic law does not account for fluid exchange with the surrounding rock matrix or for variations in fracture connectivity that influence the actual flow pathways. As mentioned, fracture media are anisotropic and heterogeneous, paths change as the direction of the gradient changes (Bear et al., 1993). The observed preferential pathways can be explained by natural processes or by human activities. In addition to these causes, geochemical process including changes in fluid chemistry can entail mineral precipitation or dissolution on the fracture walls (Frape et al., 1984). In fact, any change in the void geometry of a fracture system will alter the flow and transport behaviour (NRC, 1996). More specifically to this study, in addition to the mine

openings and any potential leaching, mine dewatering is influenced by fracture flow. Indeed, it is important to determine the hydraulically significant fractures which form a fracture network. The flow and transport in fractured rock can be directly quantified with pressure and tracer tests done in the laboratory or *in situ* (Neuman, 2005). Assuming that the flow is laminar in a fracture, that the aperture is constant within a planar axis surface and that the diffusion is solely the only transport mechanism within the porous blocks surrounding the fractures, simplifies numerical modelling (Bear et al., 1993). The use of the effective aperture can be used to evaluate the flow. The equation mostly used when assuming the flow in a fracture, governed by the cubic law, is the following:

$$Q = \frac{b^3}{12\mu}\nabla P, \tag{2.1}$$

Where Q is the volumetric flow rate per unit width, b is the aperture or the distance between the plates, P represents the pressure, in this case the pressure gradient and μ is the dynamic viscosity. This equation has mostly been used to model macroscopic fracture flow, but it has also recently been applied to a microscopic level (NRC, 1996).

The hydraulic conductivity (K_{fr}) and the permeability (k_{fr}) equations can be interchanged. In a fracture, they are defined respectively and as follows:

$$K_{fr} = \frac{\rho g}{\mu}\frac{b^2}{12} \tag{2.2}$$

$$k_{fr} = \frac{b^2}{12} \tag{2.3}$$

It is important to note that fracture orientation and connectivity create directional variations in the flow through a fractured rock domain. The hydraulic conductivity is often much higher in the dominant fracture (Bear et al., 1993). The notion of anisotropic hydraulic conductivity can be considered. However, this also includes assumptions due to the complexity of choosing a REV and

the irregularity of all the fracture physical properties. In fact, the observed anisotropy can vary with the chosen scale. It is recommended to start with steady state flow when conceptualizing a numerical model (NRC, 1996).

Not only is the transmissivity important to consider but also the specific storage (S_S). The general equation can be defined as follow:

$$S_s = \rho g(\beta_w + \beta_f) \tag{2.4}$$

Where β_w is the compressibility of water (negligible) and β_f is the compressibility of fracture.

To calibrate the model, these parameters can be evaluated with hydraulic testing through multiple boreholes (NRC, 1996). It also helps to better understand the network connectivity and permeability in the domain which is discussed in the next subsection.

2.2.2 Permeability and Network Connectivity

The permeability in fractured rock is primarily governed by the physical properties of the fracture and not the matrix porosity (NRC, 1996). In numerical modelling, these physical properties are scale dependent. In other words, the REV is critical for the proper simulation of the domain. Anisotropy is not always well represented. In fact, the cubic law doesn't directly consider it. Eq. 2.3 does assume uniform fracture physical properties. To potentially exhibit some anisotropy in transient flow, the tensor-based Darcy's law for anisotropic media can be used. Directional permeability tensors are used to model fractures orientation, spacing and connectivity (Anderson et al., 2015). To better understand this concept it is relevant to review the notion of flux through a REV. Anderson et al. (2015) describe the concept of a REV with a volume expressed with **ΔxΔyΔz** as shown in Fig 2.7 As noticed in the diagram, the flux direction through a REV is a vector that can be divided in three components. The flow rate is equal to the change in storage capacity (S_s) which deviated from eq. 2.4. and goes as follow:

$$S_s \frac{\partial h}{\partial t} = \left(\frac{\partial q_x}{\partial x} + \frac{\partial q_y}{\partial y} + \frac{\partial q_z}{\partial z} - W \right) \Delta x \Delta y \Delta z \tag{2.5}$$

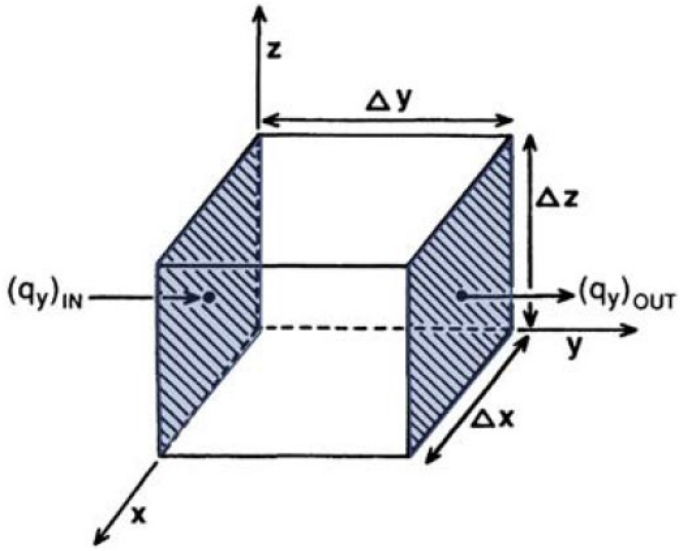

Figure 2.7: An example diagram of a REV (ΔxΔyΔz) showing the components of flow along the y-axis (Anderson et al., 2015)

Where *W* represents the volumetric inflow rate from a source/sink of water. In fact, the expanded form and components of the specific discharge vector, *q* are the following:

$$\begin{aligned} q_x &= -K_{xx} \frac{\partial h}{\partial x} - K_{xy} \frac{\partial h}{\partial y} - K_{xz} \frac{\partial h}{\partial z} \\ q_y &= -K_{yx} \frac{\partial h}{\partial x} - K_{yy} \frac{\partial h}{\partial y} - K_{yz} \frac{\partial h}{\partial z} \\ q_z &= -K_{zx} \frac{\partial h}{\partial x} - K_{zy} \frac{\partial h}{\partial y} - K_{zz} \frac{\partial h}{\partial z} \end{aligned} \tag{2.6}$$

Where K_x, K_y, K_z are the principal components of the hydraulic conductivity tensor and $\frac{\partial h}{\partial x}, \frac{\partial h}{\partial y}$ *and* $\frac{\partial h}{\partial z}$ are components of the vector gradient, the gradient of head in 3D transient flow. 2D transient flow is possible with a two-dimensional coordinate system. If equations 2.5 and 2.6 are combined to represent the flux, it can be summarized with eq. 2.7.

$$S_s \frac{\partial h}{\partial t} - W = \frac{\partial}{\partial x}\left(K_{xx}\frac{\partial h}{\partial x} + K_{xy}\frac{\partial h}{\partial y} + K_{xz}\frac{\partial h}{\partial z}\right) + \frac{\partial}{\partial y}\left(K_{yx}\frac{\partial h}{\partial x} + K_{yy}\frac{\partial h}{\partial y} + K_{yz}\frac{\partial h}{\partial z}\right) + \frac{\partial}{\partial z}\left(K_{zx}\frac{\partial h}{\partial x} + K_{zy}\frac{\partial h}{\partial y} + K_{zz}\frac{\partial h}{\partial z}\right) \quad (2.7)$$

FEFLOW and SUTRA have this capability (Anderson et al., 2015). Nevertheless, these models can properly represent flows that are dominated by the fracture network connectivity. However, the connectivity of fractures through a domain is also a function of its size (Bear et al., 1993). In fracture networks dominated by short, isolated or unfavourably oriented fractures, hydraulic properties can be limited because these features do not form continuous or intersecting flow paths. The threshold percolation is a key concept to assess whether a fracture medium can support bulk flow or remain hydraulically disconnected (Bear et al., 1993). If the percolation is below the threshold, this would mean that the fracture is not well connected and are possibly isolated. In the case of a percolation above this threshold, or when a critical value is crossed, the fracture medium can enable significant permeability and percolation happens. The threshold is the case depend. It can be estimated with numerical modelling and analytical methods by simulating the fracture network and identifying the fracture density and observing when there is a continuous pathway formed across the domain (NRC, 1996). A group of fractures or a region in a fracture network with high connectivity is also referred to as a connected fracture domain. If the fracture density is low, fractures can be found as disconnected clusters. This can also potentially trap contaminants and reduce the bulk permeability. Another indicator of connectivity can be the fracture trace length, also referred to as a footprint: a line or shape where a 3D fracture intersects with a 2D surface (NRC, 1996). There is a correlation with longer or more connected trace length and greater flow potential in a domain. Certainly, the complexity of flow and storage in fractured media cannot be fully captured with the evaluation of all the fracture physical properties. To better understand and represent the combined behaviour of fractures and the surrounding rock matrix, conceptual models such as dual porosity/permeability approaches discussed in the following sub-section.

2.2.3 Dual Porosity/Permeability Concepts

The dual porosity and permeability concepts were briefly introduced in sub-section 2.1.1. Both concepts are used in modelling to approximate field conditions; they are based on two continua models for the fracture and matrix of the domain. In fact, one way to simulate with advection and Fickian dispersion equations are to include a term to describe the exchange of solute between the fractures and the surrounding porous matrix while using the dual porosity approach (Anderson et al., 2015). More specifically, there is an option to use this approach in MODFLOW (i.e. MT3DMS) and FEFLOW while simulating mass transport in highly conductive preferential flow paths (Anderson et al., 2015). The dual-permeability approach allows flow to occur both within the rock matrix and within the fracture network, as well as between them. Because both continua are hydraulically active, dual-permeability models generally require greater computational effort than dual-porosity models (Bear et al., 1993). In dual-permeability formulations, the two media can transmit flow at different rates, with fractures typically dominating. In contrast, the dual-porosity approach assumes that the surrounding matrix contributes negligible advective flow compared to fractures and primarily serves as a storage domain that exchanges fluid and solute with the fractures through diffusion. The transfer of fluids or solutes between these two overlapping continua is linearly proportional to the pressure (or concentration) differential between them at each point in space and time (Neuman, 2005). Besides, the dual-porosity model can be considered of a special case of dual-permeability model if the flow in the rock matrix is ignored and is used for storage allowing fluid exchanges with the fracture network with diffusive mechanisms (Bear et al., 1993). The geometry of the fracture network is simplified to the point of representing a small portion of the domain. The application of both approaches has found success in field scale for waste-disposal storage, petroleum reservoirs or extraction resources in fractured rock, or fractured rock aquifers (Berkowitz, 2002). In the context of mine openings, both concepts are particularly relevant. In fact, excavation such as drifts, shafts and stopes disrupt the pre-existing fracture network, leading to localized changes in permeability, fracture connectivity and storage properties (Zhou et al., 2023). Mine openings can complexify the flow regime where fractures act as dominant conduits for rapid groundwater movement while the surrounding matrix continues to contribute to storage but only minimally to flow (Chen et al., 2022). Due to the complex interaction between the fracture network and rock matrix, single-porosity models sometimes fail to adequately capture both storage and flow dynamics. The concepts of dual porosity/permeability provide a structured framework to

model these processes with separate continua but linked by fracture-matrix exchange terms. This justifies treating these processes in a more detailed way in numerical modelling (Berkowitz, 2002). While these concepts can significantly improve the representation of flow and mass transport in fracture environments, additional complexities arise when considering solute and contaminant migration at depth. In particular, fractured rock aquifers exhibit unique challenges for predicting the movement of dissolved species which is of critical importance in mining operations, waste management, and environmental protection (NRC, 1996; Neuman, 2005). These aspects are discussed in the following section.

2.3 Hydrogeochemical mining overview

The flow and mass transport of groundwater contaminants are governed by the hydraulic gradient, the hydraulic properties (mainly hydraulic conductivity and porosity) of subsurface material and the geological characteristics of the area. In the Canadian Shield, high salinity in fractured rock aquifers can be attributed to multiple sources including marine intrusions, ancient brines resulting from prolonged water-rock interactions, and sometimes human activities (Walter et al., 2017). In the absence of surface contamination, shallow aquifers generally present lower salinity concentration compared to deeper aquifers. This can be explained by the geochemical evolution of groundwater, which is more pronounced in deep regional groundwater flow systems than in local and intermediate systems (Tóth, 1999). This is reflected particularly in the chemical composition of groundwater, which trends to shift from an anionic facies dominated by bicarbonate to facies dominated by sulfates and ultimately chlorides in flow systems with increasing distance and percolation time. Stable and radiogenic isotopes also provide valuable tools for tracing groundwater sources, recharge mechanisms, and flow paths (Douglas et al., 2000). For the purpose of this study, it is important to first review some major ion indicators for impacted groundwater in fracture bedrock. This is followed by the presentation of solute transport mechanisms in fracture, the influence of fracture networks characteristics and modelling approaches for solute transport.

2.3.1 Operational Indicators of Salinity

In underground mines developed in the Canadian Shield, saline groundwater and water affected by brines may be encountered at depth. From an operational perspective, salinity is typically evaluated using integrated indicators that can be measured. The most common indicators are TDS and water electrical conductivity (EC), which reflect the overall abundance of dissolved ions in water rather than the presence of a single contaminant (van Dam et al., 2014). The EC is often used as a rapid screening tool because it responds to the ionic strength of water. While TDS provides a mass-based measure that supports comparisons among mine levels and through time. These indicators are essential in the underground mine water context where source concentrations may vary with depth and where mine development and dewatering can modify hydraulic gradient and mixing conditions. Neither parameter is used to identify the origin of the salinity. However, they help to provide a practical basis to classify mine waters, track changes during mine development, and flag the potential for operational issues such as corrosion and scaling associated with high dissolved-ion loads. In the Canadian Shield, saline waters commonly contain major ions such as Ca, Na, Mg, Cl, SO_4, along with minor constituents such as B, Br and Sr (Bottomley et al., 1994). These ions collectively contribute to TDS and therefore control EC. For interpretation beyond screening, the relative proportions of major ions can be used to support salinity sources and geochemical evolution, which is addressed in the following sections (Frape et al., 1984; Bottomley et al., 1994; van Dam et al., 2014)

2.3.2 Major Ions as Process Indicators

Bicarbonate (HCO_3^-) and sulfate (SO_4^{2-}) often contribute to TDS in mine waters, but they are especially useful as process indicators because their concentrations reflect water-rock interaction and redox conditions rather than conservative mixing alone. As previously mentioned, in fractured settings, changes in hydraulic gradients caused by mine dewatering and development can modify flow paths and promote mixing between shallow and deep waters, which can in turn influence the distribution of these species (Frape et al., 2014). HCO_3^- is often the dominant alkalinity species around typical groundwater pH. It is closely linked to the carbonate system and is commonly generated by the dissolution of CO_2 followed by carbonate equilibria in soils and groundwater as shown below in Eq. 2.8. (Frape et al., 2014). As a result, shallow groundwater can be mildly acidic

due to soil CO_2, while deeper waters may show different HCO_3^- trends depending on the geochemical conditions and mineral controls (Frape et al., 2014). From an operational perspective, HCO_3^- is primarily relevant because it controls alkalinity and buffering capacity and together with Ca^+ and Mg^+ it can contribute to scaling/precipitation risks and overall water-treatment requirements. In some settings, elevated HCO_3^- has also been associated with biological or thermogenic CO_2/CH_4 processes, but these mechanisms are site-based and are discussed here mainly to support the interpretation rather than detailed prediction as shown in Fig 2.8 (Taulis et al., 2007).

$$CO_{2\,(g)} + H_2O \rightleftharpoons H_2CO_{3\,(aq)} \rightleftharpoons HCO^-_{3\,(aq)} + H^+ \tag{2.8}$$

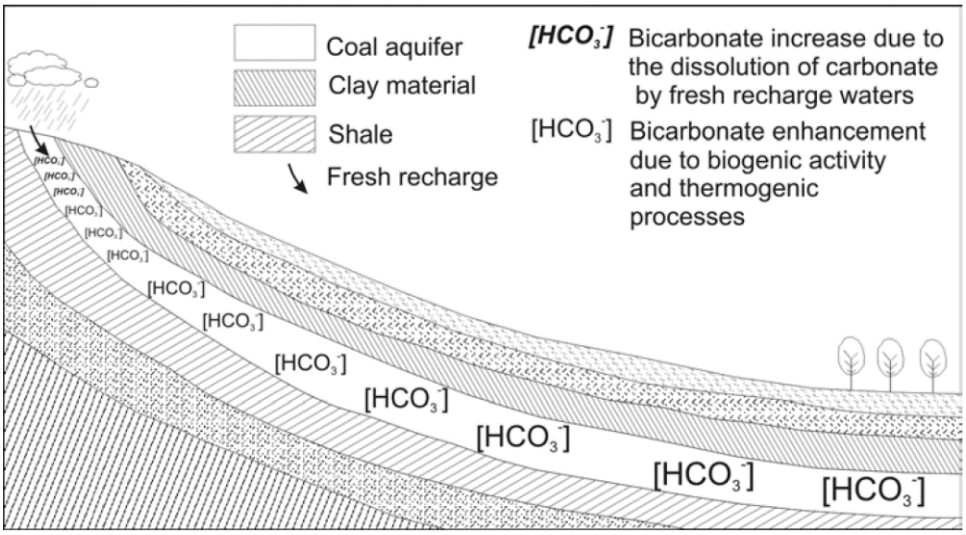

Figure 2.8: Bicarbonate concentration increasing in an aquifer with carbonate presence (Taulis et al., 2007)

Sulfate (SO_4^{2-}) is commonly observed in crystalline-rock groundwaters and may increase with depth in some Canadian Shield settings as observed in Fig. 2.9 (Frape et al., 2014). Potential sources include mixing with saline and by-products, dissolution of sulfate-bearing minerals (where present) and oxidation of sulfide minerals when oxygenated recharge penetrates deeper along

preferential pathways (Bowell et al., 2004; Frape et al., 2014). In the mining context, sulfide oxidation can be particularly relevant where mine development enhances access of oxygenated water to reactive zones as shown in Fig 2.9. Conversely, sulfate can be reduced under sufficiently reducing conditions, although SO_4^{2-} reduction may be limited in some shallow saline groundwater (Bowell et al., 2004). Beyond its contribution to TDS, sulfate can be relevant for water management because its toxicity responses are often hardness-dependent and can vary by jurisdiction (Taulis et al., 2007). Overall SO_4^{2-} and HCO_3^- provide complementary information to conservative tracers such as Cl^-. They help interpret the processes controlling mine water quality and support decisions around monitoring and treatment selection.

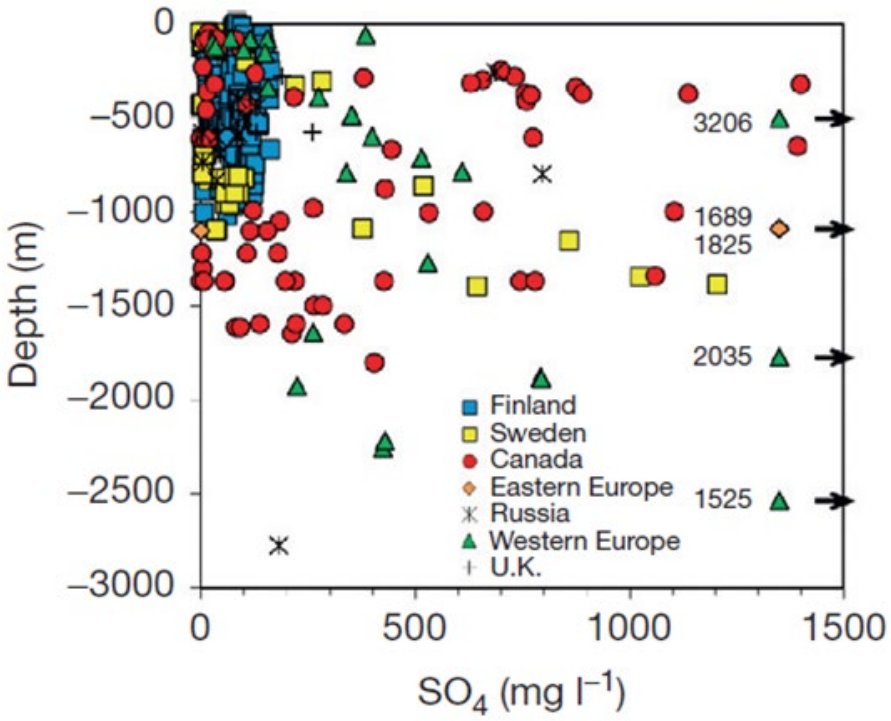

Figure 2.9: Sulfate concentration varying according to the depth across different world regions – in red, the Canadian Shield (Frape et al., 2014)

2.3.3 Mine-relevant Water Quality Parameters

Beyond the major-ion context discussed in this study, underground mine water quality is commonly screened using a relatively small set of operational parameters directly impact handling, treatment and compliance (INAP, 2021). pH and redox indicators (e.g. dissolved oxygen and/or Eh when available) provide first-order context for whether conditions may allow metal mobility or the formation of precipitates and sludge, which can strongly influence treatment performance. A key practical issue, specifically considering that underground water is pumped and discharged on the surface, is turbidity and total suspended solids (TSS). Turbidity (optical response) and TSS (a mass concentration) can increase due to fine particles generated or mobilized by blasting and drilling fines, wall-rock degradation, resuspension of settled solids in sumps and drifts, and precipitated solids (INAP, 2021). These suspended materials drive clarification/filtration needs and can cause operational problems such as ponds/pipe sedimentation, increased sludge production, and fouling of downstream processes (Pouw et al., 2014). This is why solids control is typically treated as a core element of mine water management.

2.3.4 Major Ions Used to Identify Sourcing and Mixing

Chloride (Cl^-) and sodium (Na^+) are widely used as practical indicators of salinity and mixing because they are commonly abundant in saline waters and can be measured reliably. In shallow fractured settings, elevated Cl^- and Na^+ can reflect surface inputs or other anthropogenic sources, whereas higher concentration at depth is common in parts of the Canadian Shield where saline end-members and brines occur (Al Yacoubi, 2021). In the mining context, dewatering and development can modify hydraulic gradients and preferential pathways, which may increase the likelihood of intercepting saline waters along conductive structures. From an interpretation standpoint, Cl^- is generally treated as a conservative tracer (highly soluble and typically not strongly retarded), making it particularly useful to track salinity trends and mixing, while Na^+ can be influenced by cation-exchange reactions in some settings. Therefore, Cl^- is often preferred for mass balance or mixing interpretations and Na^+ is used a complementary saline indicator. Elevated Cl^- and Na^+ waters are also operationally relevant because they can increase corrosion potential. Fig. 2.10 illustrates how Cl^- varies with depth in different areas of the Canadian Shield. Elevated deep chloride can reflect mixing with brines (>1,000 m depth) that migrate upward into pumping zones under induced upward vertical gradients (Al Yacoubi, 2021). When comparisons to the receiving

environment are needed, the Canadian aquatic-life guidelines for chloride provide useful context: chronic (long-term) ~120 mg/L from acute (short-term) ~640 mg/L benchmarks. In lakes, rivers, and wetlands, elevated Cl^- can be toxic to invertebrates and amphibians, can enhance mobilization of toxic metals such as arsenic, and can reduce vegetation biodiversity (Kelly et al., 2010). Cl^- is only weakly adsorbed by clays and generally behaves conservatively in groundwater; owing to its high solubility, it remains dissolved and is transported widely within the hydrologic cycle (Al Yacoubi, 2021). One recommended treatment for high Cl^- and Na^+ is membrane separation, such as reverse osmosis (Pouw et al., 2014).

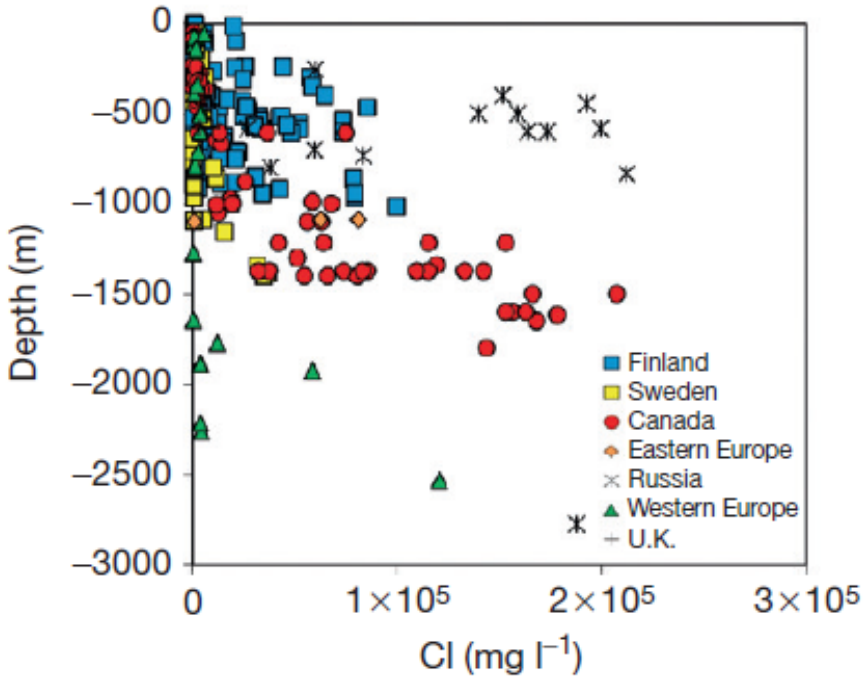

Figure 2.10: Chloride concentration varying according to the depth across different world regions – in red, the Canadian Shield (Frape et al., 2014)

2.3.5 Determination of Groundwater Origin with Isotopic and Geochemical Tracers

Groundwater that flows to greater depths traverses different hydrogeochemical facies and progressively alters its composition. Multiple tracers can therefore be used to determine groundwater origin (Bottomley et al., 1994). Tracers include physical methods (e.g., dye tests or temperature anomalies), but for this study the emphasis should be on geochemical and isotopic tracers that best address the key studied components:

- The origin of the groundwater supplying high-salinity inflows, and
- the parameters that control hydrogeochemical interactions and inter-aquifer mixing near mine openings.

At first glance, groundwater chemistry reflects interaction with the surrounding mineralogy; however, heterogeneous fracture networks can disrupt simple lithology–chemistry associations. An adequate sample set is therefore critical for robust interpretation. Water could be classified as follows:

- meteoric/recent recharge
- local versus regional groundwater and surface water
- deep/brine water
- seawater.

Useful isotopic systems include the stable isotopes of water ($\delta^{18}O$, $\delta^{2}H$) together with tritium (^{3}H), the strontium ratio $^{87}Sr/^{86}Sr$, the stable isotopes of chlorine ($\delta^{37}Cl$) and bromine ($\delta^{81}Br$), sulfur ($\delta^{34}S$), boron ($\delta^{11}B$), lithium (typically expressed as $\delta^{7}Li$), and carbon ($\delta^{13}C$) (Al Yacoubi, 2022). Each water source tends to occupy characteristic isotopic ranges that help constrain origin and mixing. For example, Frape et al. (2014) concluded that meteoric signals can be detected at a depth where mine dewatering imposes downward hydraulic gradients (Fig. 2.11). More negative $\delta^{18}O$ values are consistent with ancient recharge that occurred under colder climate conditions. The resulting mixtures of meteoric and deep waters complicate source attribution and therefore argue for a multi-tracer approach. Douglas et al. (2000) demonstrate such an approach by apportioning source contributions to mine inflows with a combination of isotopic and chemical tracers. Deep brines in shield terranes typically plot off the Global Meteoric Water Line (GMWL) with relatively high $\delta^{18}O$ and constant $\delta^{2}H$ can reflect long residence times and water–rock interaction. Tritium is a valuable indicator of modern recharge: ^{3}H is usually absent in old, deep waters but can appear in

mine workings where rapid infiltration and short flow paths deliver recent water along fractures and engineered openings (Frape et al., 2014). On the other hand, chloride (Cl^-) is a conservative tracer frequently used to identify brine contributions; high-Cl^- brines are common in the Canadian Shield (Douglas et al., 2000). The chlorine isotope composition $\delta^{37}Cl$ can add source/process insight (e.g., halite dissolution, ion-filtration, and broader water/rock interaction), while bromide (Br^-) and $\delta^{81}Br$ provide further discrimination of salinity sources (Frape et al., 2014; Al Yacoubi, 2022). Elevated Sr and the $^{87}Sr/^{86}Sr$ ratio help characterize water-rock interaction because ^{87}Sr is radiogenic (produced by the decay of ^{87}Rb hosted in K-bearing minerals such as biotite, muscovite, and K-feldspar), whereas ^{86}Sr is a non-radiogenic stable isotope. Consequently, comparing groundwater $^{87}Sr/^{86}Sr$ with that of local lithologies (e.g., plagioclase and carbonates versus potassium-rich silicates) constrains flow paths and reaction histories (McNutt et al., 2000; Al Yacoubi, 2022). Major-ion chemistry can also be informative when determining the groundwater origin. For instance, sulfate (SO_4^{2-}), calcium (Ca^{2+}), and magnesium (Mg^{2+}) often increase with salinity or reflect redox-dependent reactions; however, low SO_4^{2-} should not be taken to mean "meteoric water" by itself, as it can equally indicate sulfate reduction along longer flow paths (Bottomley et al., 1994, 2005). Ratios such as K/Br and B/Br can help distinguish marine-derived salinity from rock-interaction signatures, although diagenetic processes (e.g., smectite illitization) can blur this separation and produce marine-like ratios in non-marine settings (Bottomley et al., 1994; Bottomley & Clark, 2004). Dissolved gases also provide origin and process constraints. Shallow, recently recharged crystalline-rock groundwater commonly contains dissolved atmospheric O_2, N_2, and CO_2, whereas deep shield waters show distinct gas signatures shaped by long isolation and reactions (Frape et al., 2014). Noble gases (He, Ne, Ar, Kr, Xe) are especially powerful for reconstructing recharge conditions, residence times, and mixing because their solubilities are governed by temperature and salinity in predictable ways; interpreting noble-gas concentrations and isotopic ratios can therefore identify mixing between old, isolated fluids and recent meteoric waters (Greene et al., 2008).

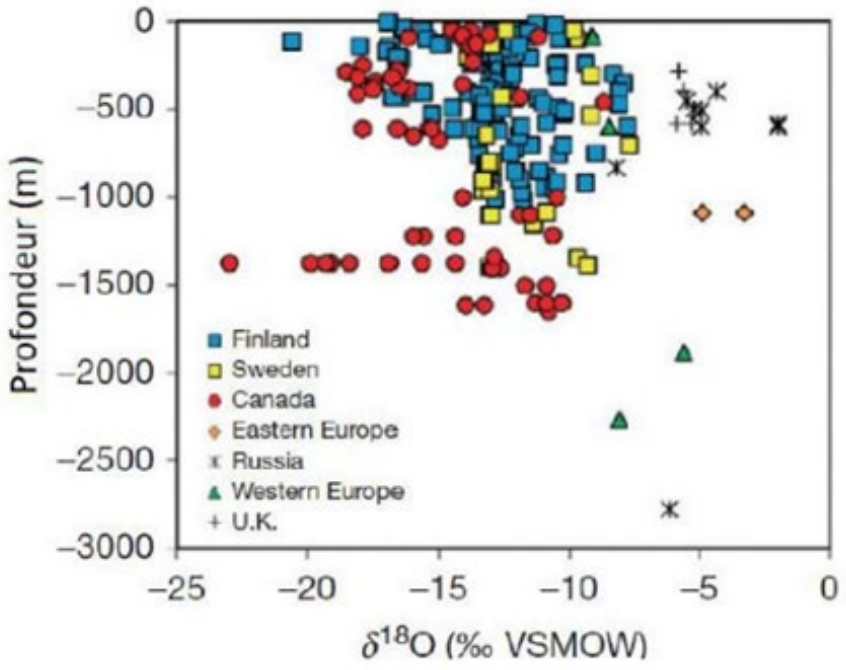

Figure 2.11: $\delta^{18}O$ values varying according to the depth across different world regions – in red Canadian Shield (Frape et al., 2014)

2.4 Solute Transport Mechanisms in Fractures

In addition to scaling and having the proper REV, the solute transports mechanisms are influenced by the unique structure, dynamics and the density of the fractures. In numerical modeling, the solute advection of the grid portion without fractures can happen across the defined porous volume of the surrounding matrix. Advection refers to the movement of the tracer (dissolved constituents) caused by the movement of the host fluid (NRC, 1996). In the classical approach to transport modeling, the average velocity is used; the transport of tracer along this average flow field is referred to as advection (NRC, 1996). Hence the advective transport is not fully described by the tracer movement which can spread and mix. Groundwater flow in fractured rock aquifers is predominantly governed by advection; solutes can travel long distances. This makes it difficult to capture the full extent of transport processes at a single modelling scale without refining the grid or adding more cells to the model (MacQuarrie & Mayer, 2005). In fact, flow channelization creates differential advection in the plane of the fracture (NRC, 1996).

Transversal dispersivity of the solute implies a perpendicular spread to respect with the flow direction and longitudinal dispersivity of the solute implies a spread along with the flow direction. In fracture systems, transversal and longitudinal dispersion is expected. In a homogeneous porous medium, in 2D, transversal and longitudinal dispersion includes the dispersivity and the molecular diffusion (Freeze & Cherry, 1979):

$$D_l = \alpha_l \bar{v}^m + D^* \tag{2.9}$$

Where α_l represents the dispersivity along a curvilinear coordinate direction l, $\bar{v}$ is the average linear groundwater velocity, m is an empirically determined constant between 1 and 2, and D^* is the coefficient of molecular diffusion.

The dimensionless Péclet number indicates the balance between advection and dispersion in a contaminant plume (Freeze & Cheery, 1979):

$$Pe = \frac{\bar{v} l}{D_l} \tag{2.10}$$

When Pe < 1, diffusion dominates in the solute transport, when Pe is between 1 and 10 there is a relative balance between advection and dispersion, when Pe > 10 advection dominates the solute transport (Freeze & Cheery, 1979; Huyakorn et al., 1983; Bear et al., 1993). In a mine scale, the Péclet number is expected to be very high because of the different groundwater flow velocities and heterogeneity which would indicate that the transport is dominated by advection, but molecular diffusion can become negligible. Dispersivity is a scale-dependent parameter, increasing with the size of the flow domain or the length scale over which transport is evaluated (Freeze & Cheery, 1979). Simulation of contaminant transport can have values that are an order of magnitude larger

than in a laboratory setting. Therefore, in numerical modelling, it is important to set an appropriate scale to represent the REV.

Modern studies suggest that dispersion cannot always be treated as a Fickian process: in a heterogenous environment the solute must travel a certain distance before Fickian dispersion is established (NRC, 1996). Hence, the representation of dispersivity depends on how detailed the heterogeneity is modelled. In fact, the advection-dispersion equation is considered unreliable predictor of transport processes in a highly heterogenous environment (Anderson et al., 2015). In general, the common advection-dispersion equation considers the solute concentration, flux and dispersion tensor (MacQuarrie & Mayer, 2005). When dealing with brines, the high-density of saline water introduces density-driven flow, which can cause heavier fluids to sink along the fracture network (Douglas et al., 2000). In fact, standard advection-dispersion models may underestimate the solute transport unless the vertical migration or preferential flow paths attributed to the fluid density are explicitly included in the simulation (Bear et al., 1993). Alternatively, this can be captured by coupling models with variable density. The irregular flow paths, relatively high flow and variable velocities cause mechanical dispersion to dominate, often more than molecular diffusion or matrix diffusion ($D_l = \alpha_l \bar{v}^m$) (Anderson et al., 2015). By the definition, molecular diffusion occurs when a solute move from high to low concentration areas. In a fractured environment, molecular diffusion dominates in zones with low flow and fracture-matrix interfaces ($D_l = D^*$). It also can govern matrix diffusion where solutes slowly penetrate the rock matrix (Bear et al., 1993). As for any other transport mechanisms, there is research needed to determine how the fracture geometry governs preferential flow paths and the surface area affects matrix diffusion and reactive transport (NRC, 1996). In fact, channelized transport and matrix diffusion are concepts that are developed in the study of solute transport in fracture rocks (NRC,1996; Hadgu et al., 2017). Moreover, defining the specific interstitial surface and the flux between the fractures and the surrounding matrix can further help to consider the diffusion of some chemical components (MacQuarrie & Mayer, 2005). A proper REV can help represent the diffusion between the surrounding matrix and its fracture network. Continuum media can better consider this transport mechanism (Selroos et al., 2002; Hadgu et al., 2017; Zhou et al., 2023). Essentially, if the domain geometry is well understood, the rock matrix and fractures can be represented separately to accurately simulate diffusion between these two media. Nevertheless, there are numerous complex geochemical reactions. For example, on some occasions, the alteration of the adjacent matrix to the

fracture surface can be limited by a small zone due to the molecular diffusion and the relevant kinetic reactions (MacQuarrie & Mayer, 2005).

2.5 Influence of Mine Openings on Fracture Connectivity

Deep geological settings experience high confining stress which can reduce the fracture apertures and permeability unless stress is relieved or redistributed by mining activity for example (Bear et al., 1993). Mine openings can induce significant geomechanical and hydrogeological changes that exposes sealed fracture or create new ones (Hoek et. al., 2002). When a mine gallery is built, the horizontal stresses can be higher than the vertical stresses which causes the main stresses to be redistributed: the ceiling and ground of the gallery is under compression whereas the walls are under tension (Gagne, 2014). In addition, mine opening can impact on the flow paths and hydraulic connectivity and the geochemistry as shown in Fig. 2.12. Construction of an underground structure can be expected to disturb the regional groundwater flow system, controlled by discontinuities in the rock mass which include faults and joints (Douglas et al., 2000). With an increase connectivity within the fracture network, there can be mass transport over long distances. This can make a model more complicated to predict mine inflows or solute migration. Steep hydraulic gradients can be created between the surface and depth which would induce flow towards excavated areas, as it was observed in Con Mine: there is evidence of groundwater circulation and mixing in crystalline rock (Douglas et al., 2000). One of the characteristics of these crystalline aquifers was described by Frape et al. (2014) is the fact that water intrusion from the glacier melt can be found at depth. In mine dewatering, there is a chemical interaction between the groundwater and the rock mass. Mine openings allow the introduction of oxygen in the deep geological setting which causes oxidation. In addition to this impact, pumping can also cause groundwater mixing with meteoric water which creates isotopic and chemical dilution (Frape et al., 1984). As observed in the Canadian Shield, deep systems often contain saline groundwater (Al Yacoubi, 2021). As mentioned in the previous subsection, fracture physical properties influence the movement of these denser fluids through advection and density-driven flow. Afterall, underground mines can provide valuable observation points for detecting and analyzing in groundwater flow and mass transport. In fact, it is in the best interest to understand how the mine impacts the local aquifers (Gagne, 2014). Though, at depth,

limited access and borehole data increase uncertainty. Thus, fracture network assumptions with respect to the fracture physical properties, significantly affect the numerical model outcomes.

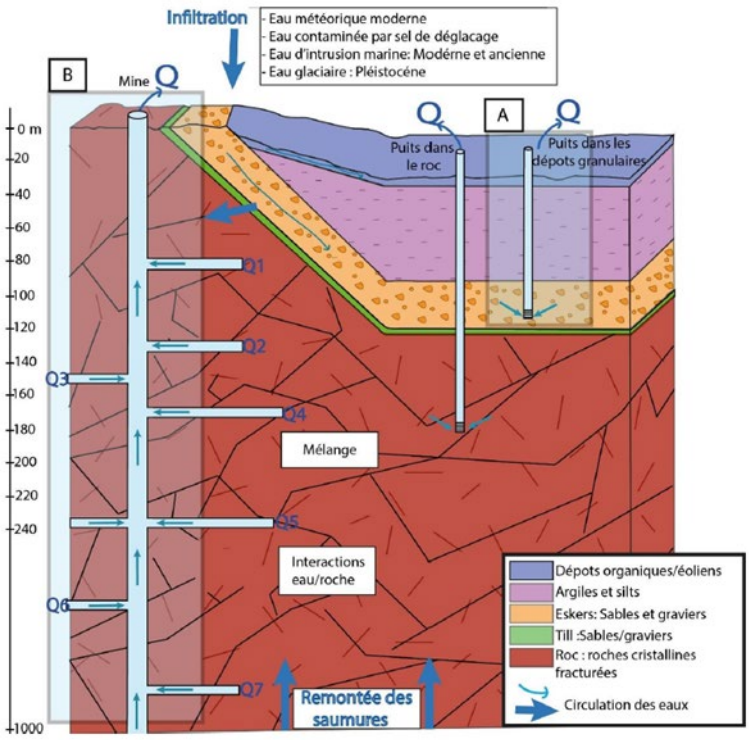

Figure 2.12: Illustration of the hydrogeochemical interactions and exchanges in fractured-rock aquifer with mine openings adapted from Al Yacoubi (2021)

2.6 Modelling Approaches and Applications for Solute Transport in Mine Openings

Modelling fractured crystalline aquifers has advanced through a variety of mathematical frameworks (Abdelghani et al., 2015). As with groundwater-flow modelling, the central challenge for solute-transport modelling in fractured crystalline rock is how the fracture network is represented. Widely common representation methods are (i) discrete fracture (DFN/DFM) approaches and (ii) equivalent-continuum models (ECM) at a representative elementary volume

(REV) scale; both can be effective for simulating contaminant behaviour in this type of subsurface, depending on data and objectives. Numerous studies have compared fracture representations in transport models (Selroos et al., 2002; Neuman, 2005; MacQuarrie & Mayer, 2005; Chesnaux et al., 2012; Karay & Hajnal, 2015; Hadgu et al., 2017; Zhou et al., 2023). Although homogenizing fractures into a continuum can simplify computation and calibration. Particularly, in mine dewatering in the Canadian Shield, water is induced and mixed in crystalline rock. 3D modelling can be challenging especially considering the heterogeneity, anisotropic, variable properties of mine workings. While there is a broad understanding of plausible contaminant sources—partly informed by radioactive-waste and deep-shield studies—it remains best practice to conceptualize the model case by case (Hadgu et al., 2017; MacQuarrie & Mayer, 2005; Selroos et al., 2002). Many factors can influence model outcomes. Preferential pathways commonly develop along connected fractures (Chesnaux et al., 2012). Chesnaux et al. (2012) showed how fracture location and connectivity govern groundwater flow using GeoStudio (SEEP/W for flow; CTRAN/W for transport). Abdelghani et al. (2015) modelled 2D solute transport from a waste-rock deposition in a fractured-rock open pit with HydroGeoSphere, where the simulated plume advanced relatively smoothly through time (Fig 2.13). However, such uniform fronts can be an artefact of assumptions about fracture geometry and properties. As shown in Karay & Hajnal, (2015) (refer to Fig. 2.14), fracture length, aperture and spacing vary over metres to tens of metres, producing channelized, non-uniform advance. Within fractures, flow is often laminar and well described by the cubic law (discharge proportional to the aperture and hydraulic-head gradient), but non-Darcian behaviour can arise locally where velocities and roughness induce inertial losses. In those cases, cubic-law corrections (e.g., Forchheimer terms or effective-aperture/roughness factors) are needed; simply asserting that “Darcy’s law does not apply” can be considered an understatement (Karay & Hajnal, 2015).

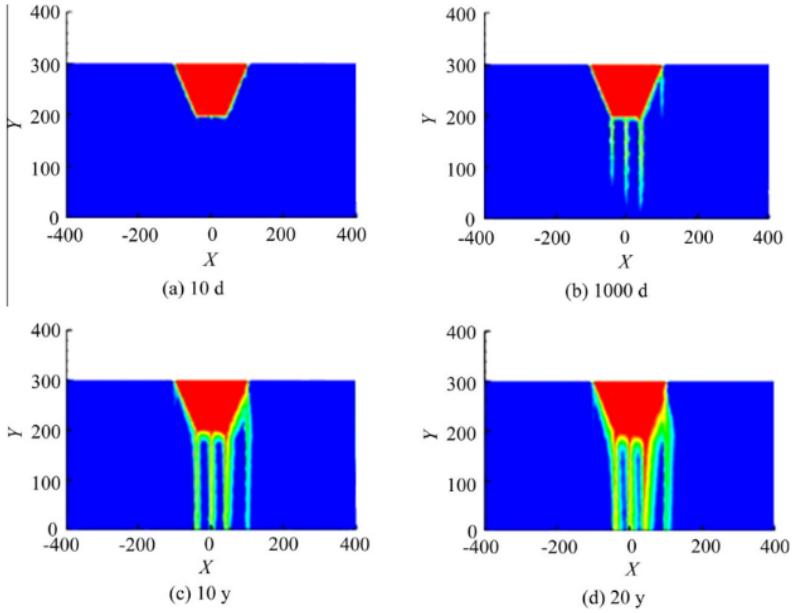

Figure 2.13: Simulation of contaminants through an open pit mine filled with waste rock through homogeneous and vertical fractures through different time periods. Blue representing low concentrations and red representing high concentrations. (Abdelghani et al., 2015)

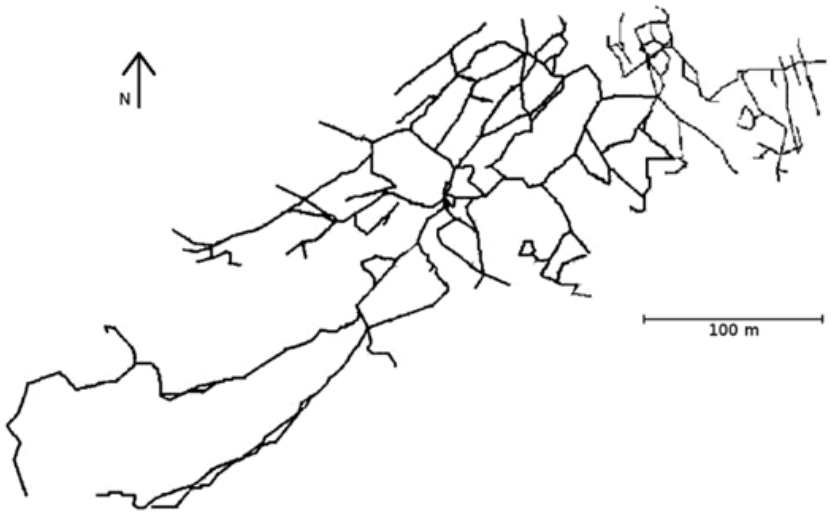

Figure 2.14: Fractures representation in the Molnar Janos cave (Karay & Hajnal, 2015)

Beyond fracture representation, appropriate boundary conditions are critical for transport studies (Karay & Hajnal, 2015). Pumping tests and controlled dewatering provide head/flow responses that help constrain boundary conditions and transmissivity. Where helpful, laboratory analogue models (as in Karay & Hajnal, 2015) can inform parameters, followed by numerical analysis (e.g., with MODFLOW-family codes for flow and linked transport solvers). A consistent water balance is essential because recharge and operational fluxes alter boundary conditions and drive transport (Zhou et al., 2023). Porosity and permeability can vary markedly over short distances in fractured media (Zhou et al., 2023). Transport processes to include are advection along fractures, matrix–fracture diffusion, longitudinal and transverse dispersion, sorption/retardation, and (where relevant) mineral reactions (Zhou et al., 2023). The standard advection–dispersion equation governs conservative transport (MacQuarrie & Mayer, 2005). For linear sorption, retardation can be represented with a distribution coefficient (ratio of sorbed to dissolved concentrations) and bulk density/porosity; non-linear Langmuir or Freundlich isotherms may be required (MacQuarrie & Mayer, 2005). Flow-coupled reactions such as mineral dissolution/precipitation can further modify concentrations (MacQuarrie & Mayer, 2005). Fig. 2.15 illustrates common fractures-matrix interactions that should be characterized during site investigation because they strongly affect numerical predictions.

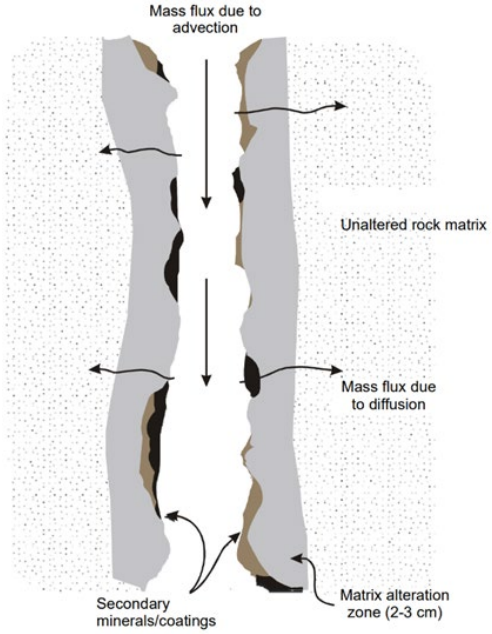

Figure 2.15: Chemical interaction between rock mass and fractures
(MacQuarrie & Mayer, 2005)

When designing a model, it is useful to formulate governing equations for a single aqueous phase with multiple solutes, and to extend to multiphase only where gas or NAPL phases are demonstrably present (Chesnaux et al., 2012). Comparative sites can help distinguish natural signals from anthropogenic impacts (Chesnaux et al., 2012). Hadgu et al. (2017) evaluated a 1-km³ fractured-rock volume in PFLOTRAN, comparing an ECM and discrete-fracture formulations to estimate effective permeability and porosity. In practice, DFN/DFM approaches count fractures within the domain and characterize their transmissivity, aperture and orientation together with matrix properties. The effective permeability controls both flow and transport; better fracture characterization reduces bias. Fig 2.16 shows normalized breakthrough curves from four realizations; concentrations rise faster and earlier in fracture-explicit cases than in continuum equivalents. Hadgu et al. (2017) suggest using DFN/DFM where fractures materially control connectivity and travel times; ECMs better capture matrix diffusion and sorption when fractures are short, sparse, or poorly connected.

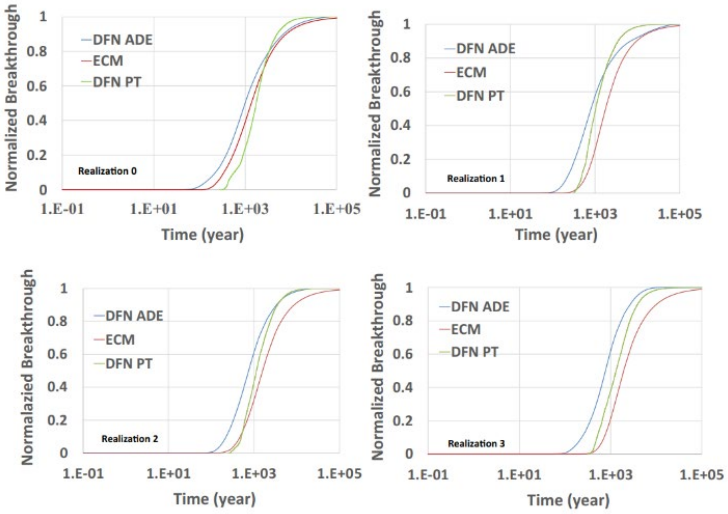

Figure 2.16: Normalized curves comparing DFN and ECM (Hadgu et al., 2017)

As discussed earlier, hybrid approaches that combine fracture channels with matrix diffusion (e.g., stochastic channel networks, dual porosity/dual permeability, or multi-rate mass-transfer formulations) are often advantageous (Selroos et al., 2002). A DFM becomes complex in a large

scale compared to an ECM. Also, heterogeneity can affect the dispersion patterns which lead to non-Fickian transport behaviours (NRC, 1996). Numerical tools such as MODFLOW-USG and FEFLOW have been adapted for fractured environments, often integrating dual-porosity and variable-density capabilities (Anderson et al., 2015). In general, there are several geochemical reactions to capture. It is recommended to couple models to better encompass multicomponent reactive transport (Hu et al., 2020). In addition, it is important to distinguish with tracers natural groundwater from solute introduced by mining activities. For example, as highlighted by Stotler et al. (2009) in a study on the Lupin Mine, Nunavut, mine water can be contaminated with drilling brine and with blasting nitrogen species. In the context of the study, more specifically in mining operations, there can be significant exchanges between the fractures, and the rock matrix can be captured with a model that integrates dual porosity. In addition, a model that can use variable-density solute transport approaches can capture the groundwater mixing caused by the mining activities. Mine galleries, shafts and drifts are often modeled as drains, sinks or highly permeable zones to consider the influence on domain flow and solute migration (Zaidel et al., 2010). In fact, considering the large scale, it is suggested to model under transient conditions to consider the long-term evolution of solute fronts under changing conditions through the life of mine. However, these elaborated models require the collection of data to accurately simulate and estimate local hydraulic parameters in fracture systems. Analytical solutions are useful for simplifying parameter estimation from hydraulic tests, but their underlying assumptions can bias results in fracture network which can sometimes lead to overestimation of hydraulic properties compared to more detailed numerical models (Gagne, 2014). Regardless of the framework chosen, flow caused by the fracture network must be understood first; a pragmatic approach is to run a coupled flow model, then implement a dual-domain transport (fracture domain for advection/dispersion; matrix domain for diffusion/sorption) to ensure that both domains are represented (Hadgu et al., 2017). Therefore, choosing numerical tools that support tight coupling between flow and transport and use robust iterative solvers for fractured networks can be challenging (MacQuarrie & Mayer, 2005; Karay & Hajnal, 2015). Furthermore, when assembling inputs and setting spatial/temporal discretization and evaluating and calibrating results field data is to prioritize (Chesnaux et al., 2012). This would include hydraulic heads and gradients, pumping/flow rates, fracture-test data (e.g., packer tests, transmissivity), groundwater chemistry and tracers, and geologic/structural mapping; grain-size data are relevant mainly for overburden or weathered zones (MacQuarrie & Mayer, 2005). To

summarize, it is important to define the adequacy of the study scale considering the heterogeneity and anisotropy of the environment. Nevertheless, it is important to calibrate the transport models using tracer tests, mine water quantitative and qualitative data, hydraulic head data, and inflow measurements (Rapantova et al., 2007). Essentially, when conceptualizing a numerical model to study the flow and transport through a fractured environment, the model strategy and fracture representation will depend on the data availability and hydrogeological setting. Particularly in a mine site, often times, the priority falls into understanding the overall context of the dewatering system to plan operational and capital expenses which can lead to a simplified parametrization scheme (Skeekanth et al., 2020). In fact, while comparing *in situ* data and simulation results, sensitivity analysis can help evaluate which parameters have the most influence. As previously discussed, in a mine setting, numerical modelling with GeoStudio can exhibit numerical instabilities and artificial dispersion when the spatial (and temporal) discretization is too coarse to resolve the dominant advective front, particularly under conditions with high Péclet number as expected in a mine scale. Therefore, the Pe number is adjusted to ≤ 2 to stabilize the model and have a more realistic representation of the plume behaviour (Geo-Slope, 2012). The Pe number is adjusted by increasing the dispersivity and/or refining the mesh. Moreover, the Courant number is also considered. It is a dimensionless ratio that measures how far a solute particle is transported across an element during a single time step. For many marching schemes, numerical stability requires the Courant number to remain below a method-dependent limit (Anderson et al., 2015). In 1D advection, the Courant number is expressed as follows:

$$Courant\ Number = \frac{\bar{v}\Delta t}{\Delta x} \tag{2.12}$$

Where Δx is the nodal spacing, Δt is incremental time step.

In GeoStudio, when Courant number ≤ 1, the model can be stable since the front moves less or one element length per time step whereas when Courant number > 1, the model can be unstable since it jumps elements within a time step.

CHAPTER 3 SITE CONDITIONS AND SETTING

This chapter summarizes the climatic, physiographic, geological, hydrogeological, and hydrogeochemical setting of the reference site to frame the physical processes relevant to fractured-rock underground mines. Although Éléonore provides a concrete context, the numerical models that are developed use idealized fracture geometries and settings inspired by the site and are not intended to reproduce the Éléonore detailed conditions.

3.1 Climate and Surface Conditions

The reference site, Éléonore mine, is located in the territory of the Cree Nation of Wemindji, in the *Eeyou Istchee* – James Bay region, Northern Quebec within a cold and humid subarctic climate typical of the Canadian Shield setting (refer to Fig 3.1). Several minerals and metals of economical interest such as gold, diamond, iron, lithium, uranium are found in the region. The terrain is relatively flat, with hills and depressions caused by the uneven surface of the Canadian Shield, as well as regional slopes inclined towards James Bay to the West. The region is characterized by a cold and humid subarctic climate. The temperature varies from -20 °C during the winter months to 16°C in the summer months (Al Yacoubi, 2022). The average annual precipitation is 650 mm. The region is known to encompass several significant water resources, notably the Opinaca Reservoir (south) and the Opinaca River (north). These resources are sensitive to environmental changes and may be significantly impacted by anthropological activities such as the development of hydroelectricity and mining operations. The climate, surface conditions, and geology of the site are described extensively in Al Yacoubi (2022). Here the focus is mainly set on existing information pertaining to fracture characterization and local hydrogeological modelling progress. Cold-climate Shield setting typically combine abundant surface bodies with shallow fracture bedrock, making surface water-groundwater connectivity essential for boundary conditions consideration.

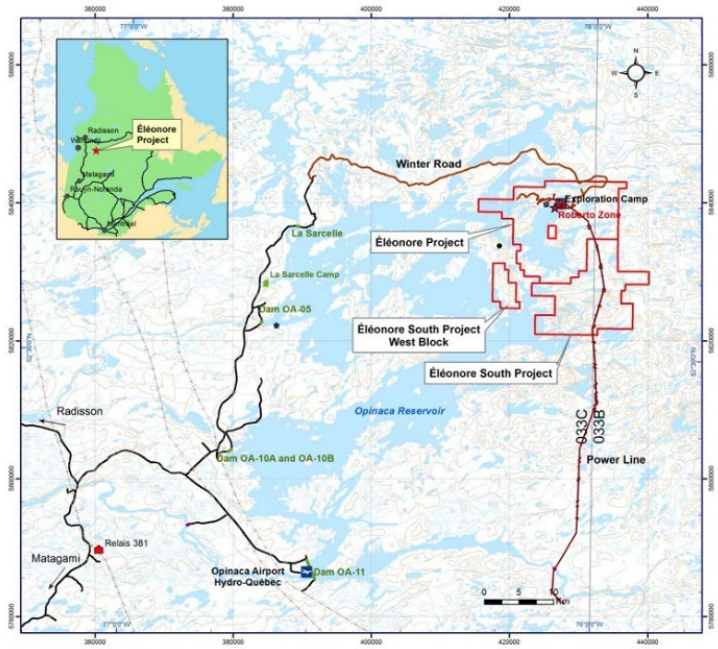

Figure 3.1: Reference site location based on the NI 43-101 Technical Report (Charland et al., 2018)

3.2 Geological Setting

The reference site, Éléonore mine, is found in the Superior geological province, near the limit between the Opinaca and La Grande geological Subprovinces. The contact between the two subprovinces, also referred to as the transition zone, is poorly constrained. It generally coincides with regional-scale deformation zones and a sharp change in metamorphic grade (Charland et al., 2018). In some areas the contact is masked by the late intrusion of one or the other subprovinces (Bandyayera et al., 2007). This contact can be noticed in the northeast corner of the property, as observed in Fig. 3.2. The regional faults are mostly present in the La Grande Subprovince. In the Opinaca Subprovince, faults and shear zone are mostly located along the fold limbs. The Opinaca geological subprovince is characterized by gneiss, metatexites and diatexites whereas the La Grande geological subprovince is characterized by volcano-plutonic rock, intrusive rocks such as tonalite, granodiorite and leucogranite (Charland et al., 2018). Locally, the Éléonore site is located within the Low 2 Formation, which consists mainly of Neoarchean sedimentary rock, refer to Fig 3.3 (MRNF, 2025). Reactivated structures and folded turbidites create a strongly anisotropic rock mass, which leads to groundwater that is controlled by fractures (secondary permeability). Shallow sub-horizontal joints enhance hydraulic connectivity with the Opinaca Reservoir (Charland et al.,

2018). Although the hydraulic conductivity decreases with depth, there are discrete zones that remain transmissive where fractures concentrate. The area immediately surrounding the mine is characterized by undifferentiated till deposits, which are bordered by bedrock outcrops to the northeast and northwest. Shallow-water marine deposits and undifferentiated lacustrine deposits occupy the lower-elevation areas on the periphery of the site. The bottom of the Opinaca Reservoir is covered with silt and clay sediments. Some areas were identified with coarser material (Fig 3.4). In most case in Shield settings, the rock mass is hydraulically anisotropic and dominated by secondary permeability, supporting the use of fracture-controlled conceptual models rather than matrix-porous media behaviour.

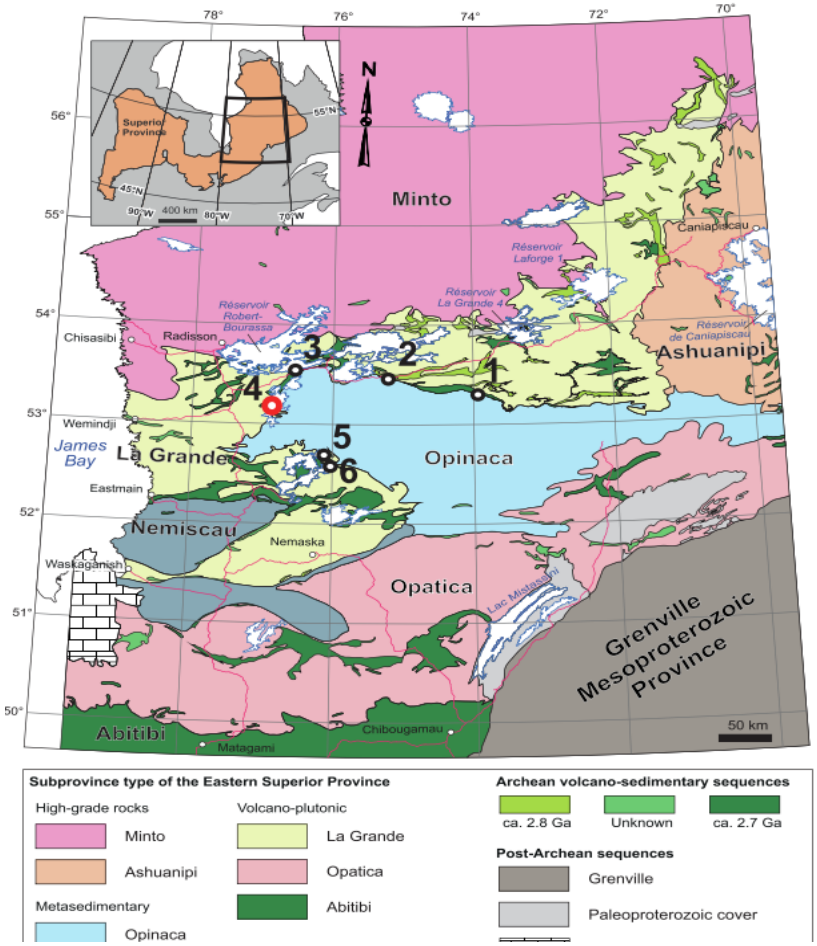

Figure 3.2: Eastern Superior Geological Province. 1. Marco zone deposit; 2. Orfée deposit; 3. Zone 32 deposit; 4. La Point deposit; 5. Roberto deposit (Éléonore Gold Mine), 6. Cheechoo/Éléonore South deposit (Fleury et al., 2021)

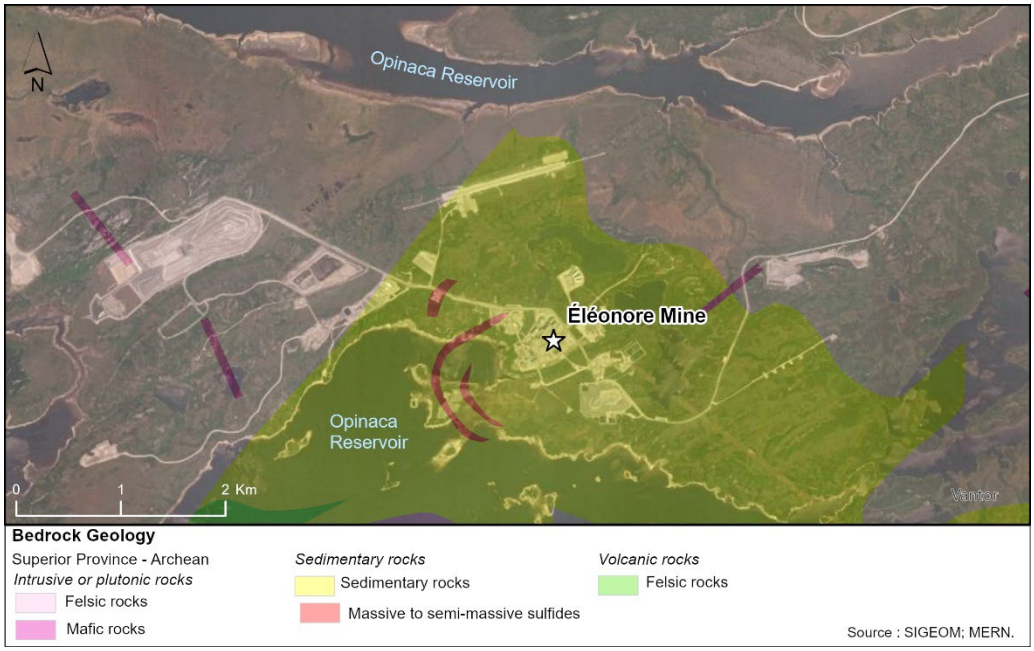

Figure 3.3: Bedrock geology of the reference site from SIGEOM (MNRF, n.d.)

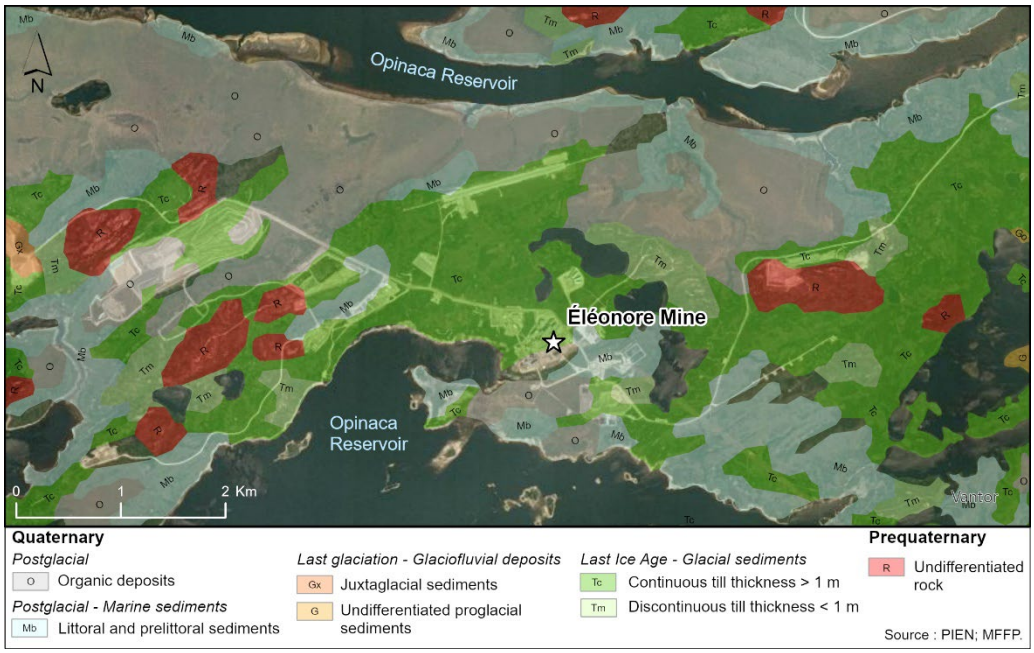

Figure 3.4: Surficial deposits of the reference site from SIGEOM (MNRF, n.d.)

3.3 Hydrogeological and Hydrogeochemical Conditions

According to site data, there is a network of observation wells to allow monitoring and sampling twice a year. Baseline studies show low chloride concentration. This indicates that the lake was not impacted by other source terms. However, in some areas, it shows the presence of deeper mineralized water. Earlier dewatering chemical results suggested the strong connection between the Opinaca and the mine openings since they were drawing freshwater. In fact, sampling results confirmed low salinity values. As the mine progresses, it was identified that groundwater quality (GWQ) gets more impacted at deeper levels and shows a clear stratification (Al Yacoubi, 2021). Shallow levels have a shorter residence time and high flow which explains the minor impacted GWQ, whereas deeper levels have longer residence time and allow salinity buildup with more abundant water-rock interactions which explain the significant impact on GWQ (Frape et al., 2014). According to site records, it was confirmed that the water chemistry is impacted by paste backfill which can be considered a source term responsible for the salinity. As suggested in previous reports, it would be beneficial for a site to better characterize the geochemistry on the different levels of the mine to have the adequate remediation strategy and best available technology economically achievable (BATEA) for closure and post-closure. Since the residence time and potential source terms depends on the depth, it is useful to consider stratification and localized solute source in conceptual transport scenarios.

3.4 Fracture Characterization and Relevant to Conceptual Modelling

In fractured settings of the Canadian Shield, sub-vertical fault zones often form the primary pathways controlling connectivity and travel times. At the reference site, these structures are interpreted to link mine openings with nearby surface waterbodies. Earlier analytical work has determined that there is water from the flooded mine area travelling upward along the steep faults, also referred to as the water-conducting faults. The connectivity of the fracture network is driven by these types of faults. In fact, a recent intersection of a known fault by the mine development confirms the extent of the fracture network. This was confirmed with the sudden loss of water in a piezometer. Moreover, pumping tests completed to this date can confirm that there is a strong connection between the mine area aquifer and the nearby waterbodies. On the other hand, the transport model also indicates that there is an exchange between the surface water and the mine in

outcrops and in areas where low permeability lakebed sediments are absent. The transport simulation also revealed that if the water in the mine is maintained at or below the level of the Reservoir, the mine behaves as a sink. Therefore, solute migration from the waterbody to the mine would not be expected. However, this could potentially be feasible during the closure phase if mine dewatering persists. According to the model, paste backfill leachate could create localized pockets of contaminants at deeper levels in low-flow zones. Upon closure, it was evaluated that the mine is expected to flood relatively quickly. This rapid filling can cause water to mix at different levels. Even during closure, the model suggests that there would be stratification of salinity: higher concentration at deeper levels. However, the brines are expected to rise over the long-term as water-rock interaction continues. With time, there could be additional ion mobilization. The travel time is driven by the high permeability fracture network. More specifically, advective flow dominates with minimal dispersion/attenuation since there is not enough travel time to allow for dilution or diffusion. Preliminary model results indicate that even with conservative source concentrations, discharge from the upper mine levels is expected to remain below acceptable thresholds. This finding can be supported with more geochemical inputs. Prior site-specific models (used with different platforms) consistently highlight the importance of transmissive structures and surface water boundaries in controlling inflows and potential solute pathways. The current models were inspired by each previously mentioned model approach. To contextualize, a limited number of transmissive structures can dominate advective pathways and travel times which highlight the importance of exploring simplified fracture geometries in numerical modelling.

Although Chapter 3 describes the site-specific geological and hydrogeological conditions at Éléonore, Chapter 4 focuses on simplified conceptual representations of fractures. These simplified models are not meant to reproduce site conditions directly, but rather to explore the behaviour of idealized fracture geometries and hydraulic parameters that inform later numerical analyses.

CHAPTER 4 METHODOLOGY

This chapter describes the methodology that was used to develop the model on GeoStudio 2024.2.1 using SEEP3D and CTRAN3D (Seequent, 2024). It includes the modelling approach used, the geometry and domain definition utilized, material properties and input parameters used, as well as the boundary conditions and initial conditions applied. Moreover, the chapter discusses the model calibration and validation applied with its sensitivity analysis and the model limitations and assumptions that are part of this development.

4.1 Model Selection

As outlined in Chapter 2, a range of software programs exists for simulating groundwater flow and dissolved solute transport. The selection process is often complicated by the fact that each software program has its own set of advantages and disadvantages. Amongst the extensive range of software available, the GeoStudio 3D suite is of particular interest because it combines numerous components that can be used to simulate water flow (SEEP3D), non-reactive solute transport (CTRAN3D), heat transport (TEMP3D), and gas flow (AIR3D) in a coupled manner. This is particularly relevant in mining contexts, where these components are essential for evaluating the exchange of water, dissolved solute, heat, and gas that can influence mine operations and the effectiveness of environmental protection measures. Furthermore, the CTRAN3D component of GeoStudio has only been available since 2021 and remains relatively underutilized in the mining context. It is important to mention that the only geochemical process that CTRAN3D can uptake is solute transport through advection dispersion. There is also the option to add the sorption process. However, it was not used for the purpose of this study. Consequently, there is an opportunity to test the coupled simulation of water and dissolved solute flows with SEEP3D and CTRAN3D to evaluate flow in fractured rock in a mining context.

4.2 Conceptual Model and Modelling Approach

GeoStudio uses a finite element method. Here, the SEEP3D & CTRAN3D solvers were used. These components of the GeoStudio software are applicable to groundwater flow through fractured bedrock and mine openings and allow for solving governing flow equations and supporting the inclusion of high-permeability linear features to represent fracture systems. The simulation was developed using a branch of analyses, starting with a steady-state groundwater flow analysis used as a parent analysis for daughter CTRAN3D steady state and transient analysis. The domain geometries are all limited to 2 km × 2 km × 2 km volume and were developed based on the data representative of real geological faults and structures observed at the Éléonore mine site and using a simple conceptual model (Fig 4.1). In the three main geometries, also referred to as the Conceptual Geometry 1, 2 & 3 as labelled A-B-C in Fig. 4.1, respectively, it is assumed that regional groundwater flow is sub-horizontal (i.e. negligible vertical gradient), that recharge waters from the surface area dilute and that brine originates from a depth of 2 km. The models developed here focus specifically on the fractured bedrock and for simplification purposes, the surface deposits were not explicitly included in the simulations.

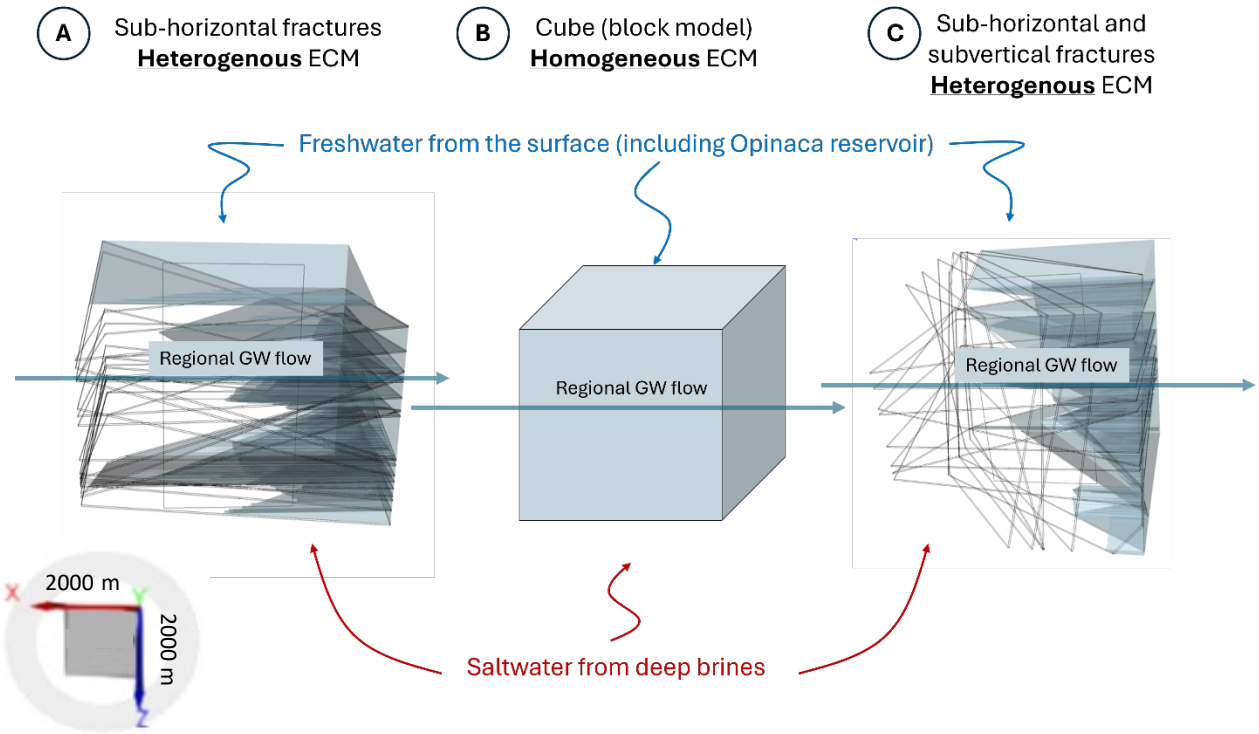

Figure 4.1: Study model conceptualization for developing SEEP3D and CTRAN3D analyses.

The first model domain geometry (Fig 4.1A) focused specifically on sub-horizontal structures representing joint sets and water bearing features in the mine site, thus simplifying the actual geological conditions. The model is spatially heterogeneous in that it includes discrete fracture zones intersecting an impermeable rock mass. This geometry was selected as a starting point because it allows for simulating unidirectional flow along the x-axis, facilitating direct comparisons with a 1D analytical solution. The geometry, continuity and internal heterogeneity of fractures are generated from available structural data. An additional level of simplification was implemented in GeoStudio to ensure model stability which is further discussed in this chapter. Once the SEEP3D steady-state analysis converged, it was possible to proceed with CTRAN3D simulations. Advection dispersion (including diffusion) processes were simulated. Adsorption process function was not defined for this transport model.

The second model domain geometry (Fig 4.1B) was developed to represent a homogeneous ECM approach. This model is also referred to as the "block model". The advantage of this model is that it allows comparison with a model comprising discretized zones that correspond to fractures (Fig.4.1A) and a domain that is considered to be a strict EPM (Fig 4.1B).

The third domain geometry considers both horizontal and vertical structures. This geometry is closer to real conditions but is too complex to be compared with results from an analytical solution. This third geometry is used for more complex simulations involving mine dewatering scenarios. It is important to note that only half of the vertical and horizontal structures were kept in the third geometry. This was done because GeoStudio 3D could not handle the complexity of geometries with more than 18 planar structures.

The conceptual model focuses on using water-conducting structures and other main faults that steer the flow direction and the permeability of the environment. The latest mine survey was initially used to size the domain. In terms of water balance, we must keep in mind, for the mine to be able to operate it needs to pump or dewater the underground working due to its positive water balance. In fact, the mine site estimates pumping rates of 300 m^3/hr for the mine operation and avoid major underground infiltration. The main contributor of these underground infiltrations is the Opinaca Reservoir. As per Bense et al. (2013), an equivalent continuum approach was used to simulate the groundwater flow. Given the complexity and the uncertainty associated with characterizing each fracture in the study area, a simplified geometrical form of the main faults and structures previously

discretized were used. In the case of the first domain geometry (Fig 4.1A), the use of simplified sub-horizontal structures helps to ensure the computational stability to adequately identify dominant flow and understand the overall flow and solute transport in fracture zones. In other words, the domain flow is reduced and applied to 3D planes and their volume. It is worth mentioning that SEEP3D and CTRAN3D do not allow through open free-flow channels within the domain. In the models developed here, their permeable features are embedded in a "heterogeneous" ECM domain where 3D plans are drawn, assuming that the rock matrix between planes is impervious.

This model approach can represent a balance between the simplification of conditions and real-time conditions: the key structural features were captured while remaining computationally efficient and suitable for the site scale analysis with the information and geological characterization provided. From an operational perspective, this approach is preferred over a discrete approach not only due to the limited detailed fracture system characterization, but also due to the need to have site-scale predictions rather than localized behaviours.

4.3 Model Geometry and Domain Definition

The fault and geological structure files were available in DXF files which were imported individually in GeoStudio. It is important to note that the original geological fault and structures have a z-axis that corresponds to the elevation. However, in GeoStudio, the vertical dimension is defined along the y-axis. As a result, the import process effectively rotates the model's coordinate system, where the initial X-Z planes become the X-Y plane. This change is purely geometric and does not affect the conceptual or hydrogeological interpretation. Once the background mesh is imported, a 2D plane was created for each structure to ensure to place as many points as possible matching the fault geometry. The plane was extruded to have a finite 3D plane with 6 surfaces: each structure was given initially the same thickness of 10 m. Due to the relatively large extent of the structure length, the model could not converge with a smaller thickness of 5 m.

A 2 km cube was built perpendicular to the X-Z axis sized to enclose all structures. The intent of the cube was to trim the fault solids with the cut function to ensure faults stay inside the defined volume. The domain captures the mine and rock mass surrounding the infrastructure. The model basepoint was reset to 0,0,0 for simplification, only affecting the absolute positioning of the model

in the domain. While the actual Cartesian coordinates were not preserved in GeoStudio, the relative spatial relationship between features were maintained. This adjustment does not affect the internal geometry or hydrogeological behaviour which allows the model to preserve its functional integrity.

In the area of interest, the 3D planes intersect with mine workings as well. The intersections provide important information regarding the flow interpretation and help understand the preferential flow paths or mechanical hinge. The intersection of the 3D planes is computed analytically and then clipped to the polygonal boundaries of each plane to obtain a segment. In reality, faults can intersect more than once between each other, the pairwise approach is appropriate to better understand the kinematic and hydrogeological implication. Since the intersections are predicted to be a control of inflows through the system, it is important to resolve where each fault intersects between each other. As known, each structure was simplified and represented in a Cartesian coordinate (x, y, z). Using either three non-collinear points (A, B, C) on a surface or the structure strike, dip and a reference point, the plane is presented in a vector form, and the line of intersection can be found:

$$n_i = (\cos\alpha \sin\delta\,, -\sin\alpha\ \sin\delta\,, \cos\delta) \tag{4.1}$$

Where α is the strike angle (° in radians) clockwise from the North, δ the dip (° in radians). For a fault or plane i, n_i is the unit normal.

On the other hand, with three non-collinear points:

$$A_i = x_a, y_a, z_a; B_i = x_b, y_b, z_b; C_i = x_c, y_c, z_c$$

$$u_i = B_i - A_i\,; v_i = C_i - A_i$$

$$n_i^* = u_i\ x\ v_i \tag{4.2}$$

Where n^*_i is a vector perpendicular (not necessarily normalized) to a plane and u_i and v_i are non-collinear vectors that lie in the plane i. The plane equation is as follows:

$$n_i * r + D_i = 0, \qquad D_i = -n_i * p_i \tag{4.3}$$

Where the offset D_i. r is a point in space and p_i is a known point in the plane. Therefore, for any plane *i, j,* the direction (*d*) of their intersections is:

$$d = n_i x\, n_j \tag{4.4}$$

A particular point on this line is obtained in close form as r_0 :

$$r_0 = \frac{(D_j n_i - D_i n_j) x\, d}{||d||^2} \tag{4.5}$$

Where ||*d*|| is also referred to as a scalar magnitude.

And the parametric line (*L*) can be defined as follows:

$$L(t) = r_0 + td \tag{4.6}$$

Where *t* is a scalar parameter that refers to the distance and the direction in which along the line from a chosen starting point. The vector line equation of all intersecting faults (in pairs) can be found in Appendix A.

All model geometries cover all the defined faults and geological structures as mentioned above and extends to all the extremities of the mine even if another level of simplification was implemented. To ensure to have similar properties than the block model, the model using the actual sub-horizontal structures (equivalent to the conceptual model shown in Fig. 4.1A) was first conceptualized due to irregular geometrical shape and their complex representation in GeoStudio, 18 structures are defined in this model. As previously mentioned, these simplified structures are a conjunction of joint sets and has water bearing features. Vertical faults were also implemented in the third model (equivalent to the conceptual model shown in Fig 4.1C). These are the primary hydraulic structure and pathways connecting the shallow levels and the underground mine workings. Vertical faults

are known to dominate the groundwater inflows and solute transport in the study area. The homogeneous ECM (equivalent to the conceptual model shown in Fig. 4.1B) was built as a uniform cube and hydraulic properties were adjusted to obtain flow rates similar to those in the heterogeneous models. To alleviate the geometrical complexity in GeoStudio, models were conceptualizing according to the structural orientation. It is important to keep in mind that horizontal fracture sets are typically discontinuous, poorly constrained, and largely sealed under in situ stress, contributing minimally to regional transmissivity (Selroos et al. 2002; Neuman, 2005). Their bulk effect on storage and diffusion in a large scale like the reference site is represented implicitly through rock-matrix parameters. This simplification reduces geometric uncertainties and computational cost while preserving the key hydraulic behaviour relevant to mine dewatering and post-closure mixing (Frape et al., 2014; Hadgu et al., 2017). Table 4.1 summarizes all the known faults and their dip and dip direction. Angles are already considered as structures are imported in GeoStudio. However, this information is presented to have it as a reference. For the sub-horizontal structures, the actual dip value varies from 0 to 25° and was assumed to be 12.5° for all faults. Since the sub-horizontal faults are almost parallel to the azimuth of the horizontal line, it was assumed that the dip is 0° for all faults. Sub-vertical faults orientation information is available except for NW_FX6 and NW_FX9. In this context, NW refers to the general orientation of the fault and FX refers is a fault identifier. However, since the visible orientation of FX6 is similar to FX7 and FX9 to FX8, the values were assumed accordingly.

Table 4.1: Summary of dip values and dip direction of water-conducting faults and structures (in **bold** are the structures used for the Conceptual Geometry 3 shown in Fig 4.1C)

Water-conducting faults/structures used	**Actual Orientation**	**Dip dir. (°)**	**Dip (°)**
F1-110, F1-200, **F2-110**, F2-200, **F2-290**, **F1-140a**, **F1-530**, F1-410, F2-530, **F2-560**, F2-140, F2-170, **F2-1010**, **F2-740**, F1-770a, F1-230, F1-770	Sub-horizontal structures	12.5	0
RAMP_FX1, NW_FX2, NW_FX3, **NW_FX6*,** NW_FX7	Sub-vertical faults	55	70
NW_FX1, NW_FX1a, NW_FX5, NW_FX8, NW_FX9*		35	81

*NW_FX6 and NW_FX9 orientation are not available but are similar to NW_FX7 and NW_FX8, respectively

Ultimately, the fault orientation should be considered to better simulate the extent of the defined geological structures. In fact, these geological structures were interpreted as planes in the model. The 2D planes were extruded to create a 3D object that has thickness. As mentioned previously, this facilitates the material assignation to each surface of the geological structures. The area of interest is defined to be the area where the mine workings are located as well as all the geological structures that were mentioned. With an area of 4 km^2, it can be assured that all faults are enclosed within the medium. Since the objective of this numerical modelling is to have a site-scale assessment, it was important to have the area interest as well as a larger area which includes the surroundings. This will ensure to have a REV. In fact, the depth of the model is 2 km which is deeper than the underground workings. Moreover, the domain encompasses most of the surroundings, including the Opinaca River and the Opinaca Reservoir, the main boundary conditions for this modelling work. A representative cross-section (1,000 m × 2,000 m) was extracted from the centre of the domain to support interpretation of flow and transport behaviour (Fig. 4.2). For reference, in Fig. 4.2, the origin point is where the red and blue lines cross. The blue line represents the z-axis, the red line the x-axis and the green line the y-axis. The planes are located on the negative side of the coordinate system relative to their origin. While the entire section was used for visualizing model outputs, only the portions of structures intersecting this cross-section were considered in subsequent analyses. The orientation of the section is inverted relative to the

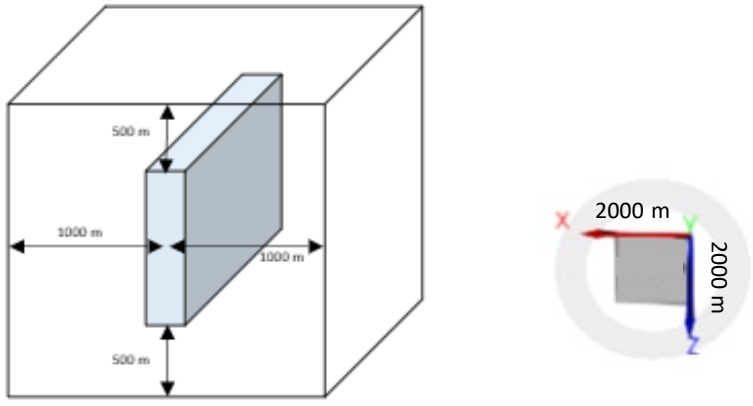

Figure 4.2: GeoStudio 3D model result evaluation: 2D grey rectangle plane representing the cross-section used in the centre of the domain. 3D planes representing the faults are illustrated in orange for the fault model.

domain layout. This location was determined to be the most optimal when using GeoStudio 3D. For the interest of a mine site, it is relevant to observe the general effect in the centre of the domain where the core of the mine openings would be located. The initial mesh size is 50 m. It allowed obtaining reasonable Péclet and Courant Numbers in the defined cross-section area.

4.4 Material Properties and Input Parameters

To allow better modelling convergence, faults were attributed permeable properties. The hydraulic conductivity assigned is 1×10^{-5} m/s. Despite the flow and transport is led by the main fracture orientation (vertical flow), the hydraulic conductivity is defined as isotropic in the model (Kx=Ky=Kz) and all faults were attributed similarly for simplification and model convergence. More specifically, the scale of the model is larger than the local structure anisotropy. The porosity and water content for the water-conducting structures is 0.1 representing the effective porosity used for transport calculations. An effective porosity of 0.1 helps to better represent the effective storage and flow capacity of a permeable fractured medium in this early-stage model setup. These parameters values were based according to Neuman (2005). The compressibility is assumed to be 1×10^{-11} kPa^{-1} which can also be assumed to be nil and therefore ignored. Neuman (2005) refers to a range from 1×10^{-13} to 1×10^{-11} kPa^{-1} in fractured dominated zones. This can also help to better simulate the storage and transient flow behaviour from its initial state to the evolution of the groundwater movement under stress gradients (Bear et al., 1993), although here, the focus was on steady state flow. The dry density 2000 kg/m^3 was assigned to the fracture zones, reflecting the lower density brecciated material relative to intact crystalline rock (Bense et al., 2013). For this study, we do not explicitly link the stress and pore pressure changes.

Anisotropy transport can be represented with the dispersivity tensors (MacQuarrie & Mayer, 2005; Neuman 2005). Here, in the CTRAN3D simulations, the anisotropy is expressed through dispersivity, allowing the plume to spread in the direction of the main flow. In fact, the longitudinal dispersivity is 100 m and the transversal dispersivity is 1m. The block model has similar parameters as the fault model. The value of each parameter for the block model was calculated by multiplying each parameter by a correction factor. This correction factor was calculated by estimating the geological structure surface area intersecting with the cross-sectional rectangular area as shown in Fig 4.2 and dividing it by the total surface area of the cross-section. Table 4.2 presents a summary

of the properties assigned to the models. The compressibility and inclination of each fault were also important to list.

Table 4.2: SEEP3D & CTRAN3D flow initial input parameters values for through steady state flow (saturated conditions)

Parameters	units	Value	
		Geological Structures model	**Block (Cube) Model**
Saturated Hydraulic Conductivity, K	m/s	1×10^{-5}	8.93×10^{-7}
Porosity, n	-	0.1	8.93×10^{-3}
Hydraulic conductivity Anisotropy	-	1	1
Compressibility	1/kPa	1×10^{-11}	1×10^{-11}
Longitudinal dispersivity, α_L	m	100	100
Transversal dispersivity, α_T	m	1	1
Mesh size, Δx	m	50	50

4.5 Boundary Conditions and Initial Conditions

The boundary conditions were assigned separately for the three conceptual geometries illustrated in Fig. 4.1 to meet the various objectives of the modelling process (Table 4.3). The main objective of the simulations performed with Conceptual Geometry 1 (Fig. 4.1A) was to simulate the flow and solute transport processes along the x-axis within a heterogeneous ECM, for a simple case that can be compared with calculations based on an analytical solution. Thus, in SEEP3D, a hydraulic gradient of 1% was imposed along z with hydraulic heads of h = 2020 m at x = -2000 m and h = 2000 m at x = 0 m. These hydraulic heads allow for maintaining saturated conditions throughout the model. The other boundaries (at the ends of y and z limits) are impermeable, which forces unidirectional flow along x. To simulate transport processes, an arbitrary solute concentration set at 100 g/m^3 was imposed at x = -2000 m, and a free solute output was assigned to the faces located at the other boundaries of the model. This allows for simulating how a solute would migrate along x under a 1% hydraulic gradient. It should be noted that in all models, the effects of changes in fluid density induced by solutes are not represented in GeoStudio; the simulated upward movement reflects the imposed pressure gradients along the structures rather than fully coupled density-

dependent flow. Thus, the absolute concentrations imposed in CTRAN3D do not affect water flow. The main objective of the simulations performed with Conceptual Geometry 2 (Fig. 4.1B) was to simulate the flow and solute transport along the x-axis within a homogeneous ECM, for a simple case that can be compared with calculations based on an analytical solution. The boundary conditions were imposed in the same way as explained above for conceptual geometry 1 (heterogeneous), with the aim of allowing comparison between heterogeneous and homogeneous ECMs. The simulations performed with Conceptual Geometry 3 (Fig. 4.1C) involved three scenarios (Run 1, Run 2, Run 3 in Table 4.3). The objective of run 1 was to create an analogue to Conceptual Geometries 1 and 2, but this time including vertical fracture zones. The boundary conditions were therefore imposed in the same way as for conceptual geometry 1. The objective of run 2 was to better represent non-reactive solute transport in the absence of dewatering. For this run, the boundary conditions in SEEP3D remained unchanged, but the boundary conditions in CTRAN3D were adjusted. At x = -2000 m, a concentration of 10 g/m^3 was imposed to conceptually represent regional groundwater flow. At z = 0 m, a concentration of 0 g/m^3 was imposed to represent the inflow of fresh water from the Opinaca Reservoir. At z = -2000 m, a concentration of 100 g/m^3 was imposed to conceptually represent the inflow of deep brine. The objective of Run 3 was to better represent flow and non-reactive solute transport conditions under dewatering conditions. Thus, the boundary conditions in SEEP3D were modified to impose a hydraulic head of 2020 m at all model boundaries except for the x = 0 m plane, where a potential seepage boundary condition was assigned (this allows for simulating dewatering along the x = 0 m plane). The boundary conditions imposed in CTRAN3D remained the same as those imposed in Run 2.

Table 4.3: Boundary and initial conditions throughout model domains

Conceptual model domain	**Solver**	**Applicable surface**					
		x = -2000 m plane	x = 0 m plane	y = -2000 m plane	y = 0 m plane	z = -2000 m plane	z = 0 m plane
Conceptual geometry 1 (Fig. 4.1A)	SEEP3D	h = 2020 m	h = 2000 m	No flow	No flow	No flow	No flow
	CTRAN3D	C = 100 g/m^3	Free exit	Free exit	Free exit	Free exit	Free exit
Conceptual geometry 2 (Fig. 4.1B)	SEEP3D	h = 2020 m	h = 2000 m	No flow	No flow	No flow	No flow
	CTRAN3D	C = 100 g/m^3	Free exit	Free exit	Free exit	Free exit	Free exit
Conceptual geometry 3, Run 1 (Fig. 4.1C)	SEEP3D	h = 2020 m	h = 2000 m	No flow	No flow	No flow	No flow
	CTRAN3D	C = 100 g/m^3	Free exit	Free exit	Free exit	Free exit	Free exit
Conceptual geometry 3, Run 2 (Fig. 4.1C)	SEEP3D	h = 2020 m	h = 2000 m	No flow	No flow	No flow	No flow
	CTRAN3D	C = 10 g/m^3	Free exit	Free exit	Free exit	C = 100 g/m^3	C = 0 g/m^3
Conceptual geometry 3, Run 3 (Fig. 4.1C)	SEEP3D	h = 2020 m	**Seepage**	h = 2020 m	h = 2020 m	h = 2020 m	h = 2020 m
	CTRAN3D	C = 10 g/m^3	Free exit	C = 10 g/m^3	C = 10 g/m^3	C = 100 g/m^3	C = 0 g/m^3

4.6 Model Calibration and Validation

The modelling objective was primarily conceptual understanding and sensitivity analysis rather than detailed predictive calibration. This approach is consistent with early-stage conceptual or sensitivity models where the primary objective is to evaluate relative system responses rather than the reproduction of exact field conditions (Anderson et al., 2015). The model validation focused on numerical stability, convergence, and physical plausibility of results. For example, prior to the sensitivity analysis, the mesh density was progressively refined until the hydraulic heads and flow vectors stabilized. This was a key indicator for model convergence independent of the mesh size. Model conditions were applied for model convergence. For the SEEP3D solver, a maximum of 10 iterations was allowed to have the model re-evaluate boundary conditions when convergence was not achieved. Adaptive under-relaxation was applied to maintain numerical stability. The objective to set an under-relaxation is to have a numerical technique that slows down the solution changes between iterations to allow the solver to converge smoothly and avoid numerical instability (Geo-Slope, 2015). The conditions established are summarized in Table 4.4. Model validation can be ensured by running some simulations and apply the following four criteria to the results within the cross-section shown in Fig 4.2:

- Ensuring the median of Péclet (Pe) number is < 2
- Ensuring the median of Courant (Co) number is < 1
- Comparing the analytical method to determine the flow using the 1st principle of Darcy's Law with the seepage modelling results. The surface area needs to be adjusted to consider only the area that the structures take in the cross-sectional area. This can be estimated with GeoStudio by overlapping the 3D structures to the plane and calculate the represented surface area. This surface is then used to obtain a proportional factor to find the equivalent hydraulic conductivity and porosity used in the analytical solution. In fact, for 10 m thick sub-horizontal structures the area estimated is 178576.6 m^2. For 5 m thick sub-horizontal structures, the area estimated is 96107.1 m^2. The 10 m thick sub-vertical faults area estimated is 141980.6 m^2.
- Comparing the analytical method to determine the concentration using Ogata-Bank (Ogata, 1970) method with the transport modelling results, more specifically comparing $C/C_0 = 0.5$.

For better visualization these criteria were plotted, and for the comparative criteria, the analytical and modelling results were plotted to compare with the baseline model simulations. This is further discussed in Chapters 5 and 6.

The Ogata-Bank method provides an analytical solution to 1D advection-dispersion equation, used to simulate solute transport in groundwater through steady-state flow conditions. It assumes a constant seepage velocity and uniform dispersion, and an initial solute-free domain subjected to a constant solute concentration from the source. This analytical is ideal to use for comparison with the CTRAN3D results (Geo-Slope, 2012). The function describes a concentration with distance and time as shown in eq. 4.7:

$$C(l,t) = C_0 \left[erfc\left(\frac{l - \bar{v}t}{2sqrt(D_l t)}\right) + \exp\left(\frac{\bar{v}l}{D_l}\right) erfc\left(\frac{l + \bar{v}t}{2\sqrt{D_l t}}\right)\right] \tag{4.7}$$

Where C(l,t) is the solute concentration at position l and time t (M/L^3), C_0 is the source concentration (M/L^3), D_l is the hydrodynamic dispersion previously seen in eq. 2.9 (L^2/T), t is time (T), and l is the distance from the source (L).

Furthermore, results were assessed for physical plausibility against gradients and flow patterns derived from the site conceptualization. In fact, the results are further discussed in Chapter 5. The simulated groundwater flow reproduces the general pattern inflow toward underground openings inferred from site dewatering in field conditions. Even if the model has simplified conditions to evaluate the site-wide impacts instead of localized impacts, this study still helps to identify the applicability of the model strategy and the early-stage conceptualization using GeoStudio 3D.

Table 4.4: Model convergence conditions for SEEP3D and CTRAN3D solvers

Conditions	Solver used in GeoStudio	
	SEEP3D	**CTRAN3D**
# Iterations	500	50
Max. pressure head / concentration difference	0.005 m	10 g/m^3
Significant digits equal	2	2
Max. number reviews	10	-
Initial rate	1	-
Min. rate	0.1	-
Rate reduction factor	0.65	-
Reduction frequency (# iterations)	10	-

4.7 Sensitivity Analysis

The simpler model structure (design geometry 1; Fig 4.1A) allows a system sensitivity testing. The sub-horizontal structures as well as the ECM cube models underwent to a screen-level sensitivity analysis was conducted in order to determine which parameters influenced the most the flow and transport, particularly, the equivalent hydraulic conductivity and effective permeability. While preserving the same parameter values as the initial model as shown in Table 4.2, only one parameter at a time was changed to test if the model results are relatively similar to the analytical solution using Ogata-Bank. This solution is used to predict solute transport and concentration through a homogeneous and isotropic porous aquifer (Bear et al., 1993). Table 4.5 summarizes the different scenarios tested and analyzed. While preserving the same evaluation approach, boundary conditions and initial conditions presented in Table 4.3. On top of testing the effect of dip and dip direction on each structure presented in Table 4.1, another set of analysis is to vary the hydraulic conductivity by a factor of 10 through all structures. The initial thought, regardless of the axis, the more gradient there is the more flow there will be through the faults. However, according to what was previously reviewed with mine dewatering, the flow rate and transport would get more impacted in the vertically with respect to ground level. The second set of analysis consists of varying the porosity by increasing and decreasing initial value. Understandably, more permeable properties would allow more flow, but it will depend on the effective permeability and the interconnectivity of each pore. A higher porosity could allow more storage zone and lower the seepage if there is poor connectivity. A set of analyses evaluates the change of longitudinal and

transversal dispersivity values. The higher the value of dispersivity the more plume is expected to travel according to the impacted axis. Another set of analysis evaluates the change of gradient across all faults. The lower the value, the less flow is expected. There is also a set of analysis looking at coarser vs a finer mesh and how this impacts results. It is expected, with a coarser mesh, to have more convergence but possible underestimation of the solute transport. Another set of sensitivity analysis was done using a smaller structural thickness. The expected results are to have more flow as the structure thickness increases. Although under GeoStudio, the thickness acts like an aperture of a drainage channel (i.e. fault). In real conditions, the flow wouldn't necessarily flow through the entire thickness of a specific fault. As part of the model objective and in order to test the validity of using an ECM, two different groups of structures arbitrarily selected were each assigned a hydraulic conductivity with a relative smaller variation. Preserving the same group of structures, a similar simulation was reproduced with a larger variation of hydraulic conductivity. The analysis and interpretation results are presented in Chapter 5 & 6 respectively.

Table 4.5: Parameters considered for the sensitivity analysis for horizontal structures with 5 m and 10 m thickness and the ECM cube models

Simulation	**Modified parameters**
Sensitivity 1	Hydraulic conductivity (K) / 10
Sensitivity 2	Hydraulic conductivity (K) × 10
Sensitivity 3	Porosity (n) × 5
Sensitivity 4	Porosity (n) / 5
Sensitivity 5	Longitudinal and transversal dispersivity (α_L & α_T) × 5
Sensitivity 6	Longitudinal and transversal dispersivity (α_L & α_T) / 5
Sensitivity 7 *	Hydraulic gradient (i) / 10
Sensitivity 8	Mesh size × 2
Sensitivity 9	Mesh size / 2
Sensitivity 10	50% of K × 2; 50% of K / 2
Sensitivity 11	50% of K × 5; 50% of K / 5

**Sensitivity 7 was done by adjusting the boundary conditions H_i = 2002m to H_o = 2000*

CHAPTER 5 ANALYSIS OF RESULTS

This chapter presents numerical results from the groundwater flow and solute transport simulations. Results are organized by the overall geometry, consistent with the conceptual model: sub-horizontal structures (Fig, 4.1A), ECM cube (Fig. 4.1B) and sub-horizontal structures and sub-vertical structures (Fig. 4.1C). Results are also organized according to the simulation ran as part of the sensitivity of analysis where a single parameter was varied at a time as shown in Table 4.5. The sub-horizontal structures were also used to introduce a discretization to the hydraulic conductivity as presented in Sensitivities 10 and 11 from the Table 4.5 and Fig. 4.2. All simulations are compared with a baseline simulation for the three types of geometry that uses the initial input parameters summarized in Table 4.2. All runs are also verified with these criteria: looking at the distribution curves of the Pe number (< 2) and Courant number (< 1), comparing the analytical results for the median flow and solute concentration with model node results. All central tendencies are reported as values (Pe_{50}, Co_{50}) with the 10^{th} (Pe_{10}, Co_{10}) and 90^{th} (Pe_{90}, Co_{90}) percentiles ensure model stability throughout the distribution and also identified any isolated exceedance as part of validation criteria. Ogata-Banks method results were plotted between 40,000 and 360,000 days depending on the flow rate with different time intervals to reproduce the breakthrough curve using eq. 4.8 (i.e. analytical recovery curve). Compilation of results are summarized at each subsection:

- **5.1. Heterogeneous Sub-Horizontal Structures (Conceptual Geometry 1):** Table 5.1 summarizes results from 10 m thick sub-horizontal structures model (Fig, 4.1A), through Sensitivities 1 to 9. Table 5.2 summarizes results from 5 m thick sub-horizontal structures model (Fig, 4.1A), through Sensitivities 1 to 9.
- **5.2. Sub-Horizontal Structures with 10 m thick and variable K (Conceptual Geometry 1)**: Table 5.3 summarizes results from 10 m thick sub-horizontal structures (Fig, 4.1A) with variable K through Sensitivity 10 & 11.
- **5.3. Cube ECM (Conceptual Geometry 2):** Table 5.4 summarizes results from the ECM block model (Fig, 4.1B), through Sensitivities 1 to 9.
- **5.4. Sub-Vertical and Sub-Horizontal Structures (Conceptual Geometry 3):** Grouping 16 structures and running 3 different scenarios, to replicate simulations from geometries 1 and 2, to simulate the system under non-dewatering conditions and dewatering conditions.

5.1 Heterogeneous Sub-Horizontal Structures (Conceptual Geometry 1)

5.1.1 Groundwater Flow Results

In general, the flow rates simulated in SEEP3D and those calculated using Ogata's solution are very similar, as can be seen by comparing the simulated breakthrough curves with the breakthrough curves calculated using the analytical solution (Tables 5.1 and 5.2). The time associated with passing point $C/C_0 = 0.5$ (i.e., $C = 50$ g/m^3) in the recovery curve is a good indicator of the velocity of the advection front. The consistency observed in the group of graphs (Fig. 5.1 and 5.2) suggests that the analytical solution and the model are consistent in terms of advection.

The Ogata function is represented in green in Fig. 5.1 and Fig 5.2. The median concentration model results at given times are represented with the burgundy dots and the dash lines represent the distribution curves for the model 25th and 75th percentile concentration with respect to time. The main observations are summarized as follows, for different pairs of sensitivity analyses:

- **K variations**: In sensitivity 1, as the hydraulic conductivity decreases, the recovery curve flattens and shifts towards the right. Model and analytical results are comparable. $C/C_0 \geq 0.99$ is reached at approximately 284 400 days. In sensitivity 2, as the hydraulic conductivity increases, the recovery curve has a sharper breakthrough model and shifts to the left. $C/C_0 \geq 0.99$ is reached at approximately 2 900 days.
- **n variations**: In sensitivity 3, as the porosity increases this reduces the velocity, the recovery curve shifts to the right. Both analytical and model recovery curves are comparable. $C/C_0 \geq 0.99$ is reached at approximately 142 000 days. In sensitivity 4, as the porosity decreases, this causes an opposite effect to the velocity and peak concentration compared to sensitivity 3. Both recovery curves are comparable. $C/C_0 \geq 0.99$ is reached at approximately 5 700 days.
- **α variations**: In sensitivity 5, as the dispersion is enhanced, the peak concentration decreases and the breakthrough curve flattens. Both analytical and model recovery curves are similar. $C/C_0 \geq 0.99$ is reached at approximately 57 750 days. In sensitivity 6, as the dispersion is reduced, the peak concentration increases and the recovery curve is steeper. Both analytical and model recovery curves are similar. $C/C_0 \geq 0.99$ is reached at approximately 18 000 days.

- **i variation**: In sensitivity 7, as the gradient decreases a similar effect is observed as sensitivity 1. Model results are consistent with the analytical results. $C/C_0 \geq 0.99$ is reached at approximately 284 400 days.
- **Mesh refinement**: In sensitivity 8, as the mesh size increases, the model curve is smoother than the analytical curve near the crest. $C/C_0 \geq 0.99$ is reached at approximately 28 400 days. In Sensitivity 9, as the mesh size decreases, there is overall a sharper curve and a reduction of numerical dispersion, and peak concentration aligns better with the analytical results. Minor node differences can still ensure numerical stability. $C/C_0 \geq 0.99$ is reached at the same time as sensitivity 8 at approximately 28 400 days.

5.1.2 Numerical Quality (Péclet and Courant Number Distribution)

In the case of the baseline simulation, over the distance travelled, the Courant number was < 1 for most of the output results. Close to 80% of the results have the median Péclet number under the established criterion. The sensitivity analyses results are summarized below:

- **K variations**: In sensitivity 1, as the K decreases allowing proportionally less flow through the structures. The Courant Number and Péclet Number distributions are similar to the baseline simulation. In sensitivity 2, as the K increases allowing proportionally more flow through the structures. The Courant Number results were higher not complying to the criterion. The Péclet Number median was under the criteria but similar to the baseline simulation results. This indicates that, as the flow increases, there is model instability.
- **n variations**: In sensitivity 3, as the porosity increases, the velocity is decreased allowing comparative Courant and Péclet Number distribution is similar to the baseline. In sensitivity 4, as the porosity decreases, the velocity increases and the median Courant number does not comply with the criterion. The Péclet number results are for the most part under the criterion similar to the baseline.
- **α variations**: In sensitivity 5, as the longitudinal and transversal dispersivities increase, simulating more plume propagation, most of the Péclet and Courant Number results distribution comply with the established criteria. In sensitivity 6, as the longitudinal and transversal dispersivities decrease, simulating less plume propagation, most of the Courant Number complies with the criterion. The Péclet Number results are above the criterion

established. This indicates that as the dispersivity increases across a plane, the model can become unstable.

- **i variation**: In Sensitivity 7, as the gradient decreases forcing the flow to decrease, there are similar results as sensitivity 1.
- **Mesh refinement**: In sensitivity 8, as the mesh size increases the Péclet and Courant Number distributions generally complied with recommended criteria expect for their upper end distribution of the Péclet Number results. In sensitivity 9, as the mesh size decreases the Péclet and Courant Number distributions generally complied with recommended criteria. This might indicate, as the mesh size decreases, the numerical stability might be better compared to results from sensitivity 8.

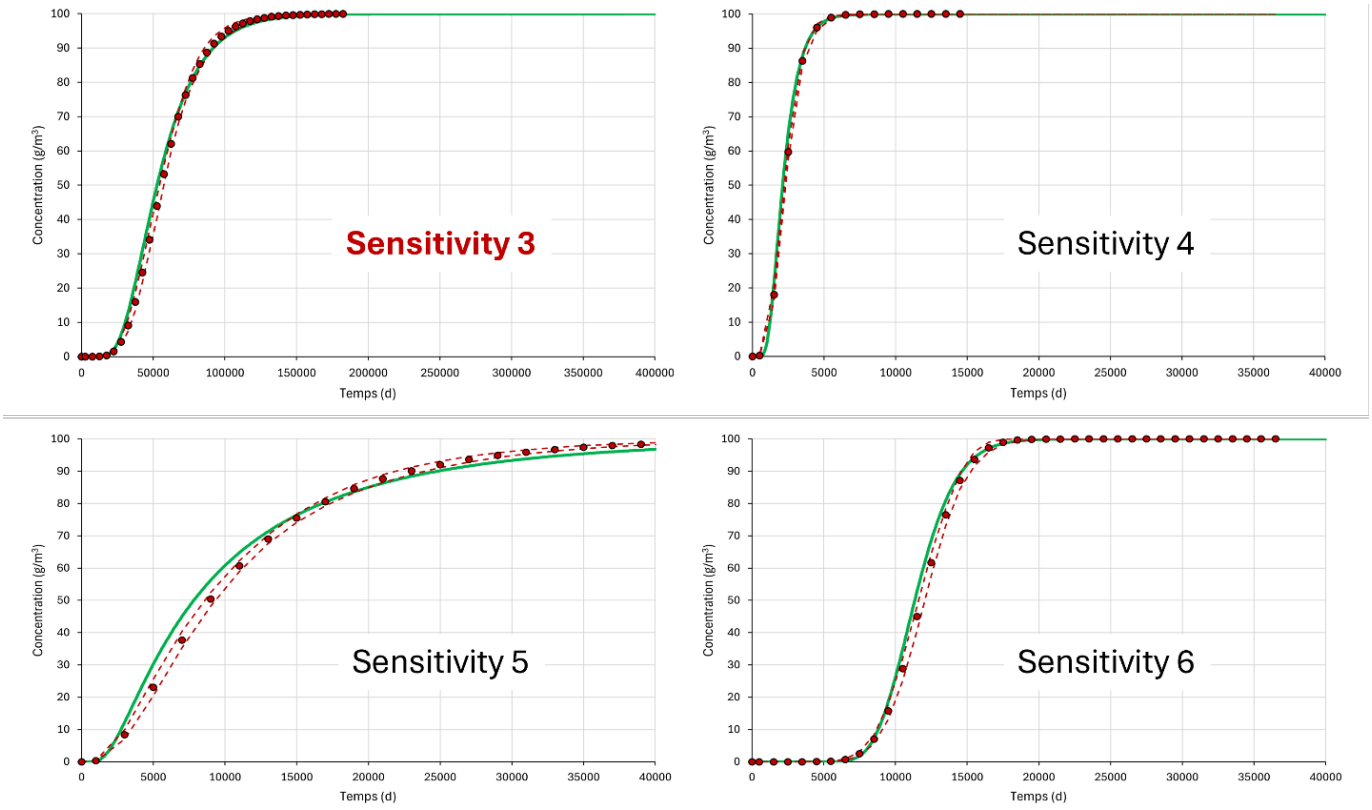

Figure 5.1: 10 m thick Sub-Horizontal Structure for Conceptual Geometry 1 breakthrough curves through the sensitivity analyses 1 to 9. In bold red characters, the breakthrough curves have a different time scale.

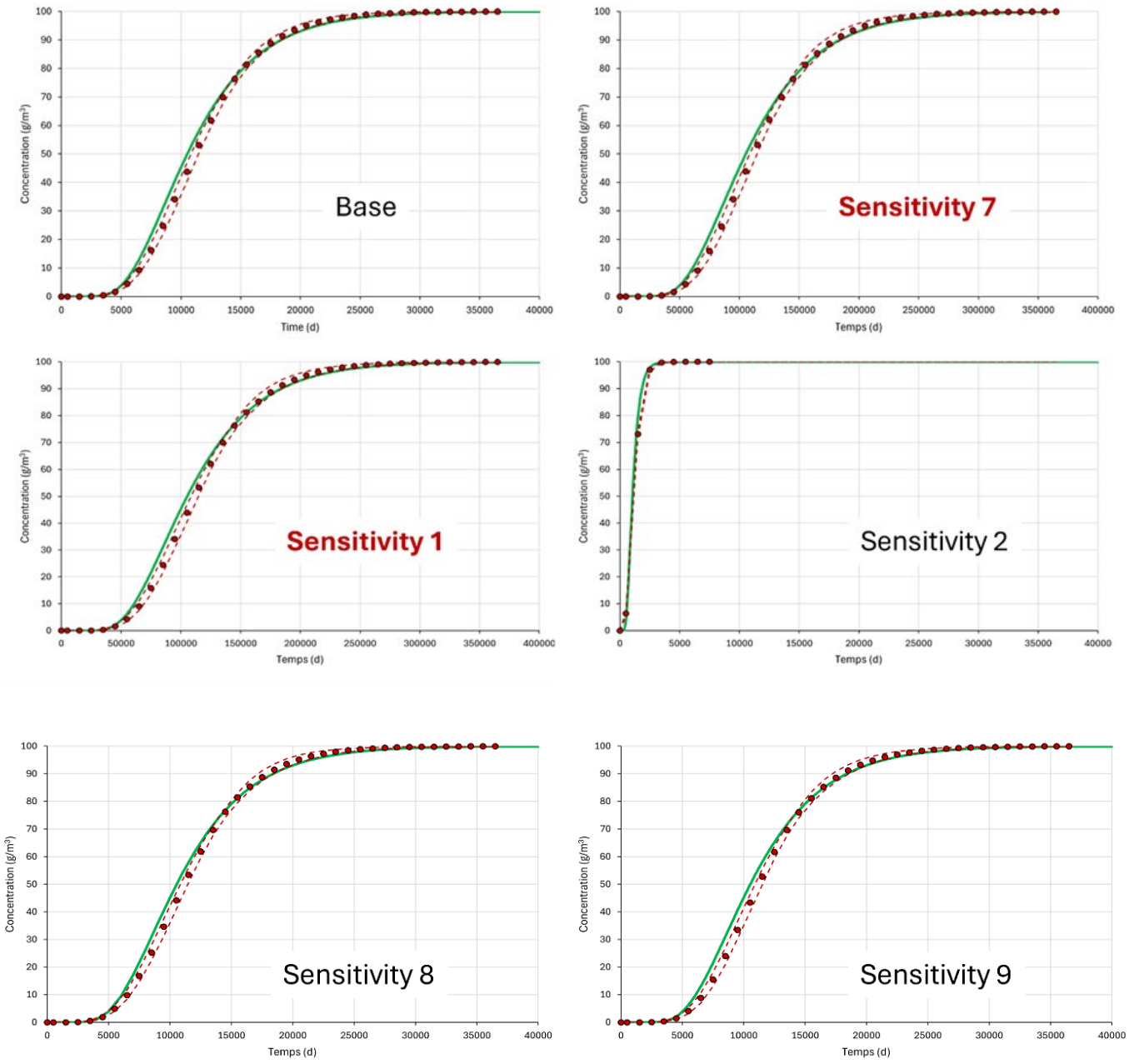

Figure 5.1 (continued):10-m thick Sub-Horizontal Structure for Conceptual Geometry 1 breakthrough curves through the sensitivity analyses 1 to 9. In bold red characters, the breakthrough curves have a different time scale.

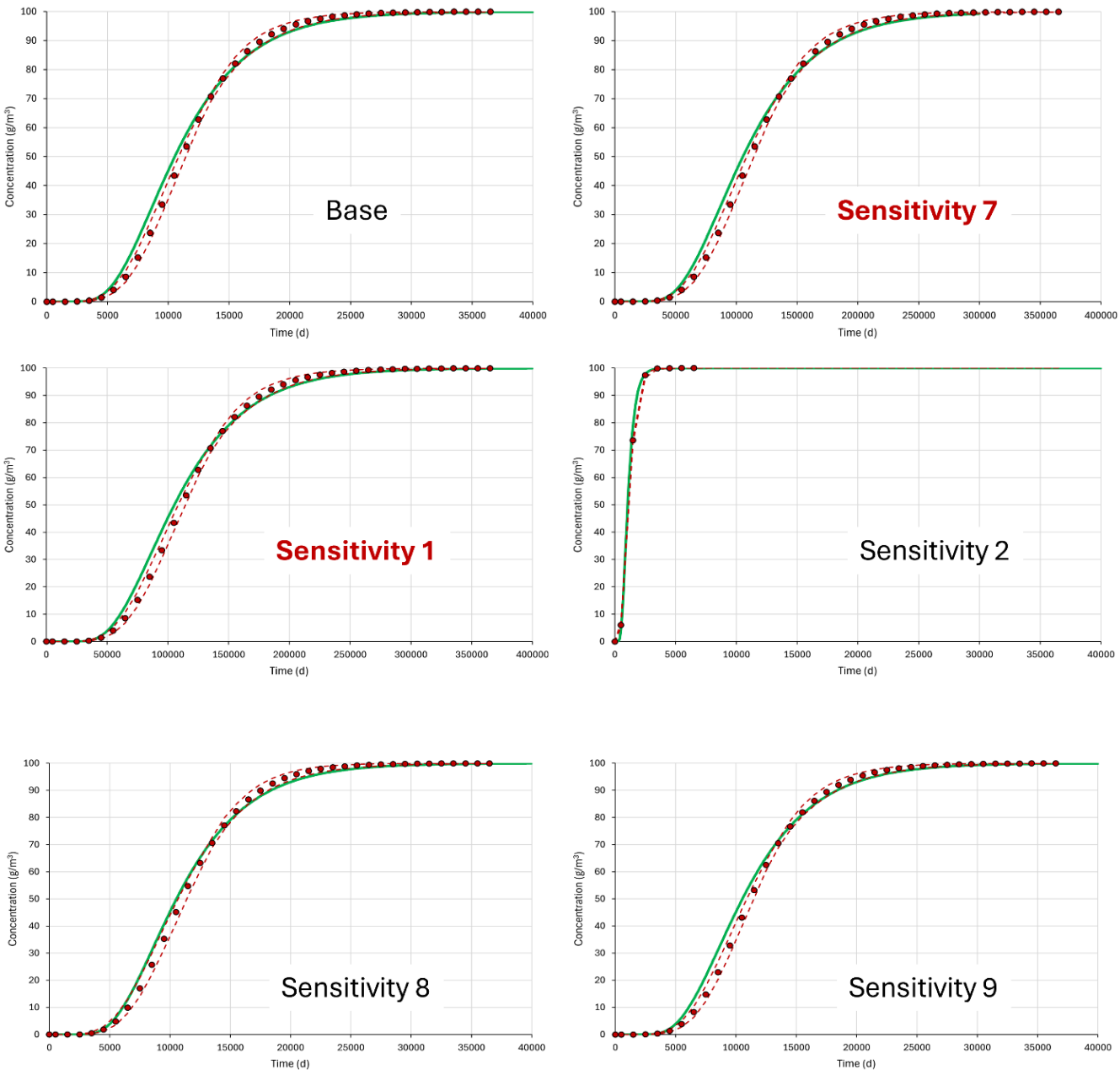

Figure 5.2: 5-m thick Sub-Horizontal Structure for Conceptual Geometry 1 breakthrough curves through the sensitivity analyses 1 to 9. In bold red characters, the breakthrough curves have a different time scale.

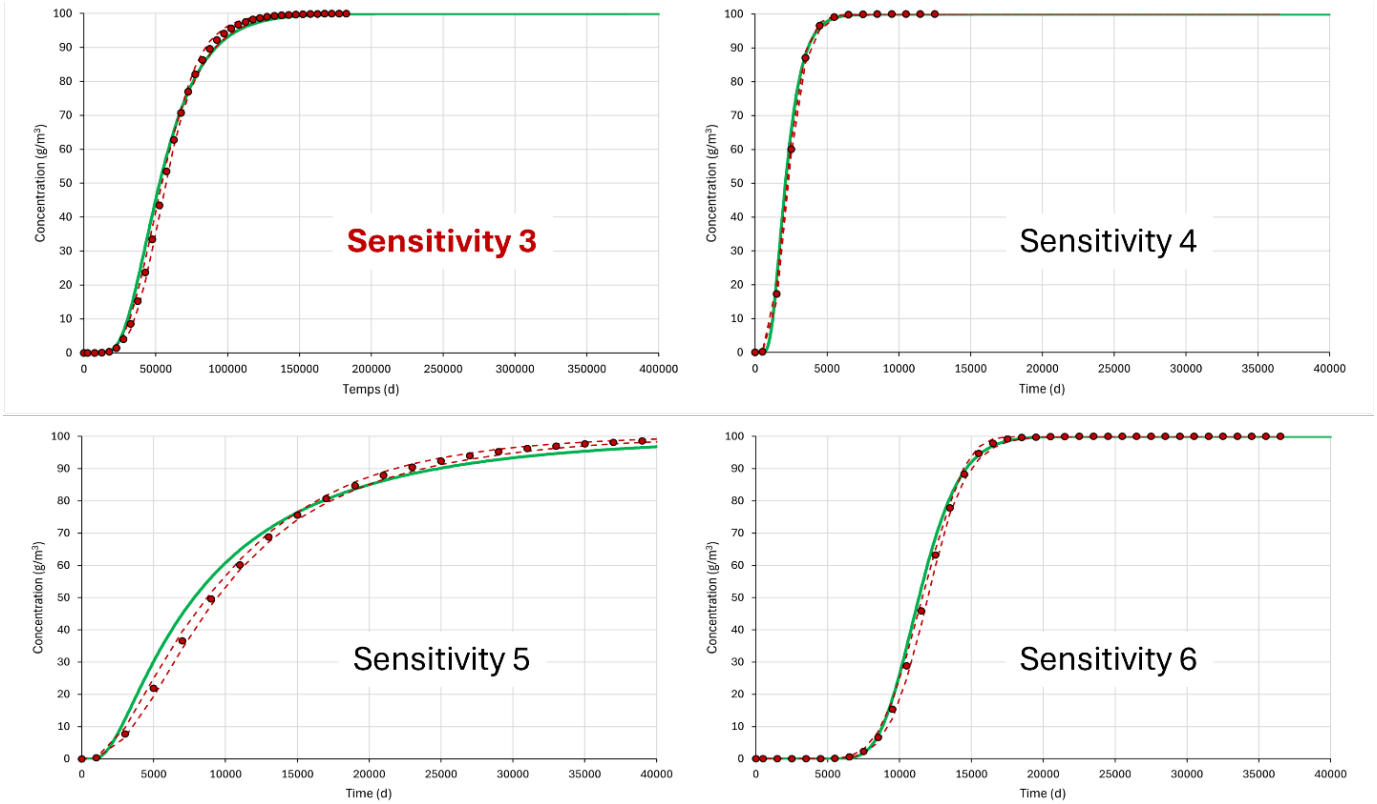

Figure 5.2 (continued): 5-m thick Sub-Horizontal Structure for Conceptual Geometry 1 breakthrough curves through the sensitivity analyses 1 to 9. In bold red characters, the breakthrough curves have a different time scale.

Table 5.1: 10-m sub-horizontal structures summary input parameters and results for comparison between model and analytical solution

Run	Approach	K (m/s)	n (-)	α_L (m)	α_T (m)	i (m/m)	Mesh (m)	Q_{total} (m^3/s)	t, $C/C_{0\ 50}$ (days)	Pe_{10}	Pe_{50}	Pe_{90}	Co_{10}	Co_{50}	Co_{90}
Baseline	Analytical	8.93×10^{-7}	0.00893	100	1	0.01		0.018	10500						
Baseline	Model	1.00×10^{-5}	0.1	100	1	0.01	50	0.018	11300	0.70	1.04	2.04	0.19	0.21	0.32
Sensitivity 1	Analytical	8.93×10^{-8}	0.00893	100	1	0.01		0.0018	105300						
Sensitivity 1	Model	1.00×10^{-6}	0.1	100	1	0.01	50	0.0018	113000	0.70	1.03	2.03	0.19	0.21	0.32
Sensitivity 2	Analytical	8.93×10^{-6}	0.00893	100	1	0.01		0.18	1050						
Sensitivity 2	Model	1.00×10^{-4}	0.1	100	1	0.01	50	0.18	1000	0.70	1.04	2.05	1.86	2.10	3.18
Sensitivity 3	Analytical	8.93×10^{-7}	0.00446	100	1	0.01		0.018	52650						
Sensitivity 3	Model	1.00×10^{-5}	0.5	100	1	0.01	50	0.018	56000	0.70	1.03	2.04	0.19	0.21	0.32
Sensitivity 4	Analytical	8.93×10^{-7}	0.00179	100	1	0.01		0.018	2150						
Sensitivity 4	Model	1.00×10^{-5}	0.02	100	1	0.01	50	0.018	2200	0.70	1.04	2.05	0.93	1.05	1.59
Sensitivity 5	Analytical	8.93×10^{-7}	0.00893	500	5	0.01		0.018	7800						
Sensitivity 5	Model	1.00×10^{-5}	0.1	500	5	0.01	50	0.018	9000	0.14	0.21	0.41	0.37	0.42	0.64
Sensitivity 6	Analytical	8.93×10^{-7}	0.00893	20	0.2	0.01		0.018	11350						
Sensitivity 6	Model	1.00×10^{-5}	0.1	20	0.2	0.01	50	0.018	12000	3.48	5.17	10.19	0.19	0.21	0.32
Sensitivity 7	Analytical	8.93×10^{-7}	0.00893	100	1	0.001		0.0018	105300						
Sensitivity 7	Model	1.00×10^{-5}	0.1	100	1	0.001	50	0.0018	113000	0.69	1.03	2.03	0.19	0.21	0.32
Sensitivity 8	Analytical	8.93×10^{-7}	0.00893	100	1	0.01		0.018	10550						
Sensitivity 8	Model	1.00×10^{-5}	0.1	100	1	0.01	100	0.018	11300	0.61	1.29	2.64	0.11	0.19	0.35
Sensitivity 9	Analytical	8.93×10^{-7}	0.00893	100	1	0.01		0.018	10550						
Sensitivity 9	Model	1.00×10^{-5}	0.1	100	1	0.01	25	0.018	11300	0.51	0.74	1.18	0.37	0.40	0.47

Table 5.2: 5-m sub-horizontal structures summary input parameters and results for comparison between model and analytical solution

Run	Approach	K (m/s)	n (-)	α_L (m)	α_T (m)	i (m/m)	Mesh (m)	Q_{total} (m^3/s)	t, $C/C_{0\ 50}$ (days)	Pe_{10}	Pe_{50}	Pe_{90}	Co_{10}	Co_{50}	Co_{90}
Baseline	Analytical	4.81×10^{-7}	0.01	100	1	0.01		0.0096	10600						
Baseline	Model	1.00×10^{-5}	0.1	100	1	0.01	50	0.0095	11500	0.44	0.72	1.67	0.20	0.26	0.46
Sensitivity 1	Analytical	4.81×10^{-8}	0.01	100	1	0.01		0.00096	106000						
Sensitivity 1	Model	1.00×10^{-6}	0.1	100	1	0.01	50	0.00095	115000	0.44	0.71	1.66	0.20	0.26	0.46
Sensitivity 2	Analytical	4.81×10^{-6}	0.01	100	1	0.01		0.096	1100						
Sensitivity 2	Model	1.00×10^{-4}	0.1	100	1	0.01	50	0.095	1500	0.44	0.72	1.67	1.98	2.55	4.57
Sensitivity 3	Analytical	4.81×10^{-7}	0.01	100	1	0.01		0.0096	52800						
Sensitivity 3	Model	1.00×10^{-5}	0.5	100	1	0.01	50	0.0095	57500	0.44	0.72	1.66	0.20	0.26	0.46
Sensitivity 4	Analytical	4.81×10^{-7}	0.01	100	1	0.01		0.0096	2200						
Sensitivity 4	Model	1.00×10^{-5}	0.02	100	1	0.01	50	0.0095	2500	0.44	0.72	1.67	0.99	1.28	2.28
Sensitivity 5	Analytical	4.81×10^{-3}	0.01	500	5	0.01		0.0096	7950						
Sensitivity 5	Model	1.00×10^{-5}	0.1	500	5	0.01	50	0.0095	9000	0.09	0.14	0.33	0.40	0.51	0.91
Sensitivity 6	Analytical	4.81×10^{-3}	0.01	20	0.2	0.01		0.0096	11400						
Sensitivity 6	Model	1.00×10^{-5}	0.1	20	0.2	0.01	50	0.0095	11500	2.20	3.58	8.32	0.20	0.26	0.46
Sensitivity 7	Analytical	4.81×10^{-3}	0.001	100	1	0.001		0.00096	105750						
Sensitivity 7	Model	1.00×10^{-5}	0.1	100	1	0.001	50	0.00095	115000	0.44	0.71	1.66	0.20	0.26	0.46
Sensitivity 8	Analytical	4.81×10^{-3}	0.01	100	1	0.01		0.0096	10600						
Sensitivity 8	Model	1.00×10^{-5}	0.1	100	1	0.01	100	0.0095	11500	0.45	1.04	2.32	0.13	0.24	0.50
Sensitivity 9	Analytical	4.81×10^{-3}	0.01	100	1	0.01		0.0096	10600						
Sensitivity 9	Model	1.00×10^{-5}	0.1	100	1	0.01	25	0.0094	11500	0.33	0.45	1.00	0.38	0.41	0.47

5.2 Sub-Horizontal Structures with 10 m thick and variable K (Conceptual Geometry 1)

5.2.1 Water Flow and Solute Transport Results

Sensitivity 10 intent was to introduce a discretization by increasing or decreasing the hydraulic conductivity in half of the geometrical structures by a factor of 2. As half of the structures have higher hydraulic conductivity, the other half has a smaller hydraulic conductivity, this is a heterogeneity test not simply looking at transmissivity. The results are summarized in Table 5.3. High-K structures would channel more water (i.e. preferential pathways) whereas low-K would behave like a drag. Overall, the equivalent hydraulic conductivity is higher than the baseline simulation. According to the model result, the $C/C_0 \geq 0.99$ would be reached after 30 500 days. The model results do not entirely match the analytical approach as shown in Fig 5.3. Some statistical measures should be integrated for prediction purposes and have a better interpretation. If the overall K increases, the heterogeneity K field shortens breakthrough time compared to the homogeneous baseline.

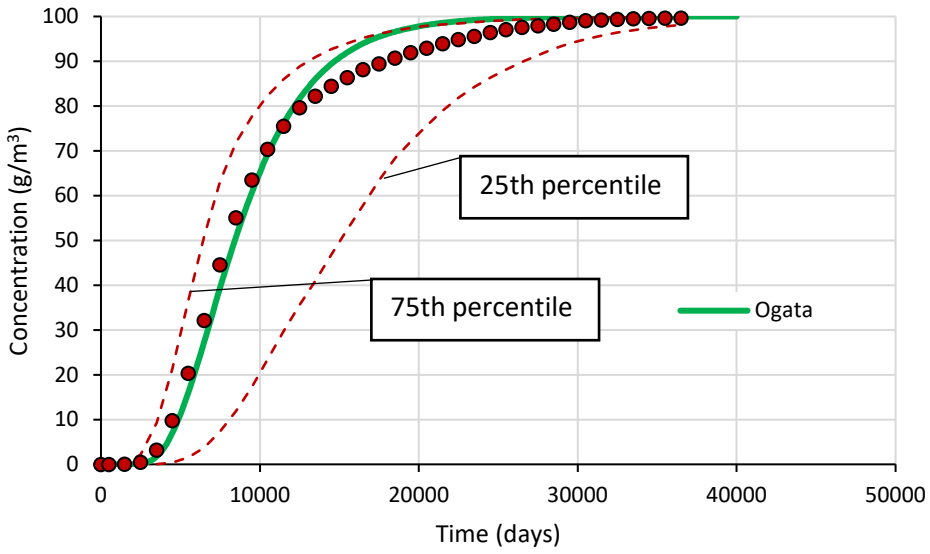

Figure 5.3: Recovery curve for variable K with a factor of 2. Comparing model and analytical results. In green the analytical approach, red dots represent the median concentration, and the dash line represents their 25th and 75th percentiles.

Similarly to sensitivity 10, the intent of sensitivity 11 was to introduce a discretization to test the heterogeneity to the hydraulic conductivity with a larger factor corresponding to 5. The one half would have a higher conductivity acting like preferential pathways, and the other half would have a lower conductivity retaining the flow. High-K structures can lead to effective advective pathways and low-K structures can be considered long-term retention spaces. The $C/C_0 \geq 0.99$ would be reached in approximately 11 000 days as shown in Fig 5.4.

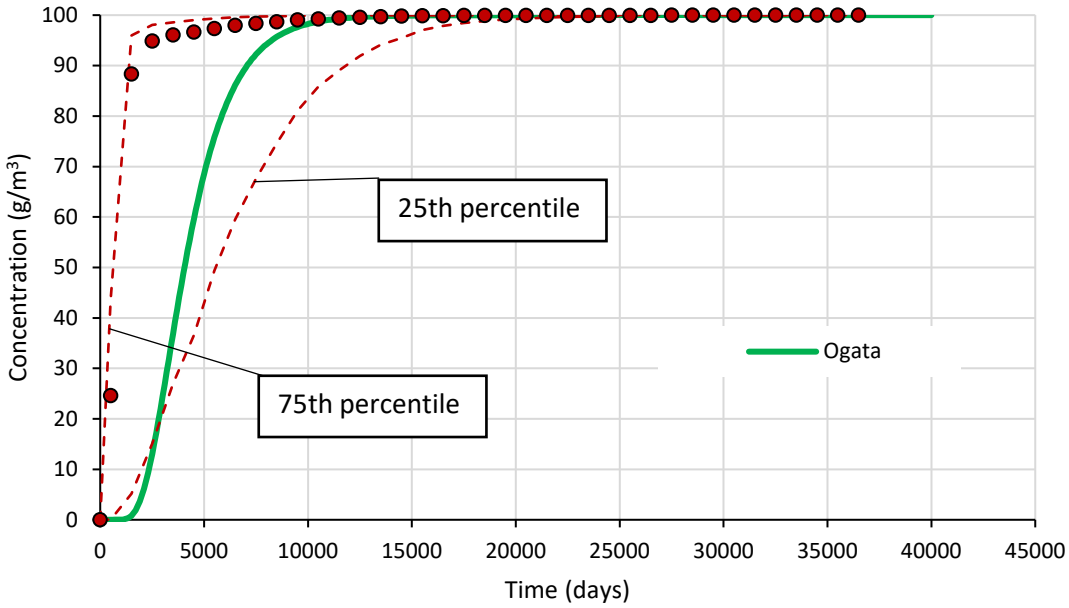

Figure 5.4: Solute transport recovery curves comparing the analytical and model results for K variable with a factor of 5. In green the analytical approach, red dots represent the median concentration, and the dash line represents their 25th and 75th percentiles.

5.2.2 Numerical Quality (Péclet and Courant Number Distributions)

The Péclet Number and Courant Number Distributions are overall under the specified criteria. Péclet Number results are slightly higher at the upper end of the distribution. This presumably shows that the overall numerical regime does not change; low Péclet and Courant values are expected because of the low conductivity. In contrast, the high conductivity causes higher values, more numerical instability.

Table 5.3: 10-m sub-horizontal structures summary input parameters and results for comparison between model and analytical solution for variable K

Run	Approach	K (m/s)	n (-)	α_L (m)	α_T (m)	i (m/m)	Mesh (m)	Q_{total} (m^3/s)	t, C/C_0 50 (days)	Pe_{10}	Pe_{50}	Pe_{90}	Co_{10}	Co_{50}	Co_{90}
Baseline	Analytical	8.93×10^{-7}	0.00893	100	1	0.01		0.018	10500						
Baseline	Model	1.00×10^{-5}	0.1	100	1	0.01	50	0.018	11300	0.70	1.04	2.04	0.19	0.21	0.32
Sensitivity 10	Analytical	1.25×10^{-5}	0.1	100	1	0.01		0.022	8450						
Sensitivity 10	Model	2.00×10^{-5} 5.00×10^{-6}	0.1	100	1	0.01	50	0.020	8000	0.71	1.26	2.15	0.10	0.34	0.48
Sensitivity 11	Analytical	2.60×10^{-5}	0.1	100	1	0.01		0.046	4050						
Sensitivity 11	Model	5.00×10^{-5} 2.00×10^{-6}	0.1	100	1	0.01	50	0.040	600	0.73	1.48	2.27	0.18	3.31	5.80

5.3 Cube ECM (Conceptual Geometry 2)

5.3.1 Water Flow and Solute Transport Results

Table 5.4 summarizes the input parameters and the comparison results for the numerical and analytical solutions. Overall, the results show that the homogeneous ECM and analytical solution results are almost identical. The Ogata function is represented in green in Fig. 5.5. The main observations are summarized as follows, for different pairs of sensitivity analyses:

- **K variations**: In sensitivity 1, as the hydraulic conductivity decreases, it takes more time for the solute to reach its peak. The model results still match the analytical results. $C/C_0 \geq 0.99$ is reached at approximately 280 000 days. In sensitivity 2, as the hydraulic conductivity increases, the recovery curve has a sharper breakthrough model peak. Model results are consistent with the analytical results. $C/C_0 \geq 0.99$ is reached at approximately 2900 days.
- **n variations**: In sensitivity 3, as the porosity increases this reduces the velocity which causes the peak concentration to decrease. Model results are consistent with the analytical results but differ slightly. $C/C_0 \geq 0.99$ is reached at approximately 142 000 days. In sensitivity 4, as the porosity decreases, this causes an opposite effect to the velocity and peak concentration compared to sensitivity 3. Model results are consistent with the analytical results but differ slightly in the upper end distribution. $C/C_0 \geq 0.99$ is reached at approximately 5700 days.
- **α variations**: In sensitivity 5, as the dispersion is enhanced, the peak concentration decreases. Model results are consistent with the analytical results but differ slightly in the upper end of the distribution. $C/C_0 \geq 0.99$ is reached at approximately 56 800 days. In sensitivity 6, as the dispersion is reduced, the peak concentration increases. Model results are consistent with the analytical results but differ slightly. $C/C_0 \geq 0.99$ is reached at approximately 18 000 days.
- **i variation**: In Sensitivity 7, as the gradient decreases, a similar effect is observed as sensitivity 1. Model results are consistent with the analytical results. $C/C_0 \geq 0.99$ is reached at approximately 285 000 days.
- **Mesh refinement**: In sensitivity 8, as the mesh size increases, the peak concentration decreases, and the model curve is smoother than the analytical curve near the crest. $C/C_0 \geq$

0.99 is reached at approximately 28 300 days. In sensitivity 9, as the mesh size decreases, there is overall a sharper curve and a reduction of numerical dispersion, and peak concentration aligns better with the analytical results. Minor node differences can still ensure numerical stability. $C/C_0 \geq 0.99$ is reached at the same time as sensitivity 8 at approximately 28 300 days.

5.3.2 Numerical Quality (Péclet and Courant Number Distributions)

The baseline simulation has Péclet and Courant number distributions which complied with recommended criteria. In fact, their median is 0.857 and 0.102, respectively, ensuring model stability and simulation validation for comparison. The sensitivity analyses results are summarized below:

- **K variations**: In sensitivity 1, as the K decreases allowing proportionally less flow through the structures. The Courant number and Péclet number are similar to the baseline results complying with the established criteria. In sensitivity 2, as the K increases allowing proportionally more flow through the structures. The Courant number results are higher than the established criterion for the upper middle part of the distribution (median = 1.021). The Péclet number median was under the criterion for the most part. This indicates that as the flow increases, there is model instability.
- **n variations**: In sensitivity 3, as the porosity increases, the flow is decreased allowing comparative Courant and Péclet number results to baseline simulations. In sensitivity 4, as the porosity decreases, the flow increases. The Péclet and Courant Number Distributions generally complied with recommended criteria.
- **α variations**: In sensitivity 5, as the longitudinal and transversal dispersivities increase, simulating more plume propagation. The Péclet and Courant Number Distributions generally complied with recommended criteria. In sensitivity 6, as the longitudinal and transversal dispersivities decrease, simulating less plume propagation, most of the Courant Number complies with the criterion for the most part. The Péclet Number results are above the criterion established (median = 4.284). This indicates that as the dispersivity increases across a plane, the model can become unstable.

- **i variation**: In sensitivity 7, as the gradient decreases forcing the flow to decrease, The Courant and Péclet Number Distributions are similar to the baseline simulation.
- **Mesh refinement**: In sensitivity 8, as the mesh size increases, the Péclet and Courant Number distributions are under compliance with the established criteria. In sensitivity 9, as the mesh size decreases, the Péclet and Courant Number distributions are under compliance with the criteria established for the most part.

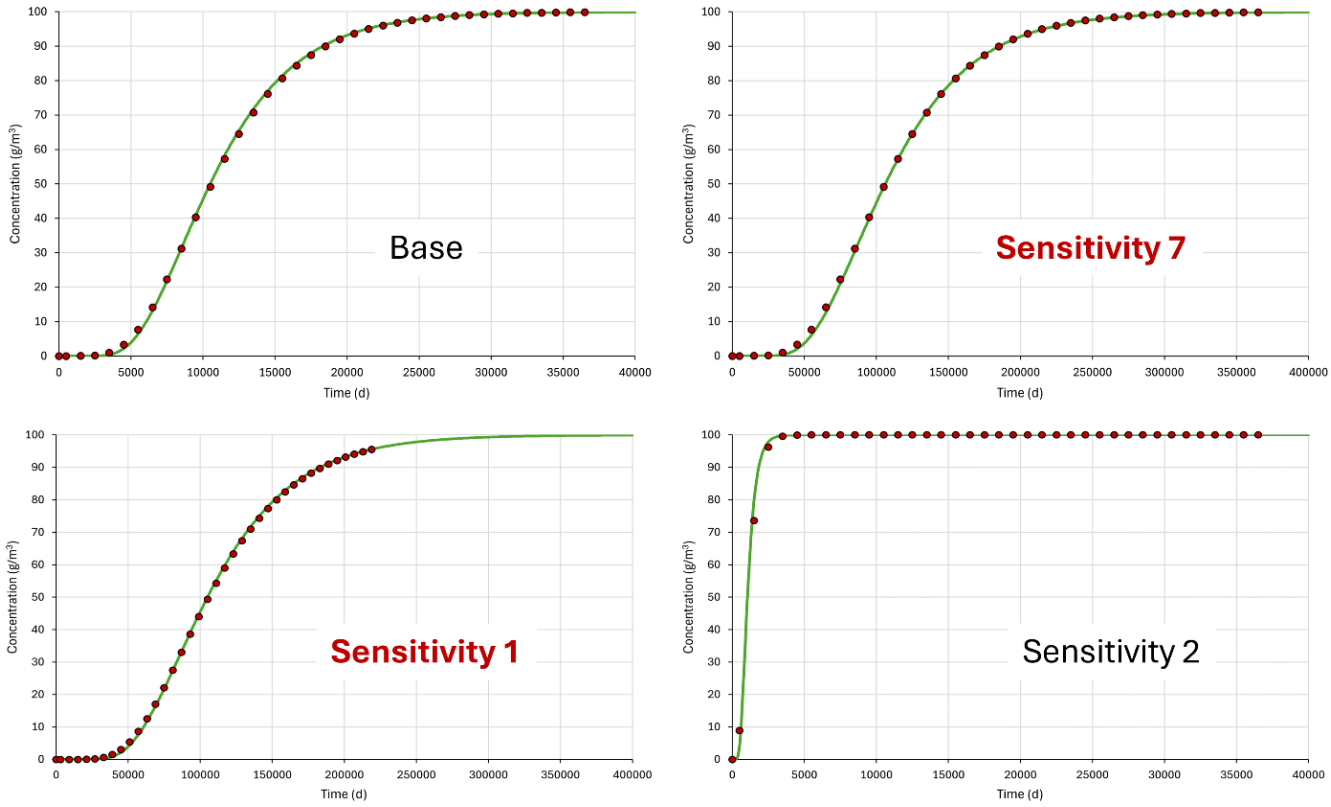

Figure 5.5: Block model for Conceptual Geometry 2 breakthrough curves through the sensitivity analyses 1 to 9. In bold red characters, are analyses that have a different time scale.

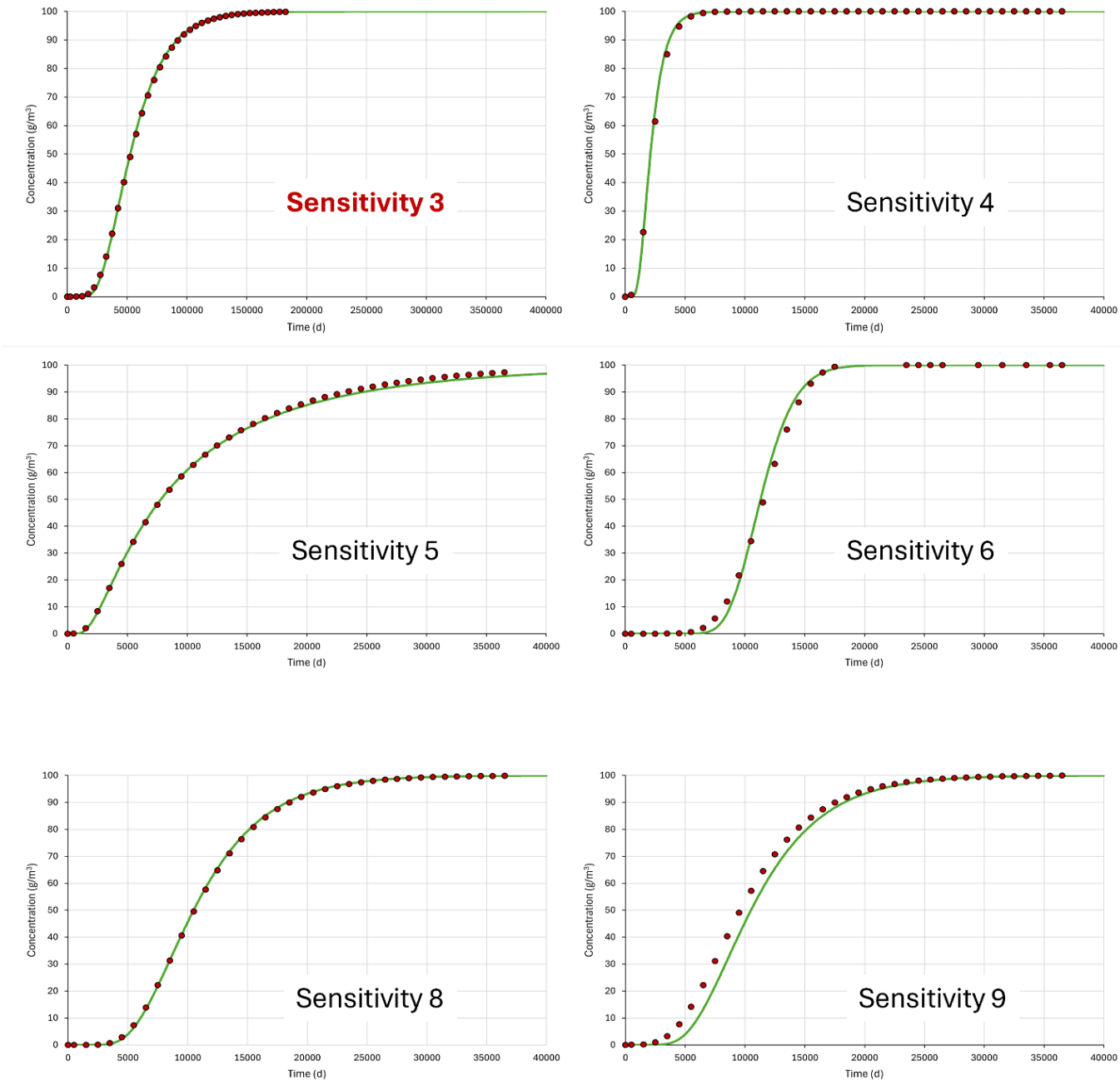

Figure 5.5 (continued): Block model for Conceptual Geometry 2 breakthrough curves through the sensitivity analyses 1 to 9. In bold red characters, are analyses that have a different time scale.

Table 5.4 Block model for ECMs summary input parameters and results for comparison between model and analytical solution

Run	Approach	K (m/s)	n (-)	α_L (m)	α_T (m)	i (m/m)	Mesh (m)	Q_{total} (m^3/s)	t, $C/C_{0\ 50}$ (days)	Pe_{10}	Pe_{50}	Pe_{90}	Co_{10}	Co_{50}	Co_{90}
Baseline	Analytical	8.93×10^{-7}	0.008923	100	1	0.01		0.018	10500						
Baseline	Model	8.93×10^{-7}	0.00893	100	1	0.01	100	0.018	10500	0.81	0.86	0.92	0.10	0.10	0.11
Sensitivity 1	Analytical	8.93×10^{-8}	0.00893	100	1	0.01		0.0018	105050						
Sensitivity 1	Model	8.93×10^{-8}	0.00893	100	1	0.01	100	0.0018	105000	0.81	0.86	0.92	0.06	0.06	0.06
Sensitivity 2	Analytical	8.93×10^{-6}	0.00893	100	1	0.01		0.18	1100						
Sensitivity 2	Model	8.93×10^{-6}	0.00893	100	1	0.01	100	0.18	1500	0.81	0.86	0.92	0.95	1.02	1.07
Sensitivity 3	Analytical	8.93×10^{-7}	0.0446	100	1	0.01		0.018	52800						
Sensitivity 3	Model	8.93×10^{-7}	0.0446	100	1	0.01	100	0.018	52500	0.81	0.86	0.92	0.10	0.10	0.11
Sensitivity 4	Analytical	8.93×10^{-7}	0.00179	100	1	0.01		0.018	2200						
Sensitivity 4	Model	8.93×10^{-7}	0.00179	100	1	0.01	100	0.018	2500	0.81	0.86	0.92	0.47	0.50	0.53
Sensitivity 5	Analytical	8.93×10^{-7}	0.00893	500	5	0.01		0.018	7800						
Sensitivity 5	Model	8.93×10^{-7}	0.00893	500	5	0.01	100	0.018	7500	0.16	0.17	0.18	0.10	0.10	0.11
Sensitivity 6	Analytical	8.93×10^{-7}	0.00893	20	2	0.01		0.018	11400						
Sensitivity 6	Model	8.93×10^{-7}	0.00893	20	2	0.01	100	0.018	11500	4.06	4.28	4.62	0.10	0.19	0.24
Sensitivity 7	Analytical	8.93×10^{-7}	0.00893	100	1	0.001		0.0018	107000						
Sensitivity 7	Model	8.93×10^{-7}	0.00893	100	1	0.001	100	0.0018	105000	0.81	0.86	0.92	0.10	0.10	0.11
Sensitivity 8	Analytical	8.93×10^{-7}	0.00893	100	1	0.01		0.018	10500						
Sensitivity 8	Model	8.93×10^{-7}	0.00893	100	1	0.01	100	0.018	10500	0.40	0.42	0.45	0.20	0.21	0.22
Sensitivity 9	Analytical	8.93×10^{-7}	0.00893	100	1	0.01		0.018	10500						
Sensitivity 9	Model	8.93×10^{-7}	0.00893	100	1	0.01	100	0.018	9500	1.64	1.75	1.84	0.05	0.05	0.05

5.4 Sub-Vertical and Sub-Horizontal Structures (Conceptual Geometry 3)

The simulations performed with conceptual geometry 3 involved three scenarios (run 1, run 2, run 3 in Table 4.3). The objective of run 1 was to create an analogue to conceptual geometries 1 and 2, but this time including vertical fracture zones. The results obtained cannot be directly compared with the analytical solution because the geometry of the model is too complex. Fig 5.6 illustrates the results obtained for the steady-state simulation in SEEP3D. In accordance with the configuration of the boundary conditions imposed (Table 4.3), the model simulates preferential flow along x, with local deformation of the equipotential lines at the intersection of the fracture zones (planar geometries). Fig. 5.7 shows the results obtained in CTRAN3D. The data suggest that the domain is largely occupied by a solute with a concentration close to 100 g/m^3, with lower concentrations near the imposed free exit boundaries (see Table 4.3). Fig 5.8 shows the breakthrough curves obtained for all mesh nodes located on the result recovery plane in the model (as a reminder, this is a plane of 1000 m along y and 2000 m along z placed at x = 1000 m). These results show that the recovery curves take various forms, illustrating the effect of heterogeneity induced by the assembly of vertical and horizontal structures.

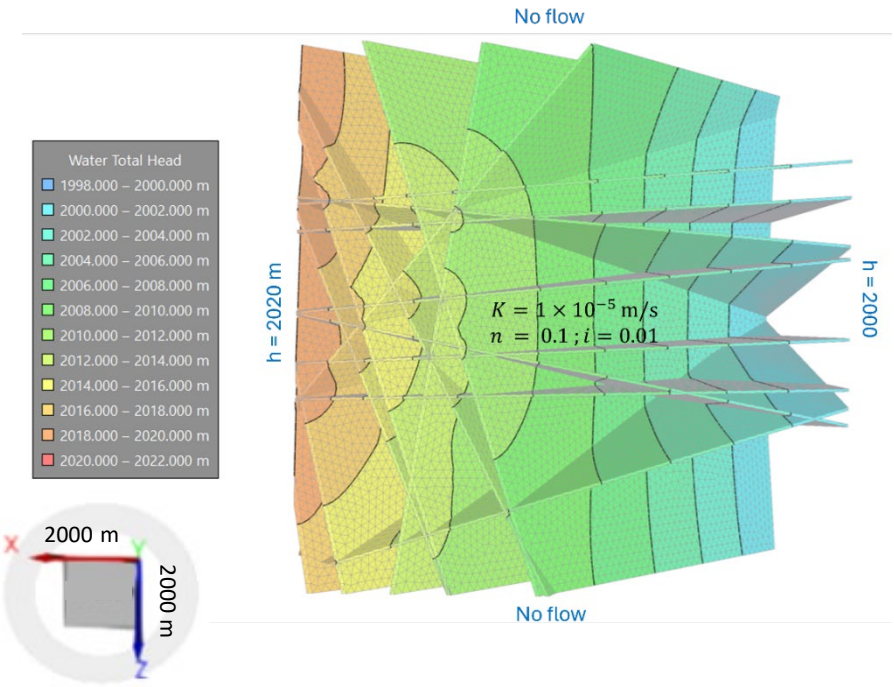

Figure 5.6: Sub-Vertical and Sub-Horizontal Structures model (Conceptual Geometry 3) simulation with SEEP3D through run 1, similar input parameters with respect to Geometries 1 and 2.

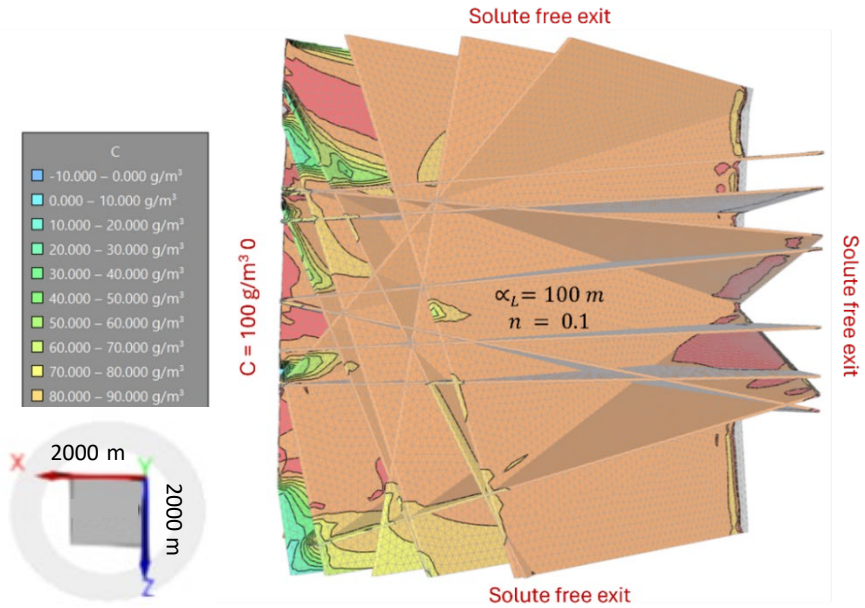

Figure 5.7: Sub-Vertical and Sub-Horizontal Structures model (Conceptual Geometry 3) simulation with CTRAN3D through run 1, similar input parameters with respect to Geometries 1 and 2.

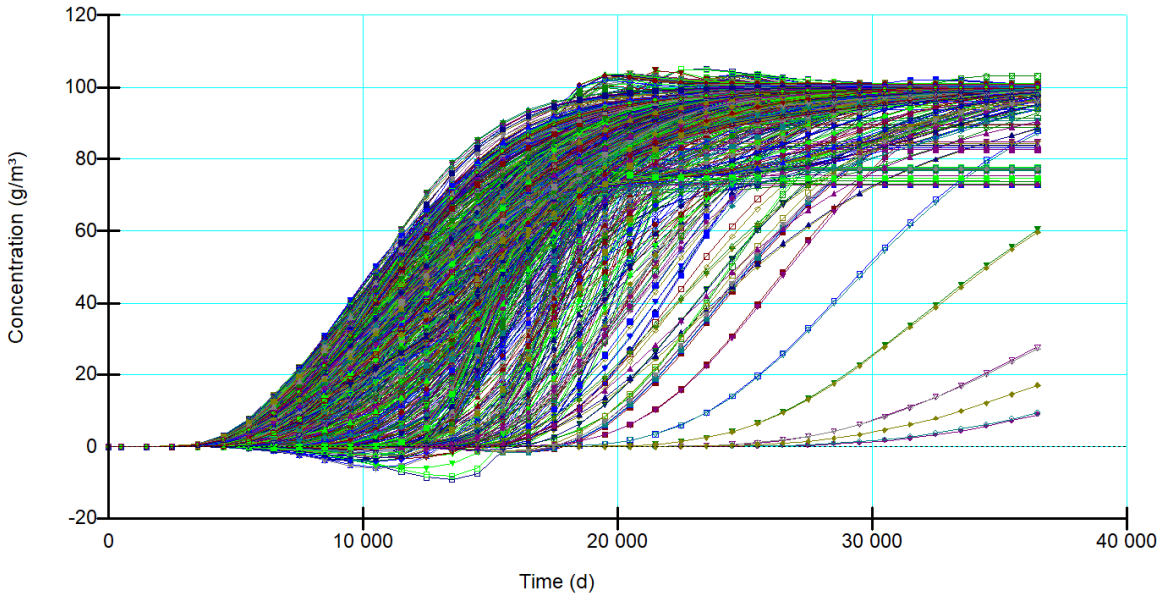

Figure 5.8: Breakthrough curves for Sub-Vertical and Sub-Horizontal Structures model (Conceptual Geometry 3) through run 1

The objective of run 3 was to better represent flow and non-reactive solute transport conditions under dewatering conditions. Although the geometry is significantly simplified compared to real conditions, this model most closely approximates dewatering conditions. As a reminder, the boundary conditions in SEEP3D were modified to impose a hydraulic head of 2020 m at all model boundaries except for the x = 0 m plane, where a potential seepage boundary condition was assigned. The boundary conditions imposed in CTRAN3D were adjusted accordingly. As stated above, at x = -2000 m, a concentration of 10 g/m^3 was imposed to conceptually represent regional groundwater flow. At z = 0 m, a concentration of 0 g/m^3 was imposed to conceptually represent the inflow of fresh water from the Opinaca reservoir located at the surface. At z = -2000 m, a concentration of 100 g/m^3 was imposed to conceptually represent the inflow of deep brines. The results from SEEP3D (Fig. 5.9) suggest flows converging toward the seepage face located at x = 0. The flow rate through the recovery face of the results is estimated at 1,690 m^3/day. The equipotential lines do not appear to be significantly distorted at the intersection of the planar structures. The results from CTRAN3D (Fig 5.10) suggest a significant rise in brine along the z-axis. For comparison purposes, Fig. 5.11 illustrates the solute concentrations measured along z at the recovery plane of the results for run 2 (without seepage effect; Fig. 5.11a) and run 3 (with

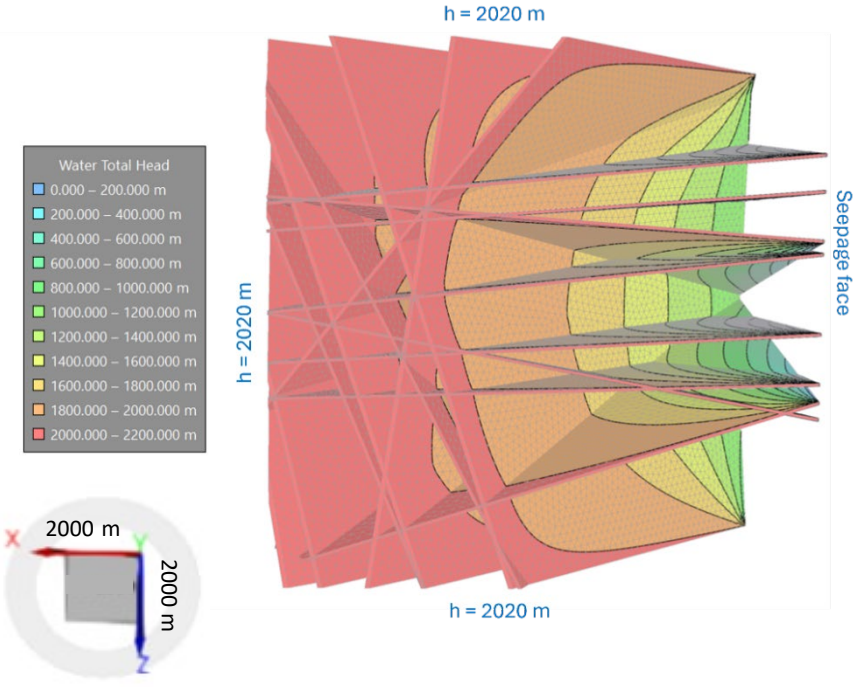

Figure 5.9: Sub-Vertical and Sub-Horizontal Structures model (Conceptual Geometry 3) simulation with SEEP3D through run 3 to simulate dewatering conditions.

dewatering effect; Fig. 5.11b). The results illustrate the effect of dewatering on the rise of saline water over more than 500 m along the z-axis.

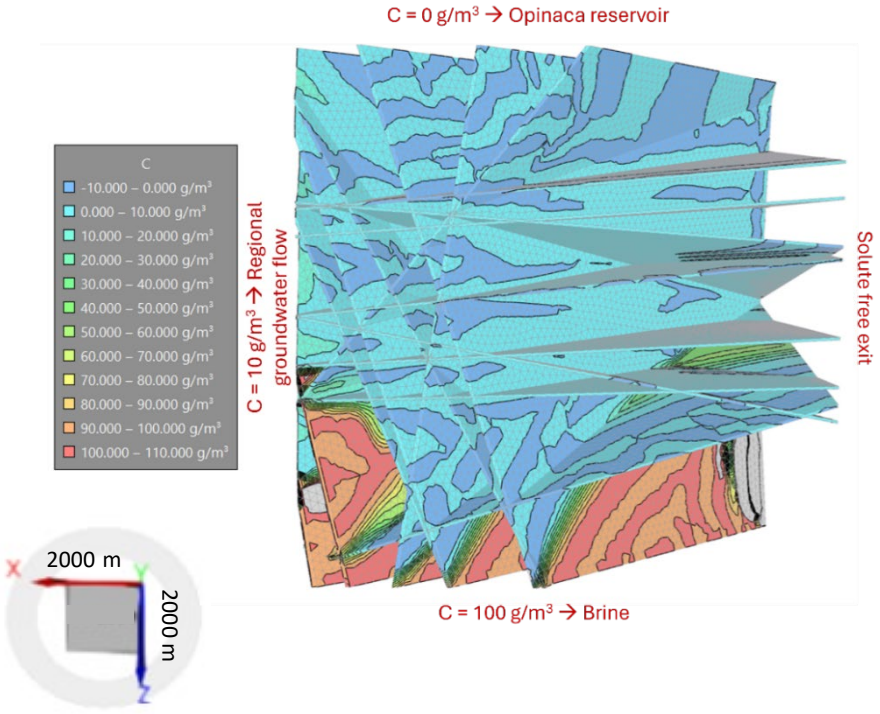

Figure 5.10: Sub-Vertical and Sub-Horizontal Structures model (Conceptual Geometry 3) simulation with CTRAN3D through run 3 to simulate dewatering conditions.

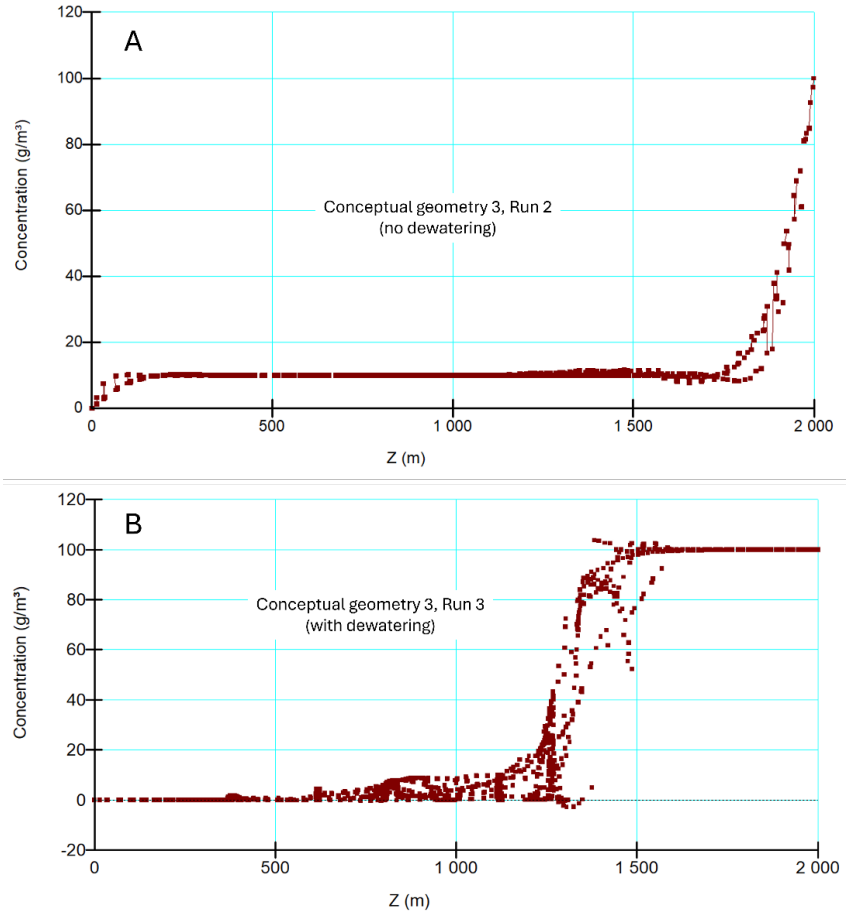

Figure 5.11: Sub-Vertical and Sub-Horizontal Structures model (Conceptual Geometry 3) simulation with CTRAN3D through run 2 to compare non-dewatering/dewatering conditions.

CHAPTER 6 INTERPRETATION OF RESULTS

6.1 Overview of the Numerical Approach

As discussed previously, numerical modelling of fracture networks can be very complex. It also highly depends on the set objectives. In the case of this study, it was important to use similar simplifications done in the past to represent the water-conducting faults using GeoStudio 3D through saturated and steady conditions. Due to its geometrical representation, geological structures and fault have been simplified, and the conceptual model used an ECM approach. As seen in Bense et al. (2013), faults are used to represent not only the geological faults but also open channels to allow flow through a fracture environment. This approach has been shown to represent the general flow in a large scale, despite the heterogeneity and anisotropy. These drainage channels act like a cluster of fractures where the flow can be impacted (Selroos et al., 2002). It has been previously discussed, having an ECM can still mask discrete pathways. In fact, the interpretation of the results arose from the current knowledge base of the site. More specifically, the primary focus is to evaluate how the fracture connectivity and the underground workings can influence the flow through an ECM. Sensitivity 1 to sensitivity 9 were used to assess how changes in input parameters affect numerical results by comparing each case to the corresponding baseline simulation for each model geometry. Overall, despite the thickness of the 3D planes, the studied models using sub-horizontal structures simulated inflows that match the analytical solution as long as the 3D structures are kept with the same parameter values. Similarly to the Conceptual Geometry 1, the ECM block model simulations have resulted in matching the analytical method. The cube model could be considered a simplification of all the previously determined preferential pathways to a volumetric equivalent continuum. In fact, the analytical solution is used to represent a single idealized fracture whereas the 3D planes have finite thickness. Small differences between the two solutions are expected even under equivalent conditions. In terms of the solute transport results, in general the numerical and analytical solutions reconciled. The ECM block model produces slower and smoother breakthrough curves than the 1D analytical approach. This behaviour reflects the inherent numerical dispersion and volumetric averaging in the ECM representation, which tends to delay peak concentrations and broaden the arrival front compared with the sharp advective front in the 1D analytical model. As such, the ECM block numerical results can be considered conservative

in terms of predicted arrival time and plume spreading. It produced a slower and smoother breakthrough curve while validating the prediction obtained with the analytical solution. In generally, in the homogeneous environment, Péclet and Courant number distributions generally complied with the recommended criteria for minimizing numerical dispersion and oscillations, supporting the numerical stability and validation. However, upset conditions were observed under conditions with high transmissivity and velocity. Local Péclet exceedances suggests that there is strong advection-dominated flow. Whereas local Courant exceedance suggests that there are narrow high-gradient zones near the advancing solute front. Moreover, these conditions can suggest that in fast homogeneous pathways, the model needs to be further adjusted to accurately capture the breakthrough behaviour.

Sensitivity 10 (variable K factor of 2) to Simulation 11 (variable K factor of 5) looked at introducing discretization partitioning the structures in two groups using the 10 m thick sub-horizontal structures. Each group was assigned their own K values. Overall, discretization has caused some variability between the analytical solution and the model results. This highlights the fact that for complex geometries, analytical solutions and homogeneous ECMs such as the cube model do not allow for representing environments that are not spatially heterogenous in terms of hydraulic properties. This also highlights the need of using at least a heterogeneous ECM for representing solute transport if the different structures present contrasted hydraulic properties. It is worth mentioning, however, that the model conceptualization did not depend on monitoring data, it was based on theoretical approaches. The Péclet distribution did not comply for Sensitivity 10. This might suggest that there is strong advection-dominated flow due to the sharp change of the K in some areas of the domain. For Sensitivity 11, the Courant distribution did not comply. This might suggest that the mesh size needs to be adjusted because of the higher inflow. Despite these discrepancies, the remaining distribution complied with the established criteria.

Previous models have helped to establish the conceptualization of this model. Understandably, a model that characterizes the fracture connectivity and the interaction between the fracture matrix could help to identify localized effects and spatial trends. All geological structures included in these models are available in DXF files. However, the challenge is the modelling improvement of the representation of the rock mass and its fracture network. Better representation of the flow and hydrogeochemical effects of the area of interest can help for decision making and potentially an improvement of the water managed through the operations. After all, looking at the model

refinement of the reference site through their LOM, it is a relevant example that can be followed to different sites in the Canadian Shield encountering similar challenges.

6.2 Interpretation Fracture Rock Flow Regime and Transport

It is understood that the groundwater flow and solute transport are strongly influenced by the connectivity of the water-conducting structures that were identified prior to the conceptual model. Hence, sub-horizontal structures representation in GeoStudio supported the validation of the initial conceptualization steps and for the sensitivity analysis. As simulations results reconciled with the analytical approach, the block model was able to be adjusted to reflect similar results as those obtained for heterogeneous ECMs. Even with an isotropic hydraulic conductivity, the solute fate and transport depend on the input parameters assigned. Not only does this ECM approach help to simplify the flow and transport regime, but also to generally understand how these drainage channels can impact the water movement and solute displacement in a mine scale. In a homogeneous environment, the analytical solution usually reconciled with the numerical solution. The baseline simulation was key to validate to use it for comparison during the sensitivity analysis. For the 10 m thick horizontal structures, as K increases and n decreases, the breakthrough curve was sharper, compared to the baseline conditions. Dispersivity and mesh size changes did not have a major effect on the breakthrough curve within the range of values tested in the study. On the opposite side, as K, i decreased or n increased, the breakthrough curve flattens. This behaviour is

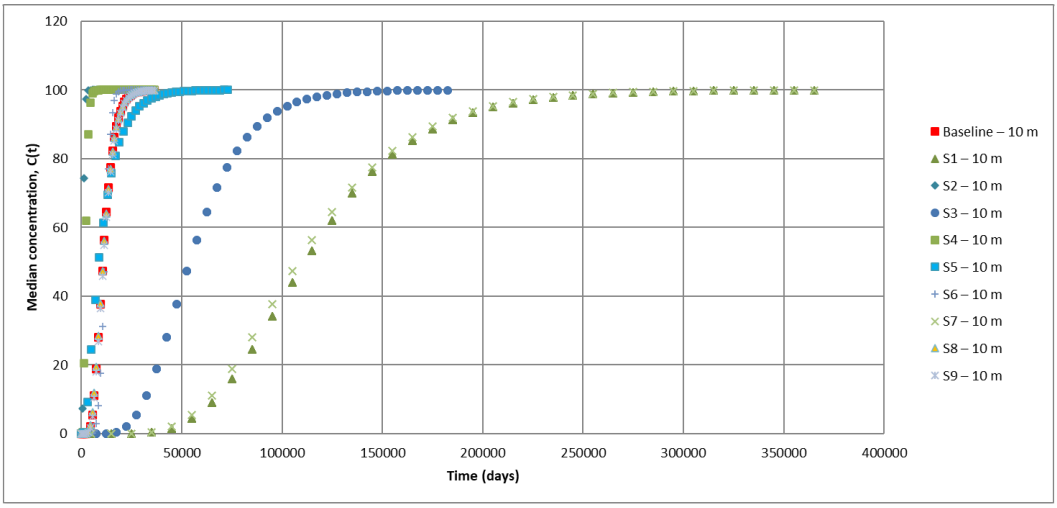

Figure 6.1: 10 m thick sub-horizontal structures breakthrough curves through Sensitivities 1 to 9

consistent with the dependence of the average pore velocity on transmissivity and porosity. Fig 6.1 compiles all the breakthrough curves for these model runs.

In general, the early-stage conceptual model helps to identify the challenges representing a geometrical DFN in GeoStudio. For example, as more complex 3D geometries are added, like with the sub-vertical faults, the model convergence becomes more restrictive, and the model validation more complex. In addition, GeoStudio 3D failed to handle more than 18 planar structures, as mesh generation was not possible. Nevertheless, the model helps to refine the understanding of water and solute transport at the reference site and lead to advancement on the understanding of the fractured bedrock and its respective hydrogeology and geochemistry. It is known that the fractured system is heterogenous and anisotropic. According to previous numerical model results, there is some evidence that there are preferential flows due to the different solute concentrations found in shallow and deep levels of the underground mine. The previous findings suggest there could be lateral and vertical flow and transport within the rock mass affecting the nearby Opinaca Reservoir. This impact depends on the thickness and the type of surficial deposits at the bottom of the water body. The simulations performed on Conceptual Geometry 3 (Run 3) are consistent with this previous observation. Indeed, the simulation suggests that concentrations representative of the Opinaca Reservoir (upper boundary condition in CTRAN3D, set at C = 0 g/m^3) occur down to a depth exceeding 500 m. This can be seen in Figure 5.9, where the simulated rise of the brine at greater depth is also shown.

Once again, this interpretation helps to highlight the importance of properly characterizing the fracture environment and to understand its connectivity according to the mine site objectives and essentially their water initiatives. More specifically, this would allow to better understand and predict areas of interest and inform the site management strategies for underground water management.

6.3 Influence of Mine Openings on Saline Water Migration

As part of the model conceptualization, it was important to ensure the reproduction of key hydrogeological mechanisms through flow-dominant structures. In GeoStudio, these structures behave as preferential flow paths to represent the conglomeration of fractures and the mine openings as part of an ECM approach. Unilateral seepage conditions were evaluated, but the final

interpretation focused on three simulation runs discussed as part of the Conceptual Geometry 3. As previously observed, mine openings have a direct impact on the groundwater flow paths. In addition to fracture connectivity, mine openings change the flow direction laterally and vertically. In fact, it is known that higher solute concentrations can be found in deeper levels at the mine site. It is also understood that mine openings could potentially allow more fracture-matrix interaction to impact the plume behaviour. Furthermore, it is also known that dewatering pumping has caused the ascent of solutes in shallower levels of the mine. Pumping rates were not evaluated as part of the model adjustment. Changing pumping rates overtime could partially be influenced by progressive opening/backfilling of stopes. In fact, blasting events can increase instantly fracture connectivity. Hence, it is typical that as the mine progresses, models should be optimized as small changes can impact the overall system. Nonetheless, the results obtained with run 3 performed on the conceptual geometry 3 (see table 4.3 and section 5.4) provide a framework for illustrating how the depressurization along the faces of planar structures can entail the upward migration of solutes. Nevertheless, more developed simulations taking density dependent flow will be needed to better analyze this process.

6.4 Opportunities to Improve the Rock Matrix Representation and Fracture Network and its Hydrogeochemical Comprehension

Depending on the objective of the mine site, it is important to adjust the representation of the rock mass and the fracture network to identify key areas of interest for a proper site water management. Mines impacted by water infiltration from significant water bodies (i.e. lakes) are faced with important dewatering considerations. Certainly, for a new project, it is hard to predict the key areas of interest. It is still relevant and recommended conducting a hydrogeological flooding model to better identify the dewatering strategies across the mine openings. However, it is valuable to continue refining the rock mass and fracture network representation as the mine operations progresses. GeoStudio 3D is limited for the use of complex geometry. Although, at a certain extent, it has shown capabilities to run an ECM approach. Understanding its limitations with reactive transport, GeoStudio could be paired with other models for a more wholesome hydrogeochemical comprehension which is essential for long-term closure planning. There are still potential avenues to refine the discretization of the geological structures (planar structures) used for the model. The

model still treats them as large rectangles with a uniform hydraulic conductivity. A hybrid approach with dual porosity is still beneficial to run deterministic and stochastic realizations to bound peak inflows during the backfilling/opening of headings. In addition to model optimization, field monitoring data collection is essential for a better presentation. *In situ* testing, like tracer tests conducted at several depths along the same fault to calibrate the current hydraulic conductivity, storage and transmissivity. Also, the dual-porosity transport model can be refined with field kinetic cells with backfill and waste rock. This could help to capture source terms that are currently ignored during fracture-matrix interactions. In this sequence, installing instrumentation at deeper levels would be relevant to better characterize the rock mass and fracture network: piezometers, packers, the use of televiewers and conducting hydro-tests. This would help to update the vertical hydraulic conductivity and reassess the recovery rate when pumping cease after mine closure. On another note, it was determined that blasting events can instantaneously increase the facture connectivity over relatively long distances. Therefore, it is relevant for a model to integrate geomechanical functions to include the fracture aperture which can vary according to local stress test scenarios for planned mine development.

6.5 Broader Benefits for Other Mines in the Canadian Shield

As previously discussed, other mines in the Canadian Shield might face similar conditions to the Éléonore site. More specifically, sites that are located within the boundaries of the historic Tyrell Sea. These sites may require additional focus due to their unique geological and hydrogeological characteristics, among others related to marine intrusion. The boundaries (thick blue lines) of the former Tyrell Sea can be observed in the Figure 6.1 below. Éléonore is a key example of a site that was able to identify the main water-conducting faults which is estimated to be responsible for more than 75% of the current inflows. Looking at this case study, the conceptual model helps to evaluate a practical representation of an ECM. Its intent is not to reproduce the detailed results of previous numerical models, but rather to provide a tool that focuses on process understanding. This tool isolates key hydrogeological mechanisms under simplified and transparent assumptions without overshadow by the complexity of the mine water balance. This model can also be updated relatively easily if any relevant future refinement is expected. The methodology can be transferred to other underground mines with fractured bedrock settings to evaluate dewatering, and salinity-mixing

processes and for closure planning without requiring high computational effort. This approach aligns with recommended multi-scale modelling practices, where simplified continuum models complement detailed site-scale simulations to strengthen conceptual understanding and scenario evaluation (Anderson et al., 2015). Nevertheless, it is of great interest for other mines to evaluate other tools to assess the underground seepage, characterize key boreholes with televiewers and have a proper underground mapping and tracer tests to focus on grouting and drainage on a few relevant faults. Other model software can couple mechanisms, evaluate transient pumping and regional flow. The reference site also reflects the importance to have remote wells in the mine dewatering risk register and have a contingency plan if the well drawdown is heavily impacted. Understandably, due to budget restrictions, it is preferable to start with an EPM model and transition to a discrete model when the data density improves. Mines planning a deep level and narrow stopes could integrate simple stress aperture relationships to forecast transient influence which could also optimize pump sizing for dewatering purposes. Previous conceptual models were able to determine when the Opinaca Reservoir would be affected by a plume if there were no mitigation measures. During mine operations and for closure/post-closure, it can become critical to predict GWQ endpoints first, then proceed with the solutions and pump shutdown schedules. For example, during operations, relative high salinity and TDS levels can impact the equipment used underground since they are exposed to corrosive water. In fact, groundwater concentrations where TDS > 1000 mg/L, Cl^- or SO_4^{2-} exceeds the range between 250 and 500 mg/L indicate potentially corrosive conditions. These concentrations were confirmed in the bottom level of the mine site (Al Yacoubi, 2022). Such water, commonly observed in saline or mine-influenced groundwater can accelerate the corrosion of metal equipment or infrastructure as well as the degradation of concrete linings (Freeze & Cherry, 1979). In the same sequence, like it was done in previous models for the Éléonore site, different scenarios for climate change scenarios should be run to better fit closure goals. Finally, the site structured data management was a key element to ensure the progress of the conceptual model instead of restarting it. It is important to establish a baseline to reduce long-term costs and any operation. More specifically in this case, it will be important to determine mitigation measures to the plume propagation to the Opinaca Reservoir. Even if backfilling can have its challenges, it is known to be a positive alternative to reduce inflows along major faults. A good example can be shown at Éléonore underground mine by backfilling the first 170 metres. This has reduced 125,000 L/min to much lower rates (unpublished internal

data). In conjunction, drainage hole or interception wells can be used to control the water ingress. Indeed, during active mining, dewatering is critical and it is important to adjust and adapt as the operation progress to maintain the required water level. Moreover, while the methodology of Éléonore mine can be transferred to other underground mines in similar conditions, its successful application still depends on site-specific structural mapping, hydraulic testing, and hydrogeochemical monitoring to constrain key water-conducting structures and boundary conditions.

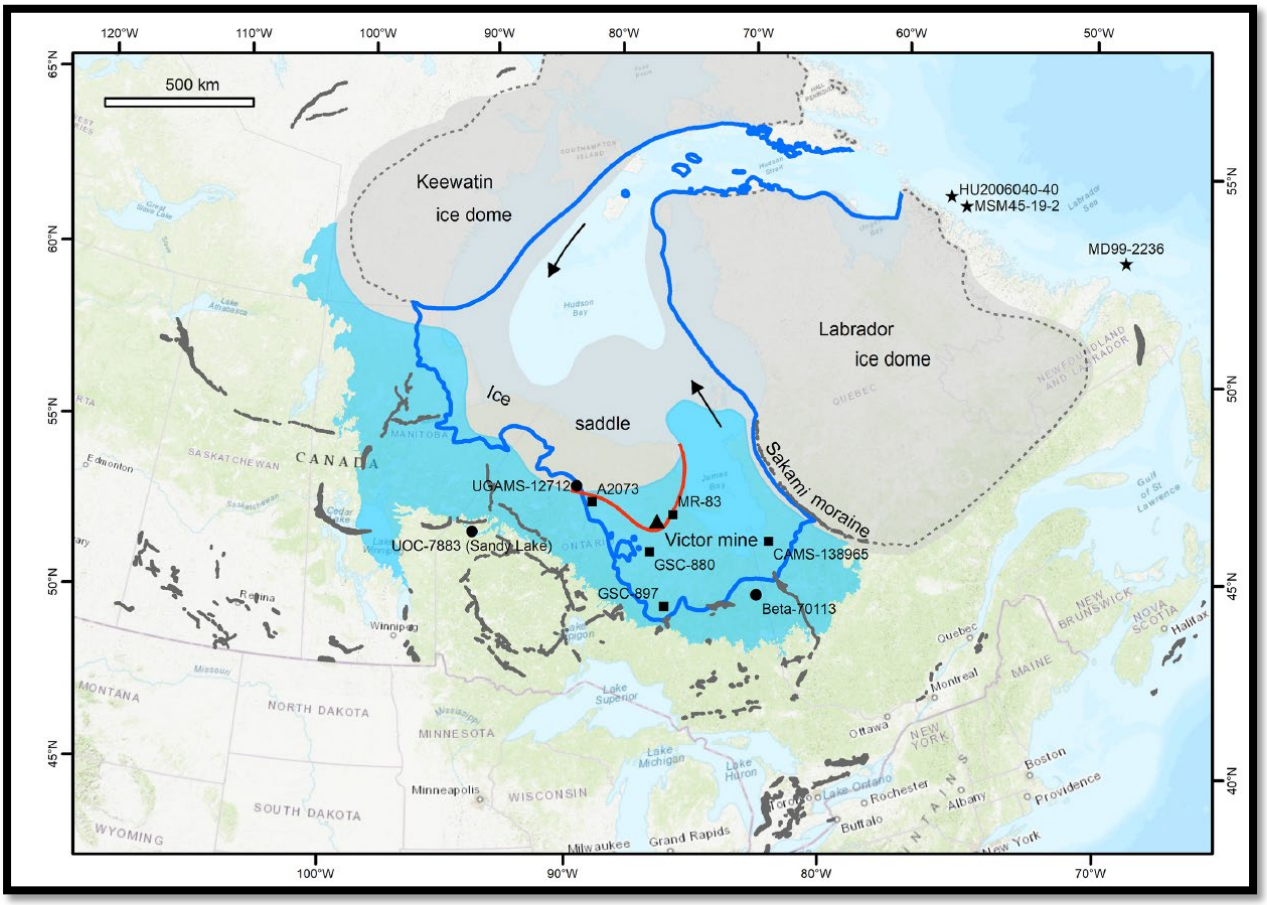

Figure 6.2:Map of the Lake Agassiz-Ojibway with the extent of Tyrell Sea with thick blue lines. The dark grey areas represent moraines. (Gao & Truton, 2025)

6.6 Model Limitations and Opportunities

At this current stage, the study conceptual model does not have calibration points that are considered far field to confirm the REV. Even if the main water-conducting faults are based

discretized geometry, the conceptual model could still be ignoring the internal heterogeneity and aperture variation with stress. In general, in homogeneous conditions, numerical stability and simulations were validated with the established criteria suggesting that ECMs representing fracture system can be reproduced in GeoStudio. Local discrepancies were observed during high transmissivity not necessarily suggesting model instability. This can possibly be adjusted by refining the model input parameters. A sort of discretization was introduced as part of sensitivities 10 and 11 using the Conceptual Geometry 1. This led to results that differ widely from the analytical method using Ogata-Bank. If monitoring data was used to conceptualize the model, these upset conditions could potentially be supported by running deterministic and stochastic realizations using statistical tools. As previously mentioned, due to the irregular shape of the fault and their complex geometry to import in GeoStudio, the fault geometry was simplified and adjusted to ease the fracture bedrock representation and facilitate the import into GeoStudio. This adjustment is considered the reproduction of the flow and transport through the known preferential pathways. In the case of this conceptual model, these structures represent volumetric zones rather than discrete planes. However, ECMs predictions of contaminant persistence or delayed release should not necessarily be considered conservative in terms of time scales. In fact, the steady-state flow assumption and saturated conditions omit the transient drawdown or rebound effect from the dewatering pumping activity. Peak inflow during new excavations or large blasts can be under-predicted by the model (unpublished internal data). Éléonore is equipped with several piezometers and have conducted several packer tests in the past. Nonetheless, in deeper levels of the mine workings, only a limited number of packer tests and piezometers have been installed underground. Boundary conditions could be refined to approximate inflow and outflow rates. For the purpose of this conceptual model and enable clean comparison with a 1D analytical solution, recharge rate was not considered. The simulations were restricted to unilateral flow through the x-axis and known lateral and vertical flow components were intentionally neglected. The recharge rate would be tied to the depth variability. In fact, there are still some interests to further investigate the Opinaca Reservoir till blanket, to better understand their physical properties and the depth variability. This is relevant to better capture the recharge and mixing between the reservoir and the groundwater in the mine openings since there are still some uncertainties tied to the long-term solute loads in previous transport models. Moreover, local diffusion gradients, matrix storage and solute retardation can be reduced, which lead to an underestimation of the plume effects (Selroos

et al., 2002; MacQuarrie & Mayer 2005). Indeed, GeoStudio is limited for reactive transport modelling capabilities. It is recommended to pair it with a software that can further investigate the hydrogeochemical effects such as MINE3P or PHREEQC. Available and additional monitoring wells can also support refinement of this modelling coupling for calibration and to see if there is field conditions alignment which improves forecasts of inflow and contaminant dispersion during and after operations. Similarly to the applicability in water balance and water quality model, it would be of great interest to conduct a sensitivity analysis using climate change to capture a more accurate recharge during closure/post-closure. In addition, GeoStudio cannot simulate the mechanical deformation of fractures which can impact the system hydraulic properties (Wu et al., 2017). For that reason, hydraulic properties are extrapolated at those levels, adding uncertainty to the model results. Finally, it also lacks automatic time-step control and advanced iterative solvers compared to FEFLOW.

To summarize, all these limitations and opportunities could help support, evaluate and determine the necessary tools for decision-making of mitigation measures to avoid the plume propagation to the receptive environment.

CHAPTER 7 CONCLUSION AND RECOMMENDATIONS

The present study investigated the groundwater flow and non-reactive solute transport in a fractured crystalline bedrock environment characteristic of the Canadian Shield with a focus on deep mine inflows and brine migration. Fractured-bedrock aquifer often contains ancient brines, raising hydrogeochemical concerns in underground mine operations. In this context, understanding how salinity moves through fracture network toward mine workings and openings is critical for both operational water management and environmental protection. The study addressed these concerns by developing a robust numerical modelling approach to simulate groundwater flow and dissolved and non-reactive solute transport in the fracture setting and by evaluating the effectiveness in representing the complex hydrogeology of the site. The modelling approach employed is an ECM to approximate the fractured-bedrock aquifer implementing using SEEP3D (for groundwater flow) and CTRAN3D (for contaminant transport) solvers in GeoStudio 3D. As part of this study main objective, homogeneous and heterogenous ECMs were compared through a series of sensitivity analysis. More specifically, the sub-objectives were to evaluate the capacity of homogeneous and heterogenous ECMs to reproduce a flow regime and non-reactive solute transport behaviour in fractured bedrock impacted by mine dewatering and to evaluate the sensitivity of ECMs while varying input parameters such as the hydraulic conductivity, fracture network representation, porosity, advection-dispersion parameters and the geometry. In fact, to recapitulate, the Conceptual Geometry 1 used a heterogenous medium with sub-horizontal geological structures through an ECM. The Conceptual Geometry 2 used a cube to represent a homogeneous medium through an ECM. The Conceptual Geometry 3 used a heterogenous medium with sub-horizontal and sub-vertical geological structures. This technique was chosen over a full DFN simulation as a practical trade-off between detailed and computational feasibility. A DFN could explicitly represent each fracture, but it would require extensive data on fracture geometry and intense computational resources. By contrast, the ECM allowed us to represent the main water-conducting structures with high transmissivity values a continuum grid. Despite the inability to represent a free-drained structure in GeoStudio, it was possible to adjust and simplify the known geological structures and incorporate dominant flow pathways without excessive complexity. Boundary conditions and initial dissolved solute distributions were defined based on the conceptual understanding of regional groundwater flow and the presence of deep brines,

acknowledging that we did not use the site data records. To build confidence in the model, the non-reactive solute transport results were compared against the analytical 1D Ogata–Banks solution for advective–dispersive transport. The Ogata–Banks solution is a classical 1D analytical solution of the advection–dispersion equation, and it provided a benchmark to ensure that the numerical implementation of transport in CTRAN3D. The ECM-based models produced concentration vs. distance profiles that were consistent with the Ogata–Banks solution under equivalent conditions, lending credibility to our approach for simulating non-reactive solute transport in the fractured medium. Furthermore, a sensitivity analysis was performed on key hydrogeological parameters, notably the hydraulic conductivity (K), the hydraulic gradient (i), and the effective porosity (n) governing solute storage and migration. This analysis revealed that model predictions of both groundwater inflow rates and salinity distribution are highly sensitive to these parameters. For instance, increasing the hydraulic conductivity or the imposed gradient significantly elevated the simulated inflow and accelerated solute migration, whereas changes in porosity affected the dispersion and attenuation of the salinity plume. These findings underscore the importance of conceptual model refinement: even in the absence of extensive field data for calibration, carefully refining the structure of the model and parameter values is crucial to obtaining realistic results. Key findings from the modelling effort highlight the controlling role of major structural features and the validity of the ECM approach within the scope of the study. The presence of one or two high-transmissivity zones was found to dominate the flow system, leading to preferential pathways. This result aligns with the field understanding that large fractures or faults often channel most of the flow in otherwise low-permeability crystalline rock. The simplified 3D model geometry proved sufficient to capture these main flow paths and the vertical salinity stratification, although it necessarily neglected any fractures outside the plane of the cross-section. Despite these simplifications, the ECM approach successfully reproduced the expected behaviour of a saline plume migrating through fractured rock towards a pumping sink, especially when benchmarked against the analytical solution. The comparison between an ECM and a notional DFN approach suggests that the ECM can serve as a practical first approximation for mine-scale problems in fractured settings, so long as the key features (e.g. major faults) are included with representative properties. Indeed, this continuum approximation smooths out the heterogeneity of individual fractures. However, given the available data and the large scale of the problem, it provided a reasonable balance between detail and manageability. Importantly, the modelling exercise

highlighted that improving the conceptual model has a profound impact on simulation outcomes. Even without direct field validation data, iterative conceptual model improvements helped produce more coherent and believable results, which is a critical step in groundwater modelling. It is important to ensure that the numerical model remains grounded in physical reality as much as possible. The numerical conceptualization refinement should continue even beyond this study, incorporating new information and exploring additional processes that may affect brine migration. For example, including diffusive exchange between fractures and the rock matrix could better represent how solutes slowly penetrate the rock over time, and considering adsorption or other geochemical interactions might become important if the solute is reactive. Additionally, introducing anisotropy in the hydraulic conductivity would make the model closer to real conditions. These enhancements would address some of the oversimplifications of the current ECM approach, aligning the model more closely with the complex behaviour of underground mine workings.

Building on the findings and acknowledging the limitations of the current model software, we recommend several steps to improve the conceptual model and discretization. A denser and more strategically refined mesh is advised, especially around critical features such as fault zones and mine openings. Finer discretization will capture steep hydraulic gradients and sharp concentration fronts more accurately, reducing numerical dispersion and improving the fidelity of flow pathways in the model. The model can also be improved by conducting future investigations should gather more detailed field data to constrain model parameters and conceptual understanding. This includes installing additional monitoring wells or piezometers to track groundwater levels, performing hydraulic tests (i.e. packer tests or pumping tests) to better estimate spatial variations in hydraulic conductivity, and conducting geochemical sampling of groundwater to delineate the distribution of salinity and other water quality indicators. Such data would not only strengthen the current input parameters but also provide validation targets for model calibration. Furthermore, the numerical model can be improved by integrating the reactive transport and geotechnical processes. The current model is considered only advective–dispersive transport of a conservative solute. We recommend extending the model framework to include reactive processes (if applicable) and to couple with geotechnical stability considerations. For instance, incorporating a reactive transport model could allow simulation of processes like mineral precipitation/dissolution or the buffering of pH and other water chemistry changes as mine water interacts with wall rock. Similarly, linking

the hydrogeological model with a geomechanical model would help assess how changing groundwater pressures during mine flooding (or dewatering) might impact rock stability or induce deformation. This integration would yield a more holistic model that addresses both the chemical and mechanical aspects of mine flooding in fractured rock. In addition, model calibration and verification are possible, as new monitoring data become available, the model should be calibrated to ensure it can reproduce these observations. Calibration may involve adjusting parameters like hydraulic conductivity in specific zones, fracture connectivity, or dispersivity values within justifiable ranges until the model output matches field measurements. Even partial calibration will increase confidence in the predictive capabilities. Moreover, if feasible, a long-term monitoring program can be implemented to verify model predictions of how salinity will evolve in and around the mine after closure (flooding), allowing further iterative improvements to the model. These recommended actions will incrementally improve the model accuracy, robustness, and relevance for decision-making: the numerical predictions become more trustworthy for guiding mine water management or remediation strategies. Finally, it should be emphasized that the approach and lessons from this study are transferable to other mining sites in similar geological settings. The Canadian Shield and other Precambrian crystalline regions host many mines where fractured rock and saline groundwater interactions pose challenges. The workflow applied here can serve as a template for hydrogeological assessments at those sites. Each site will have unique features, but the overall strategy of combining a sound conceptual model with efficient numerical tools is broadly applicable.

In conclusion, well-conceptualized modelling approach for complex fractured rock hydrogeology with an ECM approach. The current ECM model provides a useful baseline understanding of groundwater flow patterns and solute transport toward the mine, and it highlights which features and parameters most strongly control outcomes. However, it is not an endpoint but rather a foundation for continued development. Ongoing refinement and coupling of the numerical and conceptual models are strongly recommended. This includes updating the model geometry to incorporate newly identified fractures or extending to three dimensions if warranted, and incorporating additional transport processes like matrix diffusion, adsorption, and anisotropic permeability to better reflect reality. By continuously updating the model as new data and understanding emerge, we can improve predictive capability and ensure that mine closure and management plans are based on the best available science. Such a proactive, evolving modelling

practice will ultimately lead to more effective management of saline groundwater in deep mines and can be adapted to similar hydrogeological challenges in other settings.

REFERENCES

Abdelghani, F. B., Aubertin, M., Simon, R., & Therrien, R. (2015). Numerical simulations of water flow and contaminants transport near mining wastes disposed in a fractured rock mass. International Journal of Mining Science and Technology, 25(1), 37-45.

Al Yacoubi (2021). Origine des eaux souterraines saumâtres et dynamique de mélange dans les aquifères du Bouclier canadien en Abitibi et dans la région de la Baie-James. [Proposition de recherche, Institut de Recherche en mines et environnement (IRME), UQAT & Polytechnique].

Al Yacoubi (2022). Origines et évolution des saumures en contexte des Boucliers. [GML6003: Séminaire des géomatériaux, Institut de Recherche en mines et environnement (IRME), UQAT & Polytechnique].

Anderson, M. P., Woessner, W. W., & Hunt, R. J. (2015). *Applied groundwater modelling: simulation of flow and advective transport*. Academic press.

Bandyayera, D., Fliszar, A., (2007). Géologie de la region de la Baie Kasipaskatch (SNRC 33C09) et du lac Janin (SNRC 33C16), Ministère des Ressources naturelles et de la Faune, Québec, RP2007-05, 15 pages, 2 maps.

Bear, J., Bachmat, Y., Bear, J., & Bachmat, Y. (1990). The Porous Medium. Introduction to Modeling of Transport Phenomena in Porous Media.

Bear, J., Tsang, C. F., & De Marsily, G. (1993). *Flow and contaminant transport in fractured rock*. Academic Press.

Bense, V. F., Gleeson, T., Loveless, S. E., Bour, O., & Scibek, J. (2013). Fault zone hydrogeology. *Earth-Science Reviews*, *127*, 171-192.

Berkowitz, B. (2002). Characterizing flow and transport in fractured geological media: A review. *Advances in water resources*, *25*(8-12), 861-884.

Bernard, F. (1982). Caractérisation du milieu poreux équivalent à un milieu rocheux fracture par essais à l'eau In situ. Bulletin of Engineering Geology & the Environment, 26(1).

Berre, I., Doster, F., & Keilegavlen, E. (2019). Flow in fractured porous media: A review of conceptual models and discretization approaches. *Transport in Porous Media*, *130*(1), 215-236.

Billaux, D., Chiles, J. P., Hestir, K., & Long, J. (1989). Three-dimensional statistical modelling of a fractured rock mass—an example from the Fanay-Augères mine. In International Journal of Rock Mechanics and Mining Sciences & Geomechanics Abstracts (Vol. 26, No. 3-4, pp. 281-299).

Bottomley, D. J., Gregoire, D. C., & Raven, K. G. (1994). Saline ground waters and brines in the Canadian Shield: geochemical and isotopic evidence for a residual evaporite brine component. Geochimica et Cosmochimica Acta, 58(5), 1483-1498.

Bottomley, D. J., & Clark, I. D. (2004). Potassium and boron co-depletion in Canadian Shield brines: evidence for diagenetic interactions between marine brines and basin sediments. Chemical geology, 203(3-4), 225-236.

Bottomley, D. J., Clark, I. D., Battye, N., & Kotzer, T. (2005). Geochemical and isotopic evidence for a genetic link between Canadian Shield brines, dolomitization in the Western Canada Sedimentary Basin, and Devonian calcium-chloridic seawater. Canadian Journal of Earth Sciences, 42(11), 2059-2071.

Bowell, R. J., Dill, S., Cowan, J., & Wood, A. (2004). A review of sulfate removal options for mine waters. Proceedings International Mine Water Association Symposium 2, 75-88.

Cacas, M. C., Ledoux, E., de Marsily, G., Barbreau, A., Calmels, P., Gaillard, B., & Margritta, R. (1990). Modeling fracture flow with a stochastic discrete fracture network: Calibration and validation: 1. The flow model. Water Resources Research, 26(3), 479–489.

Charland, A., Perron, M., Rispoli, A., Bussières, M., & Bergeron, S. (2018). Éléonore Operations, Quebec, Canada, NI 43-101 technical report (Technical report, effective November 30, 2018). Prepared for Goldcorp Inc., Vancouver, BC.

Chen, Y. F., Ye, Y., Hu, R., Yang, Z., & Zhou, C. B. (2022). Modeling unsaturated flow in fractured rocks with scaling relationships between hydraulic parameters. *Journal of Rock Mechanics and Geotechnical Engineering*, *14*(6), 1697-1709.

Chesnaux, R., Rafini, S., & Elliott, A. P. (2012). A numerical investigation to illustrate the consequences of hydraulic connections between granular and fractured-rock aquifers. Hydrogeology journal, 20(8), 1669.

Cloutier V, Rosa E, Roy M, Nadeau S, Blanchette D, Dallaire PL, Derrien G, Veillette J (2016) Atlas hydrogéologique de l'Abitibi-Témiscamingue. Presses de l'Université du Québec, Amos.

Douglas, M., Clark, I. D., Raven, K., & Bottomley, D. (2000). Groundwater mixing dynamics at a Canadian Shield mine. Journal of Hydrology, 235(1-2), 88-103.

Elmo, D., & Stead, D. (2010). An integrated numerical modelling–discrete fracture network approach to the analysis of rock slope stability. Rock Mechanics and Rock Engineering, 43, 3–19.

ECCC (2017) Groundwater. Environment and Climate Change Canada, Government of Canada. https://www.canada.ca/en/environment-climate-change/services/water-overview/sources/groundwater.html.

Fleury, J. P., Beaudoin, G., Guilmette, C., Bédard, É., Goutier, J., Huot, F., & Davis, D. (2021). The La Pointe gold deposit, a disseminated orogenic gold deposit at the boundary between the La Grande and Opinaca subprovinces, Eeyou Istchee Baie-James, Québec, Canada. *Ore Geology Reviews*, *138*, 104355.

Frape, S., Fritz, P. et McNutt, R. t. (1984). Water-rock interaction and chemistry of groundwaters from the Canadian Shield. Geochimica et Cosmochimica Acta, 48(8), 1617-1627.

Frape, S.K., Blyth, A., Stotler, R.L., Ruskeeniemi, T., Blomqvist, R., McNutt, R., & Gascoyne, M. (2014). 7.15 – Deep Fluids in the Continents. H.D. Holland, K.K. Turekian (Eds.), Treatise on Geochemistry (second ed.), Elsevier, Oxford (2014), pp. 517-562.

Freeze, R. A., & Cherry, J. A. (1979). Groundwater (Vol. 370). Englewood Cliffs, NJ: Prentice-Hall.

Gagné, E. (2014). *Caractérisation d'aquifères régionaux en socle rocheux à partir de mines souterraines*. [Mémoire de maîtrise, Université du Québec à Chicoutimi].

Gao, C., & Turton, C. L. (2025). Early Holocene marine incursion and a freshened Tyrrell Sea in Hudson Bay Lowlands, Canada. *Quaternary Science Reviews*, *349*, 109134.

Geo-Slope International Ltd. (2012). Contaminant Modelling with CTRAN/W. Calgary, AB: Geo-Slope International Ltd. (a Seequent Company).

Geo-Slope International Ltd. (2015). Seepage Modelling with SEEP/W. Calgary, AB: Geo-Slope International Ltd. (A Seequent Company).

Genty, T. (2009). Peut-on traiter efficacement le drainage neutre contaminé à l'aide des techniques utilisant la sorption comme principal mécanisme de traitement? Synthèse environnementale. [Doctoral dissertation, Université du Québec en Abitibi-Témiscamingue].

Greene, S., Battye, N., Clark, I., Kotzer, T., & Bottomley, D. (2008). Canadian Shield brine from the Con Mine, Yellowknife, NT, Canada: Noble gas evidence for an evaporated Palaeozoic seawater origin mixed with glacial meltwater and Holocene recharge. Geochimica et Cosmochimica Acta, 72(16), 4008-4019.

Hadgu, T., Karra, S., Kalinina, E., Makedonska, N., Hyman, J. D., Klise, K., & Wang, Y. (2017). A comparative study of discrete fracture network and equivalent continuum models for simulating flow and transport in the far field of a hypothetical nuclear waste repository in crystalline host rock. Journal of Hydrology, 553, 59-70.

Hoek, E., Carranza-Torres, C., & Corkum, B. (2002). Hoek-Brown failure criterion-2002 edition. *Proceedings of NARMS-Tac*, *1*(1), 267-273.

Hu L, Zhang M, Yang Z, Fan Y, Li J, Wang H, Lubale C. (2020). Estimating dewatering in an underground mine by using a 3D finite element model. PLoS ONE 15(10): e0239682.

Huyakorn, P. S., Lester, B. H., & Faust, C. R. (1983). Finite element techniques for modelling groundwater flow in fractured aquifers. Water Resources Research, 19(4), 1019-1035.

International Network for Acid Prevention (INAP). (2021). GARD guide – Chapter 7: Management and treatment of mine water (Rev. 1). International Network for Acid Prevention.

Jing, L., & Stephansson, O. (2007). Fundamentals of discrete element methods for rock engineering: theory and applications. Elsevier.

Karay, G., & Hajnal, G. (2015). Modelling of groundwater flow in fractured rocks. Procedia Environmental Sciences, 25, 142-149.

Kleine, T., LaPointe, P., & Forsyth, B. (1997). Realizing the potential of accurate and realistic fracture modelling in mining. International Journal of Rock Mechanics and Mining Sciences, 34(3–4), Paper 158.

Kratochvil, D., Marchant, B., Bratty, M., & Lawrence, R. (2008). Innovation in ion exchange technology for the removal of sulfate. In the 69th Annual International Water Conference, San Antonio, USA.

Kratochvil, D. (2012). Sustainable water treatment technologies for the treatment of acid mine drainage. Shortcourse, ICARD 2012, Ottawa, ON.

Kelly, W. R., Panno, S. V., & Hackley, K. C. (2010). Increasing chloride in surface waters and groundwater of the Chicago region; In 2010 GSA Annual Meeting (Vol. 42, pp. 376). Geological Society of America.

Labbé, M., Molson, J., & Rosa, E. (2024). Hydrogeological Characterization and Numerical Flow Modelling of an Active Mine Tailings Site in Abitibi-Témiscamingue, Quebec, Canada. *Mine Water and the Environment*, 43(1), 16–27.

Legendre, F. (2023). GNM1018 Traitements des effluents miniers : Séance 4 – Principes de base en traitement des eaux, processus biologiques de destruction des contaminants. [Diapositives PowerPoint]. Tiré de https://moodle.uqat.ca/mod/resource/view.php?id=878053.

Ma, L., Gao, D., Qian, J., Han, D., Xing, K., Ma, H., & Deng, Y. (2023). Multiscale fractures integrated equivalent porous media method for simulating flow and solute transport in fracture-matrix system. *Journal of Hydrology*, *617*, 128845.

MacQuarrie, K. T., & Mayer, K. U. (2005). Reactive transport modelling in fractured rock: A state-of-the-science review. Earth-Science Reviews, 72(3-4), 189-227.

Mayer, K. U., & MacQuarrie, K. T. B. (2007). Reactive Transport Modelling in Sedimentary Rock: State-of-Science. Nuclear Waste Management Organization Report NWMO TR-2007-12. Toronto, Canada.

McNutt, R. H. (2000). Strontium isotopes. Dans Environmental tracers in subsurface hydrology (p. 233-260). Springer.

Molson, J., Aubertin, M., & Bussière, B. (2012). Reactive transport modelling of acid mine drainage within discretely fractured porous media: Plume evolution from a surface source zone. Environmental Modelling & Software, 38, 259–270.

Ministère des Ressources naturelles et des Forêts du Québec. (n.d.). Carte géologique – secteur de la mine Éléonore (feuillet 33C09) [Map]. SIGEOM – Système d'information géominière du Québec. https://sigeom.mines.gouv.qc.ca.

Ministère des Ressources naturelles et des Forêts (MRNF). (2025). Formation de Low. Lexique stratigraphique du Québec. https://gq.mines.gouv.qc.ca/lexique-stratigraphique/province-du-superieur/formation-de-low/.

National Research Council. (1996). *Rock fractures and fluid flow: Contemporary understanding and applications*. National Academies Press.

Neculita, C. M., Zagury, G. J., & Bussière, B. (2007). Passive treatment of acid mine drainage in bioreactors using sulfate-reducing bacteria: Critical review and research needs. Journal of environmental quality, 36(1), 1-16.

Neretnieks, I. (1990). Solute transport in fractured rock-applications to radionuclide waste repositories (No. SKB-TR--90-38). Swedish Nuclear Fuel and Waste Management Co., Stockholm (Sweden).

Neuman, S. P. (2005). Trends, prospects and challenges in quantifying flow and transport through fractured rocks. Hydrogeology Journal, 13, 124-147.

Parkhurst, D. L., Kipp, K. L., & Charlton, S. R. (2010). PHAST Version 2—A program for simulating groundwater flow, solute transport, and multicomponent geochemical reactions. US Geological Survey Techniques and Methods, 6, A35.

Ogata, A. (1970). *Theory of dispersion in a granular medium*. (U.S. Geological Survey Professional Paper 411-I). U.S. Government Printing Office.

Peterson, M. (2017). The radioactive-stable tracer diffusion method to quantify diffusive losses in fractured rocks and heterogeneous aquifers. [Doctoral dissertation, UNSW Sydney].

Pine, R. J., Coggan, J. S., Flynn, Z. N., & Elmo, D. (2006). The development of a new numerical modelling approach for naturally fractured rock masses. Rock Mechanics and Rock Engineering, 39, 395–419.

Pouw, K., Campbell, K., & Babel, L. (2014). Study to identify BATEA for the management and control of effluent quality from mines. Mine Environment Neutral Drainage (MEND). MEND Report, 3(1).

Praamsma, T. (2016). Rock outcrops in the Canadian shield: An investigation of contaminant transport from surface sources in fractured rock aquifers (Doctoral dissertation).

Pruess, K., Faybishenko, B., & Bodvarsson, G. S. (1999). Alternative concepts and approaches for modelling flow and transport in thick unsaturated zones of fractured rocks. Journal of Contaminant Hydrology, 38(1-3), 281-322.

Rapantova, N., Grmela, A., Vojtek, D., Halir, J., & Michalek, B. (2007). Ground water flow modelling applications in mining hydrogeology. Mine water and the environment, 26, 264-270.

Rouleau, A., Clark, I. D., Bottomley, D. J., and Roy, D. W. (2013). Precambrian Shield. Chap 11 in Canada`s Groundwater Resources, edited by A. Rivera, 415–442. Markham: Fitzhenry & Whiteside.

Selroos, J. O., Walker, D. D., Ström, A., Gylling, B., & Follin, S. (2002). Comparison of alternative modelling approaches for groundwater flow in fractured rock. Journal of Hydrology, 257(1-4), 174-188.

Seequent. (2024). *GeoStudio 2024.2.1* [SEEP3D & CTRAN3D]. https://www.seequent.com

Sreekanth, J., Crosbie, R., Pickett, T., Cui, T., Peeters, L., Slatter, E., ... & Herr, A. (2020). Regional-scale modelling and predictive uncertainty analysis of cumulative groundwater

impacts from coal seam gas and coal mining developments. *Hydrogeology Journal*, *28*(1), 193-218.

Stotler RL, Frape SK, Ruskeeniemi T, Ahonen L, Onstott TC, Hobbs MY. (2009). Hydrogeochemistry of groundwaters in and below the base of thick permafrost at Lupin, Nunavut, Canada. Journal of Hydrology 373: 80–95.

Taulis, M., & Milke, M. (2007). Coal seam gas water from Maramarua, New Zealand: characterisation and comparison to United States analogues. Journal of Hydrology (New Zealand), 1-17.

van Dam, R. A., Harford, A. J., Lunn, S. A., & Gagnon, M. M. (2014). Identifying the cause of toxicity of a saline mine water. PLoS One, 9(9), e106857

Tóth, J. (1999). Groundwater as a geologic agent: An overview of the causes, processes, and manifestations. *Hydrogeology journal*, *7*(1), 1-14.

Walter, J., Chesnaux, R., Cloutier, V., & Gaboury, D. (2017). The influence of water/rock−water/clay interactions and mixing in the salinization processes of groundwater. Journal of Hydrology: Regional Studies, 13, 168-188.

Wu, Y., Liu, Q., Chan, A. H., & Liu, H. (2017). Implementation of a time-domain random-walk method into a discrete element method to simulate nuclide transport in fractured rock masses. Geofluids, 2017.

Zaidel, J., Markham, B., & Bleiker, D. (2010). Simulating seepage into mine shafts and tunnels with MODFLOW. *Groundwater*, *48*(3), 390-400.

Zhou, C. B., Chen, Y. F., Hu, R., & Yang, Z. (2023). Groundwater flow through fractured rocks and seepage control in geotechnical engineering: Theories and practices. *Journal of Rock Mechanics and Geotechnical Engineering*, *15*(1), 1-36.